BioMed Research International

Biomedicine and Biotechnology: Public Health Impact

Guest Editors: Nirmal K. Ganguly, Simon Croft, Lalji Singh, Subrata Sinha, and Tanjore Balganesh

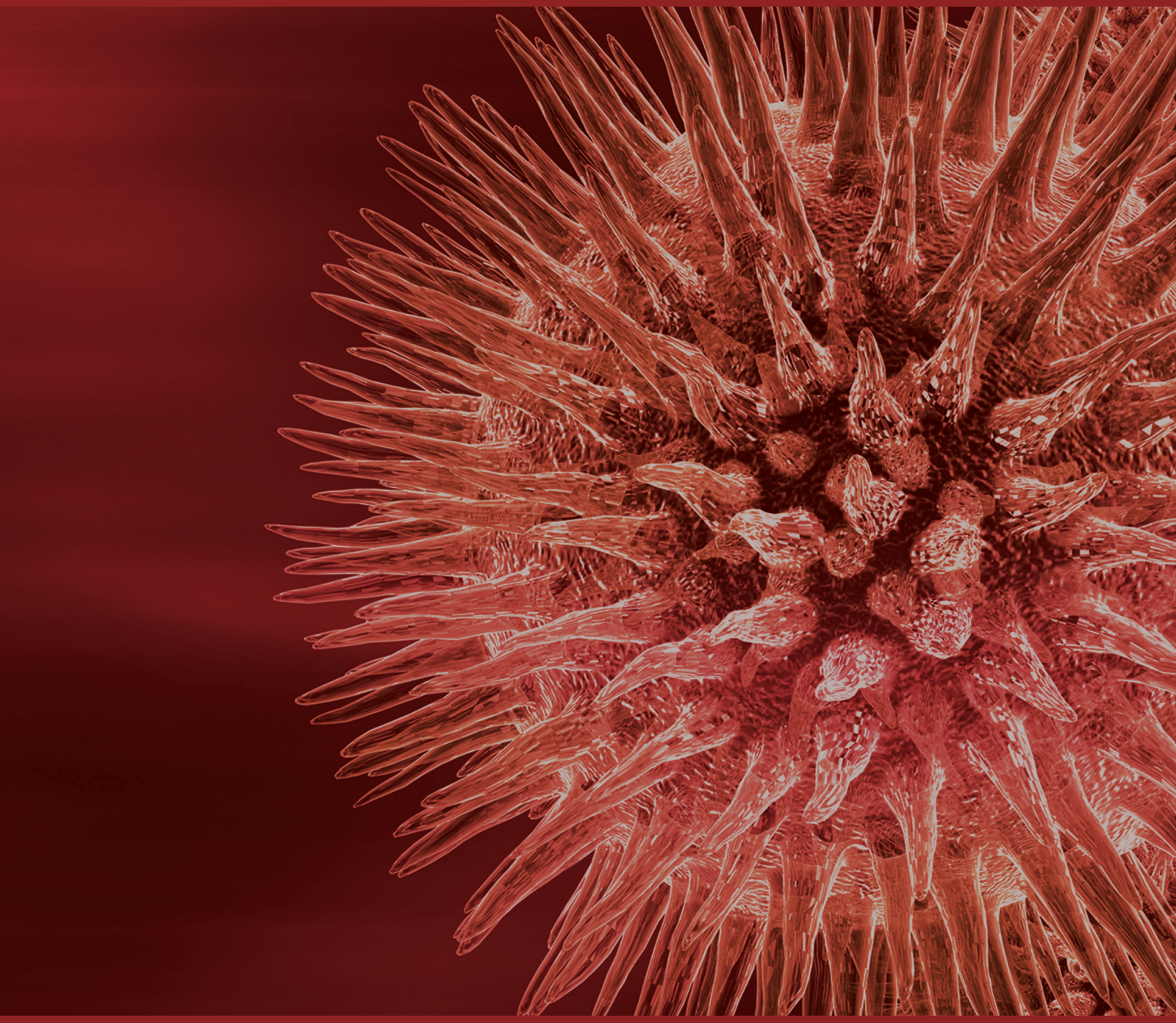

Biomedicine and Biotechnology: Public Health Impact

BioMed Research International

Biomedicine and Biotechnology: Public Health Impact

Guest Editors: Nirmal K. Ganguly, Simon Croft, Lalji Singh, Subrata Sinha, and Tanjore Balganesh

Contents

Hindawi Publishing Corporation
BioMed Research International
Volume 2014, Article ID 524785, 2 pages
http://dx.doi.org/10.1155/2014/524785

Editorial

Biomedicine and Biotechnology: Public Health Impact

Nirmal K. Ganguly,[1,2] Simon Croft,[3] Lalji Singh,[4] Subrata Sinha,[5] and Tanjore Balganesh[6]

[1] *Translational Health Science and Technology Institute (THSTI), Gurgaon, India*
[2] *The Institute of Liver and Biliary Sciences (ILBS), India*
[3] *Immunology and Infection Department, Faculty of Infectious and Tropical Diseases, London School of Hygiene and Tropical Medicine, UK*
[4] *Banaras Hindu University, Varanasi, Uttar Pradesh 221 005, India*
[5] *National Brain Research Center, NH-8, Manesar, Gurgaon, Haryana 122 051, India*
[6] *CSIR Centre for Mathematical Modelling and Computer Simulation (C-MMACS), NAL Belur Campus, Bangalore 560037, India*

Correspondence should be addressed to Nirmal K. Ganguly; nkganguly@nii.ac.in

Received 9 March 2014; Accepted 9 March 2014; Published 8 April 2014

The goal of humankind is to alleviate the suffering from disease and quest is to have good and robust health always. The gain of knowledge through research is one of the primary steps towards the same. With the newly emerging infectious diseases, increase in the antimicrobial resistance and also the increasing incidences of noncommunicable diseases have thrown at us new challenges to develop better diagnostics, drugs, medical devices, and vaccines.

The present century is the era of biotechnology and information technology. Biotechnology has become the amalgamation of several technologies ranging from the field of biomedical research and synthetic biology and further transcending to engineering, nanotechnology, and bioinformatics. Biomedicine have gone a step further converging biology, chemistry, and physics which have led to increasing the understanding of the pathophysiological processes by deciphering the molecular interaction that plays a significant role in the cellular mechanism and thus devising new strategies to produce new diagnostics and therapies.

Health innovation process needs a boost to stem the declining productivity and high turnover rates of drugs with escalating cost. So, the promotion of newer technologies and innovation is the need of the hour. It is imperative to have health innovation reach the masses and add a value to the public health system of nations across the globe. With adequate impetus we are ushering in today the era of knowledge driven, evidence-based innovation in fields of biotechnology and biomedicine, leading to development of platform technologies which can have global implications.

This special issue in the journal of Biomed Research is a step towards the path which brings us to the forefront of new innovations and technologies that transcend all aspects of translational research and have high significance in the public health arena. Hence the editors have selected the cutting edge research in the field of medical biology which has bearing in the future of science.

The paper by Y. Qin et al., which have found that DNA vaccine encoding BCR/ABL-hil2 enhances the in vivo humoral and cellular responses in BABL/c mice, hence presenting a new targeted immunotherapy approach which holds promising finding for patients with chronic myeloid leukemia (CML). The paper postulates these findings and if the research is translated to effective DNA vaccine in humans for CML patients, it will help in the treatment of residual disease after the treatment with chemotherapy or targeted therapy.

New research in antimicrobial therapy has become a very essential tool to fight infection in context of growing antibiotic resistance. The paper by J. J. G.-R. Rodríguez et al., has given alternate strategy with cloned antimicrobial peptide PaDef homologous to defensins from Mexican avocado (*Persea americana* var. *drymifolia*). This paper reports

the antimicrobial activity of defensin from avocado against *Escherichia coli* and *Staphylococcus aureus*. The alternative method of pathogen control paves the way for development of new treatment regimes against infectious pathogens.

The effect of curcumin from *Curcuma longa* L. (from the family Zingiberaceae) on fighting oxidative stress in liver and brain in mice fed with excessive alcohol was studied in the paper by C. W. Pyun et al. The finding showed that curcumin increases brain and hepatic phosphatidylcholine hydroperoxide levels in mice after consumption of excessive alcohol, hence proving the effectiveness of consumption of daily curcumin intake in protecting the liver and brain against alcohol induced oxidative stress.

The G. C. Fontes et al., paper on characterization of alginate and OSA starch bead for the use of controlled release carrier for penicillin is an important finding to alleviate the discomfort of patients undergoing conventional administration of the vital drug. This paper also has long implications on designing public health intervention for delivery of essential drugs.

The paper by M. P. L. Cunha et al., is the analysis of the vaccine adverse event reporting in the state of Rondonia, Brazil during the first ten years (1998–2008) after introduction of vaccines for BCG (Bacillus Calmette-Guerin), DTwP/Hib (hepatitis B, diphtheria, tetanus, pertussis + hemophillus influenza b), DTP (diphtheria, tetanus, and pertussis), MMR (measles, mumps, and rubella) and yellow fever (YF) is a major impact paper on public health. This study is of paramount importance which can help the regulators and clinicians alike from all over the world in gauzing the effectiveness and adverse reaction that can be anticipated from the regular vaccines that are a part of immunization programs of many countries around the world.

The simple model to analyze assessment of the antitoxin antibodies in the paper by A. Skvortsov and P. Gray also is an essential scientific finding which was once validated experimentally will be a very useful tool to assess in vitro the potential of protective antibodies for further evaluation in vivo.

The compilation of the articles in the special issue is very good read of high impact research and important scientific findings would have robust impact on strategizing innovative solutions of public health interventions globally; hence, all editors have selected the most promising research for publication.

Nirmal K. Ganguly
Simon Croft
Lalji Singh
Subrata Sinha
Tanjore Balganesh

Hindawi Publishing Corporation
BioMed Research International
Volume 2013, Article ID 986273, 9 pages
http://dx.doi.org/10.1155/2013/986273

Research Article

Antibacterial Activity of Defensin PaDef from Avocado Fruit (*Persea americana* var. *drymifolia*) Expressed in Endothelial Cells against *Escherichia coli* and *Staphylococcus aureus*

Jaquelina Julia Guzmán-Rodríguez,[1] Rodolfo López-Gómez,[2] Luis M. Suárez-Rodríguez,[2] Rafael Salgado-Garciglia,[2] Luis C. Rodríguez-Zapata,[3] Alejandra Ochoa-Zarzosa,[1] and Joel E. López-Meza[1]

[1] *Centro Multidisciplinario de Estudios en Biotecnología, Facultad de Medicina Veterinaria y Zootecnia, Universidad Michoacana de San Nicolás de Hidalgo, Km 9.5 Carretera Morelia-Zinapécuaro, Posta Veterinaria, 58893 Morelia, MICH, Mexico*
[2] *Instituto de Investigaciones Químico Biológicas, Universidad Michoacana de San Nicolás de Hidalgo (UMSNH), Ciudad Universitaria, Edificio B1, 58030 Morelia, MICH, Mexico*
[3] *Unidad de Biotecnología, Centro de Investigación Científica de Yucatán, A.C. Calle 43 No. 130 Col. Chuburná de Hidalgo, 97200 Mérida, YUC, Mexico*

Correspondence should be addressed to Joel E. López-Meza; elmeza@umich.mx

Received 2 November 2012; Accepted 4 September 2013

Academic Editor: Lalji Singh

Antimicrobial therapy is a useful tool to control infectious diseases in general and rising antibiotic resistant microorganisms in particular. Alternative strategies are desirable, and antimicrobial peptides (AMP) represent attractive control agents. Mexican avocado (*Persea americana* var. *drymifolia*) is used in traditional medicine; however, the AMP production has not been reported in this plant. We obtained a cDNA library from avocado fruit and clone PaDef was identified, which has a cDNA (249 bp) encoding a protein (78 aa) homologous with plant defensins (>80%). We expressed the defensin *PaDef* cDNA (pBME3) in the bovine endothelial cell line BVE-E6E7. Polyclonal and clonal populations were obtained and their activity was evaluated against *Escherichia coli*, *Staphylococcus aureus*, and *Candida albicans*. *E. coli* viability was inhibited with 100 μg/mL of total protein from clones (>55%). Also, *S. aureus* viability was inhibited from 50 μg/mL total protein (27–38%) but was more evident at 100 μg/mL (52–65%). This inhibition was higher than the effect showed by polyclonal population (~23%). Finally, we did not detect activity against *C. albicans*. These results are the first report that shows antimicrobial activity of a defensin produced by avocado and suggest that this AMP could be used in the control of pathogens.

1. Introduction

The excessive and inappropriate use of conventional antibiotics in the clinical treatment of human and animal infections has increased pathogen resistance against these compounds, turning them into less effective agents. As a consequence, there has been an increase in the generation of multidrug-resistant pathogens, primarily bacteria and fungi that resist the effects of most antibiotics [1, 2]. Thus, alternative methods for controlling pathogens are required. In this sense, the plants are an attractive alternative because they exhibit a huge variety of compounds with antimicrobial activity.

The antimicrobial metabolites from plant origin derive mainly from secondary metabolism. These compounds include diverse groups such as saponins, phenolic compounds, cyclic hydroxamic acids, cyanogenic glycosides, isoflavonoids, sesquiterpenes, and sulfur-containing indole derivatives [3]. Avocado (*Persea americana* Mill.) is an important worldwide agricultural crop native of Mexico

and Central America, which contains diverse metabolites with antimicrobial activity. For example, the 1,2,4-trihydroxy-n-heptadeca-16-en isolated from avocado fruit and seeds showed antibacterial activity [4]. Also, the presence of antifungal dienes from idioblast cells and exocarp and mesocarp of unripe fruits has been described [5–7]. In addition, metabolites with antiviral activity from avocado leaves have been reported [8, 9]. More recently, Sánchez-Pérez et al. [10] showed that crude root extracts from *P. americana* var. *drymifolia* inhibit the mycelial growth of *Phytophthora cinnamomi*, this activity was attributable to stigmastan-3, 5-diene. The great compound diversity with antimicrobial properties in avocado tissues is evident; despite this, the production of antimicrobial peptides (AMPs) by *P. americana* has not been reported.

AMPs are produced by a wide variety of organisms as part of their first line of defense (eukaryotes) or as a competition strategy for nutrients and space (prokaryotes) and have a broad and nonspecific activity that makes them strong candidates for a variety of pharmacological applications [11].

Plants produce AMPs as part of their defense mechanisms; these can be expressed constitutively or induced in response to pathogen attack [12, 13]. Plant AMPs have a molecular weight in the range of 2 to 10 kDa, are basic, and contain 4, 6, 8, or 12 cysteines that form disulfide bonds [13, 14]. Plant AMPs are classified in 10 families; one of the most important are the defensins, which are basic AMPs with an approximate molecular weight of 5 kDa (45 to 54 amino acids); they typically have eight cysteines and exhibit mainly antifungal activity [12, 13].

In previous works, we have reported that the expression of AMPs in bovine endothelial cells is a useful tool to explore antibacterial, fungicidal, and cytotoxic activities against a broad range of mammal pathogens and human tumor cell lines [15, 16]. In this study, we isolated the cDNA of defensin *PaDef* from avocado fruit, which was expressed as a fusion protein in the endothelial cell line BVE-E6E7. We show that the conditioned media (CM) from these cells have antimicrobial activity against *Escherichia coli* and *Staphylococcus aureus*, important pathogens from animals and humans.

2. Materials and Methods

2.1. Biological Material and Bacterial Strains. Avocado fruits of *Persea americana* var. *drymifolia* "native Mexican" were collected in the Germplasm Bank of the Instituto Nacional de Investigaciones Forestales y Agropecuarias (INIFAP; Uruapan, Michoacán, Mexico). Fruits were cut and immediately frozen in liquid nitrogen. Seeds were separated from the rest of the fruit tissue.

As representative of gram-negative bacteria, we used the enteropathogenic *Escherichia coli* strain 0111 from Instituto Nacional de Referencia Epidemiológica (SSA, Mexico) that was kindly donated by M.S. Vázquez-Garcidueñas (UMSNH, Mexico). The American Type Culture Collection (ATCC) *S. aureus* subsp. *aureus* 27543 strain isolated from a case of clinical mastitis was used as representative of gram-positive bacteria. Inoculum was prepared from bacteria that were grown at 37°C overnight in Luria-Bertani broth (LB, Bioxon, Mexico). Additionally, the ATCC *Candida albicans* 10231 strain was used. In this case, the inoculum was prepared from fungus that was grown at 21°C for 48 h in YPD broth (2% dextrose, 2% Bacto Peptone, 1% yeast extract; Difco).

2.2. Cell Cultures. The bovine endothelial cell line BVE-E6E7 immortalized with the human papillomavirus type 16 E6E7 oncogene was used to express defensin *PaDef* cDNA from *P. americana* var. *drymifolia* [17]. Cells were routinely cultured in Dulbecco's modified Eagle's medium (DMEM, Sigma), supplemented with 10% fetal calf serum (FCS, Equitech-Bio), 100 U/mL penicillin and streptomycin (Gibco) and grown in an atmosphere of 5% CO_2 at 37°C.

2.3. cDNA Library Construction and Sequencing by Sanger Method. Total RNA from frozen pulp tissue was extracted using R. López-Gómez and M. A. Gómez-Lim. [18] protocol with some modifications. All cDNA complementary libraries were built from 1 μg of total RNA using SMART cDNA library construction Kit (Clontech). The obtained cDNA sequences were cloned into TripIEx2 vector. Excision experiments were made using *E. coli* BM25.8 cells to obtain the plasmid pTriplEx2. Sequencing reactions were performed using ABI PRISM BigDye Terminators v3.0 kit (Applied Biosystems) by 5′ end of plasmids extracted from random clones. The sequences obtained were filtered by quality using PHRED [19]; vector masked and trimming of poly A/T were performed using LUCY2 software [20]. Identification of defensin *PaDef* was reported elsewhere [21].

2.4. Bioinformatic Analysis of the Defensin PaDef from Avocado. The nucleotide sequence of defensin *PaDef* cDNA and the deduced amino acid sequence were analyzed using the Blast tool in the NCBI (http://blast.ncbi .nlm.nih.gov/). The peptide structure was evaluated for the presence of a signal peptide sequence with SignalP (http://www.cbs.dtu .dk/services/SignalP/), and the possible disulfide bridge pattern was determined using the DISULFIND predictor (http://disulfind.dsi.unifi.it/).

The deduced amino acid sequence encoding for the plant defensin peptide was aligned against sequences of defensin holotype type 1 (*Raphanus sativus* Rs-AFP1, GenBank: AAA69541.1) and defensin type 2 (*Nicotiana alata* NaD1, GenBank: AAN70999.1) using ClustalX [22]. Homology models for defensin PaDef peptide were created using the Protein Model Portal (http://www.proteinmodelportal.org). The crystal structure of Rs-AFP1 (Protein Data Bank: 1AYJ) from radish was used as template. The models obtained were refined and analyzed with YASARA tools (http://www .yasara.org).

2.5. Construction of Expression Vector and Transfection of BVE-E6E7 Cells. For transfection assays the defensin *PaDef* cDNA was cloned into the mammalian expression vector pTracer-EF/V5-His-A (Invitrogen), and the construction was denominated pBME3. To obtain this construction, the defensin *PaDef* cDNA was amplified by PCR with specific

primers that were modified with restriction sites to facilitate the manipulation. The primers (Invitrogen) were: forward, 5′-TATT**ACTAGT**ATGGCGCTGGTCAAGAAG-3; reverse, 5′-ATAA**GAATTC**GCAAGGCTTGAGACACA-3′; in bold are indicated the restriction sites *Spe*I and *Eco*RI, respectively. Amplifications were performed under the following conditions: 5 min of initial denaturation at 94°C followed by 30 cycles of amplification at 94°C for 30 s, 52°C for 30 s, and 72°C for 1 min. The amplification product (249 bp) was subcloned into the *Spe*I and *Eco*RI sites of pTracer-EF/V5-His-A vector. This vector contains the resistance gene for zeocin and the reporter gene for the green fluorescent protein (GFP), which allows the selection of transfected cells by antibiotic resistance and fluorescence microscopy, respectively. The correct fusion was confirmed by sequencing. BVE-E6E7 cells were stably transfected with the construction pBME3 or pTracer EF/V5-His-A vector (negative control) by lipofection using Lipofectamine 2000 (Invitrogen) according to manufacturer's instructions. Polyclonal populations of transfected cells were selected in Opti-mem medium (Gibco) containing 500 μg/mL zeocin (Invitrogen) for 2 weeks and by expression of GFP. Cells were maintained with 200 μg/mL zeocin after selection. Next, 9 clonal populations were obtained by limiting dilution and were analyzed through this study. Expression of defensin *PaDef* by transfected BVE-E6E7 cells was analyzed by RT-PCR as described previously [23, 24].

2.6. Transfected Cells Conditioned Media. To obtain the conditioned media, polyclonal and clonal populations of BVE-E6E7 cells transfected with pBME3 (BVE3) or pTracer-EF/V5-His-A (BVpT) that corresponds to empty vector were grown at confluence in p100 Petri dishes (Costar). Culture medium was replaced with 10 mL of Optimem medium (Gibco) without serum and antibiotics, and the cells were cultured for 24 h. Conditioned media were clarified by centrifugation (10 min, 1200 ×g). The concentration of total protein was determined by the Bradford method.

2.7. Viability Assays of Staphylococcus aureus, Escherichia coli, and Candida albicans Strains. 5×10^4 CFU of *S. aureus* and 3×10^4 CFU of *E. coli* were incubated with different concentrations ranging from 10 to 100 μg/mL of total protein of CM from polyclonal and clonal populations during 4 h at 37°C in a 96-well flat-bottom plate. Then, 10 μL of 5 mg/mL of 3-(4,5-dimethyl-2-thiazolyl)-2,5-diphenyl-2H-tetrazolium bromide (MTT, Sigma) solution in PBS was added to each well and incubated for 4 h at 37°C. After that, 100 μL of acid isopropanol (95% isopropanol and 5% of 1 N HCl) was added to dissolve formazan crystals. Optical density was measured with a microplate spectrophotometer (DAS) at 595 nm [25]. Wells containing Optimem medium were used as background controls. Cells treated with gentamicin (40 μg/mL, Sigma) were used as negative control of viability. All assays were run in triplicates. In the case of *C. albicans*, 1×10^5 cells were incubated with the same concentrations of total protein for 24 h at 37°C and then evaluated as described for bacteria. Cells treated with amphotericin (250 ng/mL, Sigma) were used as negative control of viability.

2.8. Flow Cytometry Analysis. BVE3-C1 cells were plated at confluence in 24-well tissue culture plates. Then, monolayers were detached with trypsin-EDTA (Sigma) and were transferred to 1.5 mL microtubes. Cells were centrifuged at 2500 rpm and washed with PBS, and the pellet was fixed with 4% paraformaldehyde in PBS for 10 min at 4°C. Then, cells were blocked with 5% normal goat serum (Sigma) for 30 min on ice. Cells were permeabilized with 0.1% Triton X-100 for 10 min at 4°C and were incubated with primary antibody anti-V5 epitope (1 : 500, Invitrogen) overnight at 4°C and finally with the TRITC conjugated-secondary antibody against mouse IgG (1 : 50, Molecular Probes) for 45 min on ice. Cells were washed three times with PBS-Triton and analyzed in an Accuri C6 flow cytometer (Accuri Cytometers) using CFlow software. BVpT were used as control, or BVE3-C1 cells were incubated only with secondary antibody.

2.9. Data Analysis. Data were compared by analysis of variance and Student's t-test. The results are reported as mean ± the standard errors (SE). P values of < 0.05 were considered significant.

3. Results

3.1. Characteristics of Defensin PaDef from Avocado Fruit. In order to analyze the genes expressed in avocado fruit, R. López-Gómez et al. [21] prepared an EST library from the pulp of *P. americana* var. *drymifolia* fruit. From this library, one clone was identified and further characterization showed that it contains a cDNA with homology to plant AMPs, which was designated defensin PaDef (Accession GenBank KC007441). Sequence analysis of this clone revealed that it has a cDNA of 249 bp and one putative open reading frame (ORF) with a protein coding capacity of 78 amino acids (5.2 kDa). A bioinformatic analysis showed that the amino acid sequence of the ORF has homology (>80%) with plant defensins. This putative protein contains a characteristic signal peptide of 31 aa, which when removed produces a mature peptide of 47 aa. Also, an alignment with defensin holotype type 1 (*R. sativus* Rs-AFP1) and type 2 (*N. alata* NaD1) allowed us to classify it as type 1 defensin (Figure 1(a)). A comparative study with plant defensins showed that this ORF contains the conserved 8 cysteines, which could form the 4 disulfide bridges characteristic of these AMPs (Figure 1(b)). Also, the structure contains the CS$\alpha\beta$ and γ-core motifs present in these defensins (Figure 1(c)). From these analysis it was established that the ORF identified in the clone PaDef encodes a defensin from avocado.

3.2. Expression of Avocado Defensin PaDef in BVE-E6E7 Cells. To express defensin *PaDef* from avocado in BVE-E6E7 cells, we used the pBME3 construction (Figure 2(a)). This construction was introduced into BVE-E6E7 cells by lipofection. The human elongation factor 1-α (EF1-α) promoter directs the expression of defensin PaDefcDNA in BVE-E6E7, while

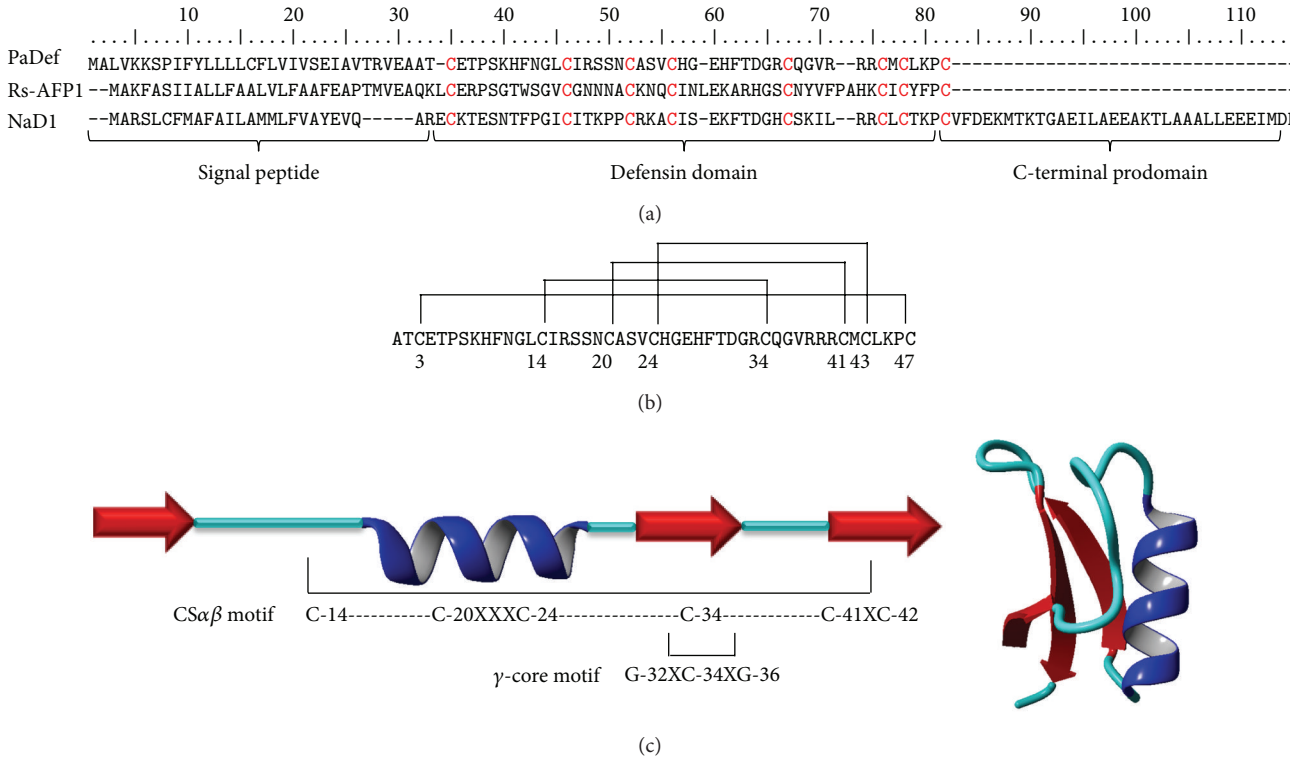

Figure 1: Characteristics of defensin PaDef from *Persea americana* var. *drymifolia*. (a) Alignment of the defensin PaDef with defensin holotype type 1 (*R. sativus* Rs-AFP1) and defensin holotype type 2 (*N. alata* NaD1). In red, the 8 conserved cysteines are indicated. (b) Prediction of disulfide bridges of defensin PaDef. The pattern was determined using the DISULFIND predictor. (c) Structural organization of defensin PaDef peptide. Left: secondary structure showing the characteristic CS$\alpha\beta$ motif of defensins. Red arrows indicate the β-sheets. Right: homology model of defensin PaDef peptide. Model was created using Rs-AFP1 (Protein Data Bank: 1AYJ) as template.

the human cytomegalovirus promoter (CMV) directs the expression of the selection marker (GFP-zeocin resistance gene fusion). Initially, we obtained a polyclonal population of BVE-E6E7 cells transfected with pBME3 construction (BVE3-PC) (Figure 2(b)). Further, with the aim to obtain homogeneous BVE-E6E7 cells transfected with pBME3, a total of 9 clones were selected from the polyclonal population using limiting dilution (BVE3-C1 to C9 clones) (Figure 2(b)). *PaDef* mRNA expression was demonstrated by RT-PCR analysis. An amplicon of ~250 bp corresponding to defensin *PaDef* was observed in polyclonal population of BVE-E6E7 cells transfected with pBME3 and the clones selected (Figures 3(a) and 3(b)), this amplicon was also obtained in the positive control (Figure 3(a), pBME3). Specific amplification was confirmed by sequencing the PCR products and by the absence of amplification in the negative control (Figure 3(a), BVpT). Also, defensin *PaDef* mRNA expression analysis of the clones showed that these have similar expression levels (Figure 3(b)). In addition, the expression of PaDef was analyzed in clone BVE3-C1 by flow cytometry using the antibody anti-V5 epitope (Figure 4). This clone showed higher relative fluorescence intensity compared to control cells, indicating that the protein of defensin PaDef is expressed in these cells (Figure 4(b)).

Further, CM from polyclonal and clonal populations were obtained as described in materials and methods and were used to assess if it have any effect on viability of BVE-E6E7 cells, which was evaluated by trypan blue exclusion technique. Results showed that none of the treatments significantly decreased cell viability (data not shown).

3.3. Antimicrobial Activity of CM from BVE-E6E7 Cells That Express Defensin PaDef from Avocado. CM from polyclonal and clonal populations were used to evaluate their antibacterial activity against *S. aureus* ATCC 27543 and *E. coli* 0111 strains. The defensin *PaDef* cDNA used to transfect BVE-E6E7 cells encodes for a signal peptide of 31 aa located at the N-terminal of the mature peptide, suggesting that defensin PaDef might be secreted to culture medium. Bacteria cells were incubated with several concentrations of total protein from CM, and their viability was estimated by MTT assay. According to previous works, we evaluated diverse concentrations of total protein of CM, ranging from 10 to 100 μg/mL. Results showed that *E. coli* viability was inhibited when bacteria were challenged with 100 μg/mL of total protein of CM from the different clones (>55%). This effect was similar for all the clones evaluated (Table 1). These values were higher than the effect showed by CM from polyclonal population (~20%). In the rest of the conditions tested we did not detect significant differences.

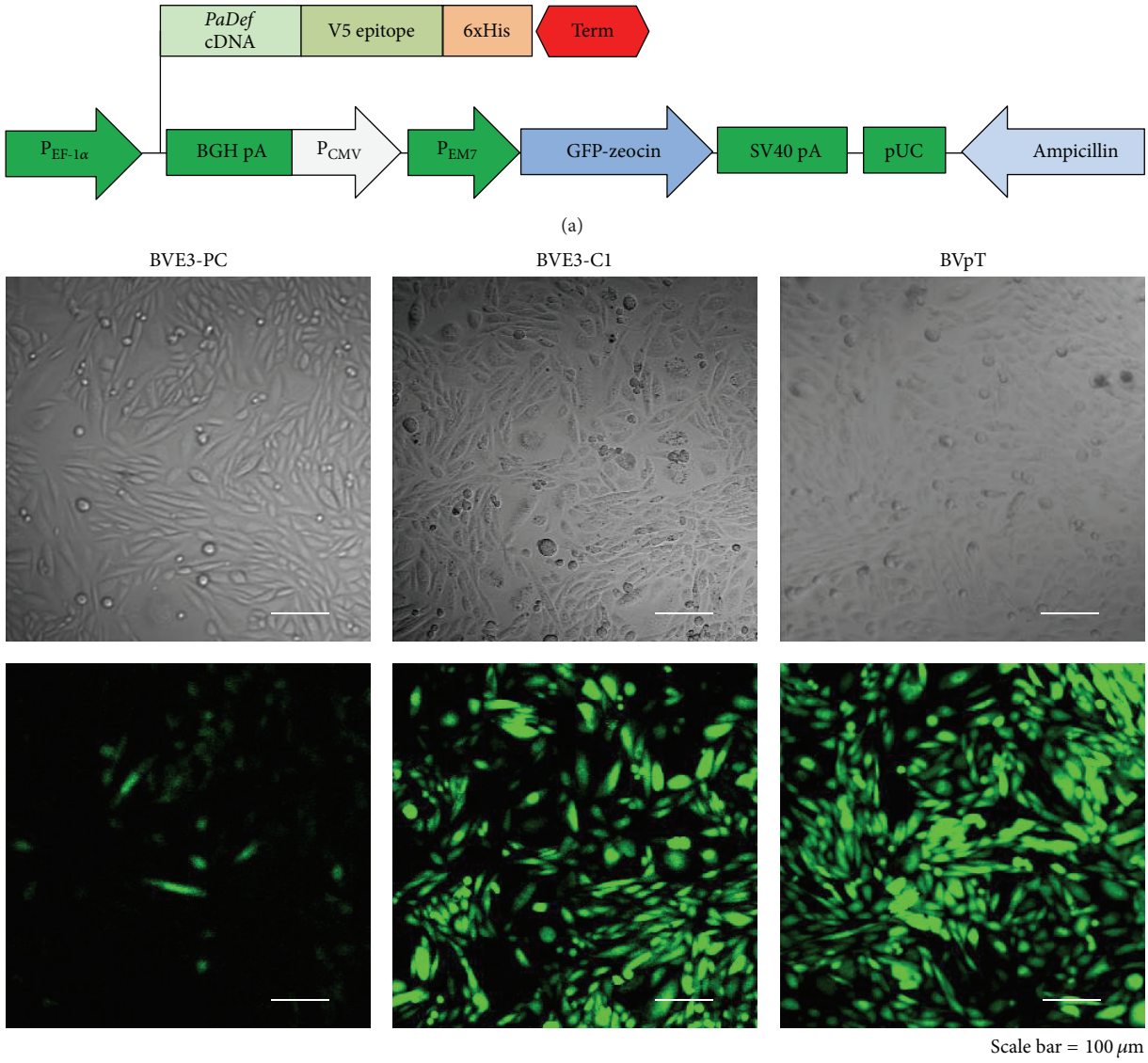

Figure 2: Transfection of BVE-E6E7 endothelial cells with pBME3 construction. (a) The pBME3 construction contains the EF1-α promoter, defensin *PaDef* cDNA, CMV promoter, EM7 promoter, GFP-zeocin resistance gene, and SV40 polyadenylation sequence. (b) Polyclonal, population (BVE3-PC) and representative cloned population (BVE3-C1) of BVE-E6E7 cells transfected with pBME3 visualized under light microscopy (upper) and fluorescence (below). Also, the control cells are showed (BVpT). Scale bar: 100 μm.

Regarding the effects on *S. aureus* viability, we observed an inhibition of viability from 50 μg/mL total protein (27–38%) when bacteria were treated with CM from clones (Table 1). This effect was more evident at 100 μg/mL of total protein; in this case the bacterial viability was inhibited at 52–65%. Similarly the effect showed for *E. coli*, CM from polyclonal population only inhibited the 23% of *S. aureus* viability at 100 μg/mL of total protein. Similar results of antibacterial activity were obtained when we compared the effect of CM from BVE-E6E7 cells expressing defensin PaDef against CM from BVE-E6E7 nontransfected (Table 1) or CM from BVE-E6E7 transfected with BVpT (data not shown). On the other hand, we did not detect antifungal activity against *C. albicans*. These results have shown that CM from BVE-E6E7 cells expressing defensin PaDef from avocado have antibacterial activity against human and animal pathogens.

4. Discussion

In this study we assessed the antimicrobial activity of defensin PaDef from *P. americana* var. *drymifolia* fruit expressed in bovine endothelial cells. In previous works, we have shown that the bovine endothelial cell line BVE-E6E7 is a valuable expression system to evaluate the antimicrobial activities of plant AMPs [15, 23]. Avocado is a worldwide important crop;

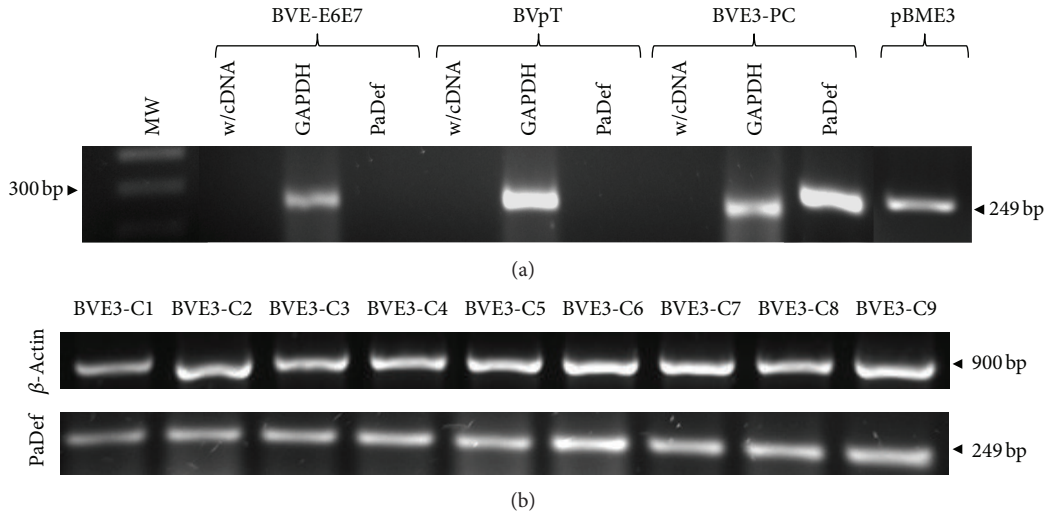

Figure 3: mRNA expression of defensin PaDef of avocado in BVE-E6E7 endothelial cells. (a) RT-PCR analysis that shows the amplification of defensin *PaDef* in polyclonal population of BVE-E6E7 cells transfected (BVE-PC). The lack of defensin *PaDef* amplification is shown in nontransfected BVE-E6E7 cells (BVE-E6E7) or only transfected with the vector (BVpT). Also, the positive control is included (pBME3). The 1 kb molecular weight marker (Invitrogen) was also included (MW). (b) RT-PCR analysis that shows the amplification of defensin *PaDef* in different endothelial cell clones.

Table 1: Antibacterial effect of CM from BVE-E6E7 cells that express defensin PaDef from *Persea americana* var. *drymifolia*[a].

Clones	Inhibition (%)[b]							
	E. coli[c]				*S. aureus*[c]			
	CM (total protein, μg)				CM (total protein, μg)			
	10	25	50	100	10	25	50	100
BVE3-PC	5.69	14.06	1.2	20.4	11.06	10.29	24.69	23.57
BVE3-C1	8.82	1.02	11.49	73.67*	4.75	4.33	38.87*	64.26*
BVE3-C2	10.37	9.74	10.51	69.64*	17.13	12.83	33.96*	63.73*
BVE3-C3	12.99	0.87	6.78	75.79*	11.64	14.35	30.86*	67.43*
BVE3-C4	23.56	15.44	14.91	65.37*	20.27	15.37	33.23*	54.59*
BVE3-C5	21.81	15.89	11.81	75.71*	13.77	6.14	30.25*	64.95*
BVE3-C6	20.26	16	7.73	78.08*	12.53	10.52	31.29*	63.86*
BVE3-C7	13.8	13.11	20.87	79.5*	11.97	3.87	31.07*	59.67*
BVE3-C8	22.15	13.4	9.56	70.88*	15.93	10.71	32.62*	58.41*
BVE3-C9	16.29	14.56	9.22	55.62*	1.47	14.45	27.02*	52.23*

[a]Bacteria were incubated during 4 h at 37°C with CM.
[b]Percentage of inhibition considering the effect of CM from BVE-E6E7 cells as 100% for each strain.
[c]Data represent the mean value ± SE of three independent experiments.
*Significant changes ($P < 0.05$) compared to CM from BVE-E6E7 cells.

in addition to its use as food, it is utilized in traditional medicine due to its curative properties [26]. Several avocado metabolites (essentially from secondary metabolism) are known to have antibacterial, antifungal, and insecticidal activity; however, very little is known about AMPs from this plant [4, 26–28].

Plant defensins have been isolated from many species and represent an alternative to agricultural biotechnology and therapeutic drug design [13]. In this work, we obtained the avocado *PaDef* cDNA from fruit. Alignment analysis of this cDNA in the NCBI database revealed a high homology (>80%) with plant AMP. Analysis of deduced amino acid sequences shows that the peptide encoding a protein (78 aa) shared the common structure of defensins, including a signal peptide of 31 aa (Figure 1). Most plant defensins are expressed as a prepeptide with N-terminal region containing a signal peptide for extracellular secretion [29]. Alignment analysis of the mature region (47 aa) showed that the defensin PaDef peptide contains 8 cysteines, which could form 4 disulfide bridges (Figure 1) and shares high similarity at deduced amino acid level with type I defensins [13]. The three-dimensional structure of plant defensins presents a CS$\alpha\beta$ motif consisting of a triple stranded, anti-parallel beta-sheet, and one alpha-helix following a $\beta\alpha\beta\beta$ pattern, which is

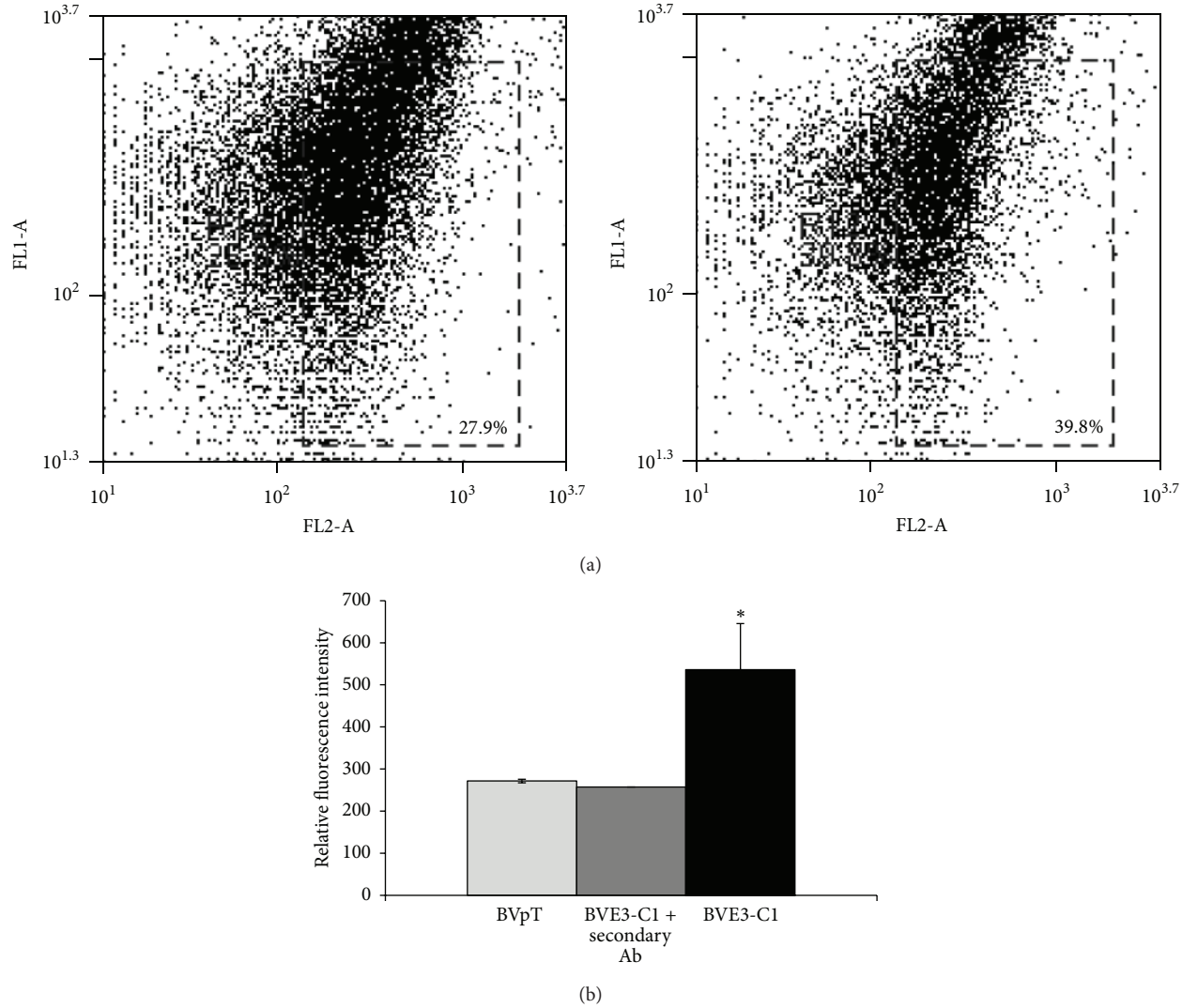

Figure 4: Defensin PaDef expression in BVE-E6E7 endothelial cells analyzed by flow cytometry. (a) Left: scatter plot of clonal population of BVE-E6E7 cells transfected with BVpT (control cells). Right: scatter plot of clonal population of BVE-E6E7 cells that express the defensin PaDef (BVE3-C1). The values inside rectangle indicate the percentage of cells that displayed fluorescence intensity higher than 2000 relative units. (b) Relative fluorescence intensity of BVE-E6E7 control cells (BVpT) and BVE-E6E7 cells that express the defensin PaDef (BVE3-C1). Fluorescence intensity was estimated from 5500 events. A control of BVE-E6E7 cells that express the defensin PaDef (BVE3-C1) only treated with the secondary antibody was included (BVE3-C1 + secondary Ab). Values of relative fluorescence intensity were obtained subtracting the fluorescence intensity corresponding to GFP expression. *Significant changes ($P < 0.05$) compared to BVE-E6E7 control cells.

stabilized by disulfide bridges [29]. This motif was also identified in defensin PaDef from avocado (Figure 1(c)). Also, defensin PaDef contains the γ-core motif, which is important to structure stabilization and has been associated with antifungal activity [30]. To our knowledge, this is the first report that shows the identification of a defensin in avocado fruit.

The defensin *PaDef* cDNA used to transfect BVE-E6E7 cells encodes for a signal peptide of 31 aa located at the N-terminal of the mature peptide suggesting that defensin PaDef might be secreted by cells to culture medium. The expression of this cDNA in polyclonal and clonal populations was demonstrated by mRNA analysis and corroborated by sequencing (Figure 3). Also, defensin PaDef protein expression was corroborated by flow cytometry (Figure 4). We tested the antibacterial activity of the CM from all clones by the MTT assay (Table 1). In general, we did not detect significant differences in antibacterial activity between the clones, which is directly related to the fact that mRNA expression is also homogeneous in clones. In respect to the effect of CM against *E. coli*, we showed that the CM from clones had a clear inhibitory effect at 100 μg/mL of total protein. On the other hand, the antibacterial activity against *S. aureus* was concentration-dependent. We attribute these differential effects to the differences in the structure of the membrane and cell walls of these organisms.

It has been established that the main activity of plant defensins is antifungal [12]. Interestingly, we did not detect antifungal activity against *C. albicans*. In agreement, Segura et al. [31] report that several defensins of spinach (So-D1, 2, 6, and 7) exhibit antibacterial activity but not fungicide activity, evaluated against *Fusarium culmorum* and *F. solani*. However, further studies are needed to evaluate a wider group of fungi, including avocado fungal pathogens in order to establish the antifungal activity of avocado defensin.

5. Conclusion

The present data is the first report that shows antimicrobial activity of a defensin produced by avocado fruit. Overall, the results of this study suggest that defensin PaDef from avocado is an AMP that could be used in the treatment of infectious diseases.

Conflict of Interests

The authors declare that there is no conflict of interests regarding the publication of this paper.

Acknowledgments

J. J. Guzmán-Rodríguez was supported by a scholarship from CONACyT (239238). This work was supported by grants from Coordinación de la Investigación Científica-UMSNH to J. E. López-Meza (CIC 14.5) and R. López-Gómez (CIC 2.2). The authors thank Luis Herrera-Estrella for sequencing support (LANGEBIO, CINVESTAV U. Guanajuato).

References

[1] O. E. Heuer, A. M. Hammerum, P. Collignon, and H. C. Wegener, "Human health hazard from antimicrobial-resistant enterococci in animals and food," *Clinical Infectious Diseases*, vol. 43, no. 7, pp. 911–916, 2006.

[2] D. Field, L. Quigley, P. M. O'Connor et al., "Studies with bioengineered Nisin peptides highlight the broad-spectrum potency of Nisin V," *Microbial Biotechnology*, vol. 3, no. 4, pp. 473–486, 2010.

[3] K. Papadopoulou, R. E. Melton, M. Leggett, M. J. Daniels, and A. E. Osbourn, "Compromised disease resistance in saponin-deficient plants," *Proceedings of the National Academy of Sciences of the United States of America*, vol. 96, no. 22, pp. 12923–12928, 1999.

[4] I. Néeman, A. Lifshitz, and Y. Kashman, "New antibacterial agent isolated from the avocado pear," *Applied microbiology*, vol. 19, no. 3, pp. 470–473, 1970.

[5] D. Prusky, N. T. Keen, J. J. Sims, and S. L. Midland, "Possible involvement of an antifungal diene in the latency of *Colletotrichum gloeosporioides* on unripe avocado fruits," *Phytopathology*, vol. 72, no. 12, pp. 1578–1582, 1982.

[6] D. Prusky and N. T. Keen, "Involvement of preformed antifungal compounds in the resistance of subtropical fruits to fungal decay," *Plant Disease*, vol. 77, no. 2, pp. 114–119, 1993.

[7] F. Domergue, G. L. Helms, D. Prusky, and J. Browse, "Antifungal compounds from idioblast cells isolated from avocado fruits," *Phytochemistry*, vol. 54, no. 2, pp. 183–189, 2000.

[8] M. D. Wigg, A. A. Al-Jabri, S. S. Costa, E. Race, B. Bodo, and U. S. Oxford, "*In vitro* virucidal and virustatic anti HIV-1 effects of extracts from *Persea americana* Mill. (avocado) leaves," *Antiviral Chemistry and Chemotherapy*, vol. 7, no. 4, pp. 179–183, 1996.

[9] A. P. de Almeida, M. M. Miranda, I. C. Simoni, M. D. Wigg, M. H. C. Lagrota, and S. S. Costa, "Flavonol monoglycosides isolated from the antiviral fractions of *Persea americana* (Lauraceae) leaf infusión," *Phytotherapy Research*, vol. 12, no. 8, pp. 562–567, 1998.

[10] J. D. L. Sánchez-Pérez, M. G. Jaimes-Lara, R. Salgado-Garciglia, and J. E. López-Meza, "Root extracts from Mexican avocado (*Persea americana* var. *drymifolia*) inhibit the mycelial growth of the oomycete *Phytophthora cinnamomi*," *European Journal of Plant Pathology*, vol. 124, no. 4, pp. 595–601, 2009.

[11] J. E. López-Meza, A. Ochoa-Zarzosa, J. A. Aguilar, and P. D. Loeza-Lara, "Antimicrobial peptides: diversity and perspectives for their biomedical application, biomedical engineering, trends, research and technologies," in *Biomedical Engineering, Trends, Research and Technologies*, M. A. Komorowska and S. Olsztynska-Janus, Eds., pp. 275–304, Intech, Rijeka, Croatia, 2011.

[12] B. P. H. J. Thomma, B. P. A. Cammue, and K. Thevissen, "Plant defensins," *Planta*, vol. 216, no. 2, pp. 193–202, 2002.

[13] F. T. Lay and M. A. Anderson, "Defensins—components of the innate immune system in plants," *Current Protein and Peptide Science*, vol. 6, no. 1, pp. 85–101, 2005.

[14] F. García-Olmedo, P. Rodríguez, A. Molina et al., "Antibiotic activities of peptides, hydrogen peroxide and peroxynitrite in plant defence," *FEBS Letters*, vol. 498, no. 2-3, pp. 219–222, 2001.

[15] J. L. Anaya-López, J. E. López-Meza, V. M. Baizabal-Aguirre, H. Cano-Camacho, and A. Ochoa-Zarzosa, "Fungicidal and cytotoxic activity of a *Capsicum chinense* defensin expressed by endothelial cells," *Biotechnology Letters*, vol. 28, no. 14, pp. 1101–1108, 2006.

[16] H. Loeza-Ángeles, E. Sagrero-Cisneros, L. Lara-Zárate, E. Villagómez-Gómez, J. E. López-Meza, and A. Ochoa-Zarzosa, "Thionin Thi2.1 from *Arabidopsis thaliana* expressed in endothelial cells shows antibacterial, antifungal and cytotoxic activity," *Biotechnology Letters*, vol. 30, no. 10, pp. 1713–1719, 2008.

[17] M. Cajero-Juárez, B. Avila, A. Ochoa et al., "Immortalization of bovine umbilical vein endothelial cells: amodel for the study of vascular endothelium," *European Journal of Cell Biology*, vol. 81, no. 1, pp. 1–8, 2002.

[18] R. López-Gómez and M. A. Gómez-Lim, "A method for extracting intact RNA from fruits rich in polysaccharides using ripe mango mesocarp," *HortScience*, vol. 27, no. 5, pp. 440–442, 1992.

[19] B. Ewing and P. Green, "Base-calling of automated sequencer traces using phred. II. Error probabilities," *Genome Research*, vol. 8, no. 3, pp. 186–194, 1998.

[20] S. Li and H.-H. Chou, "Lucy2: an interactive DNA sequence quality trimming and vector removal tool," *Bioinformatics*, vol. 20, no. 16, pp. 2865–2866, 2004.

[21] R. López-Gómez, L. E. Ibarra, R. L. M. Suárez et al., "First insights into the avocado fruit transcriptome," in *Proceedings of the 28th International Horticultural Science Congress*, Lisboa, Portugal, August 2010.

[22] M. A. Larkin, G. Blackshields, N. P. Brown et al., "Clustal W and Clustal X version 2.0," *Bioinformatics*, vol. 23, no. 21, pp. 2947–2948, 2007.

[23] A. Ochoa-Zarzosa, H. Loeza-Ángeles, E. Sagrero-Cisneros, E. Villagómez-Gómez, L. Lara-Zárate, and J. E. López-Meza, "Antibacterial activity of thionin Thi2.1 from *Arabidopsis thaliana* expressed by bovine endothelial cells against *Staphylococcus aureus* isolates from bovine mastitis," *Veterinary Microbiology*, vol. 127, no. 3-4, pp. 425–430, 2008.

[24] N. Alva-Murillo, A. Ochoa-Zarzosa, and J. E. López-Meza, "Short chain fatty acids (propionic and hexanoic) decrease *Staphylococcus aureus* internalization into bovine mammary epithelial cells and modulate antimicrobial peptide expression," *Veterinary Microbiology*, vol. 155, no. 2–4, pp. 324–331, 2012.

[25] B. Jahn, E. Martin, A. Stueben, and S. Bhakdi, "Susceptibility testing of *Candida albicans* and *Aspergillus* species by a simple microtiter menadione-augmented 3-(4,5-dimethyl-2-thiazolyl)-2,5- diphenyl-2H-tetrazolium bromide assay," *Journal of Clinical Microbiology*, vol. 33, no. 3, pp. 661–667, 1995.

[26] M. Yasir, S. Das, and M. Kharya, "The phytochemical and pharmacological profile of *Persea americana* Mill," *Pharmacognosy Reviews*, vol. 4, no. 7, pp. 77–84, 2010.

[27] J. R. King and R. J. Knight, "Occurrence and assay of estragole in the leaves of various avocado cultivars," *Journal of Agricultural and Food Chemistry*, vol. 35, no. 5, pp. 842–844, 1987.

[28] C. Rodríguez-Saona and J. T. Trumble, "Secretory avocado idioblast oil cells: evidence of their defensive role against a non-adapted insect herbivore," *Entomologia Experimentalis et Applicata*, vol. 94, no. 2, pp. 183–194, 2000.

[29] L. Padovan, M. Scocchi, and A. Tossi, "Structural aspects of plant antimicrobial peptides," *Current Protein and Peptide Science*, vol. 11, no. 3, pp. 210–219, 2010.

[30] U. S. Sagaram, R. Pandurangi, J. Kaur, T. J. Smith, and D. M. Shah, "Structure-activity determinants in antifungal plant defensins msdef1 and mtdef4 with different modes of action against *Fusarium graminearum*," *PLoS ONE*, vol. 6, no. 4, Article ID e18550, 2011.

[31] A. Segura, M. Moreno, A. Molina, and F. García-Olmedo, "Novel defensin subfamily from spinach (*Spinacia oleracea*)," *FEBS Letters*, vol. 435, no. 2-3, pp. 159–162, 1998.

Hindawi Publishing Corporation
BioMed Research International
Volume 2013, Article ID 136492, 9 pages
http://dx.doi.org/10.1155/2013/136492

Research Article

A BCR/ABL-hIL-2 DNA Vaccine Enhances the Immune Responses in BALB/c Mice

Yanan Qin,[1,2] Hongxia Tian,[3] Guanming Wang,[1] Chen Lin,[1] and Yangqiu Li[4,5]

[1] *Department of Microbiology and Immunology, Medical College, Jinan University, Guangzhou 510632, China*
[2] *Department of Otorhinolaryngology Head and Neck Surgery, The Affiliated Hospital of Qingdao University Medical College, Qingdao 266000, China*
[3] *Guangdong Academy of Medical Sciences, Guangdong General Hospital, Guangzhou 510632, China*
[4] *Institute of Hematology, Medical College, Jinan University, Guangzhou 510632, China*
[5] *Key Laboratory for Regenerative Medicine of Ministry of Education, Jinan University, Guangzhou 510632, China*

Correspondence should be addressed to Chen Lin; tlinc@jnu.edu.cn and Yangqiu Li; yangqiuli@hotmail.com

Received 5 September 2012; Accepted 20 May 2013

Academic Editor: Nirmal K. Ganguly

The use of a DNA vaccine encoding the BCR/ABL fusion gene is thought to be a promising approach for patients with chronic myeloid leukemia (CML) to eradicate minimal residual disease after treatment with chemotherapy or targeted therapy. In this study, our strategy employs genetic technology to create a DNA vaccine encoding the BCR/ABL fusion and human interleukin-2 (hIL-2) genes. The successfully constructed plasmids BCR/ABL-pIRES-hIL-2, BCR/ABL-pIRES, and pIRES-hIL-2 were delivered intramuscularly to BALB/c mice at 14-day intervals for three cycles. The transcription and expression of the BCR/ABL and hIL-2 genes were found in the injected muscle tissues. The interferon-γ (IFN-γ) serum levels were increased, and the splenic $CD4^+/CD8^+$ T cell ratio was significantly decreased in the BCR/ABL-pIRES-hIL-2-injected mice. Furthermore, specific antibodies against K562 cells could be detected by indirect immunofluorescence. These results indicate that a DNA vaccine containing BCR/ABL and hIL-2 together may elicit increased in vivo humoral and cellular immune responses in BALB/c mice.

1. Introduction

Chronic myeloid leukemia (CML), with an incidence of 1.5/100,000 people, represents 15% of newly diagnosed leukemia cases in adults in China. The Philadelphia chromosomal translocation t(9;22)(q34;q11) is essential to its pathogenesis and is found in approximately 95% of patients with CML. The result of this translocation is the BCR-ABL fusion protein, which is associated with the increased ABL tyrosine kinase activity that is directly associated with leukemogenesis [1].

Imatinib mesylate (IM), which is an inhibitor of BCR-ABL-coded tyrosine kinase activity, is the first drug widely used to treat CML. The prognosis of CML was markedly improved after the introduction of ABL tyrosine kinase inhibitors (i.e., IM and its derivatives). However, a number of patients with CML die due to ABL mutation-related drug resistance and blast crisis because IM does not kill leukemia stem cells (LSCs), which persist in a majority of patients and may cause disease relapse, and clinical resistance may develop predominantly due to point mutations in the ABL kinase domain [2]. Novel tyrosine kinase inhibitors have been developed to solve the mutation problem [3, 4]; however, their binding specificity and target profiles have not been readily predicted in pathological and normal cells [5, 6].

The success of allogeneic bone marrow transplantation, which is attributed to graft-versus-leukemia (GVL) effects targeting leukemia cells, highlights the importance of immunotherapy in myeloid leukemia [7]. Unfortunately, it is limited by the paucity of suitable donors, and it is followed by relatively high morbidity and mortality [8]. We have come to realize that immunotherapy may result in cure of the disease. Particularly, myeloid leukemia vaccines would presumably be beneficial in eradicating minimal residual disease after treatment with chemotherapy or targeted therapy [9].

Table 1: Sequences of primers used in PCR.

Primers	Sequences	Restriction enzymes
BCR/ABL-forward	5′-ATT*CTCGAG*ATGGGGCTCTATGGGTTTCTG-3′	*XhoI*
BCR/ABL-reverse	5′-GCC*GAATTC*CTAGATGTAGTTGCTTGGGAC-3′	*EcoRI*
IL-2-forward	5′-GGCAC*GTCGAC*ACAATGTACAGGATGCAACTCC-3′	*Sal I*
IL-2-reverse	5′-TAT*GCGGCCGC*TCAAGTCAGTGTTGAGATGATG-3′	*Not I*

Restriction sites within primers are italicized. GenBank accession no. AJ131466 (BCR/ABL) and NM_000586 (hIL-2).

Targeted immunotherapy using leukemia vaccines has been heavily investigated. It has been shown that immunoprotection against BCR-ABL-positive leukemia cells could be induced in preclinical systems after vaccination using peptide-based and dendritic cell-based vaccines and tumor cell lysates [10–12].

In patients with CML, specific immune responses against leukemia cells have also been demonstrated by peptide-based or dendritic cell-based vaccines [13–15]. Many peptide vaccine clinical trials have been performed with limited success. It has become clear that exogenous peptides alone fail to activate effective $CD8^+$ T cell levels, and if induced, they tended to be transient in patients with a weakened or tolerized immune system [16].

DNA vaccines present an attractive alternative strategy to peptide vaccination [17–19]. DNA vaccines are bacterial plasmids constructed to express an encoded protein following in vivo administration and their subsequent uptake by cells. The encoded antigen is processed through endogenous and exogenous pathways, thus leading to peptide presentation via both MHC-I and MHC-II [20].

DNA vaccines also offer the possibility of modifying the plasmid construct to incorporate additional immunostimulatory factors to activate directly selected immune-effector pathways. Cytokine genes as genetic adjuvants are usually added, and they can bias the immune response toward a Th1 or Th2 response. Human interleukin-2 (hIL-2) is one of the immunostimulatory adjuvants used to enhance the immune response to leukemia cells. Recombinant IL-2 can increase the antileukemic activity of donor lymphocytes, and, has been reported to be a potential enhancer of donor lymphocyte infusion (DLI). IL-2 increased the response rate with improved survival in a proportion of patients who relapsed after allo- or autolymphocyte infusions [21, 22]. The hIL-2 gene has been incorporated in many DNA vaccines [23]. Our previous research has shown that DNA vaccines containing the PML-RARα fusion and hIL-2 genes could increase the immunogenicity of vaccines and induce stronger, specific cellular and humoral immune responses in mice compared with the one encoding the tumor antigen alone [24]. In this paper, the BCR/ABL-pIRES-hIL-2 DNA vaccine was constructed to assess its efficacy, and test the possibility that the immune response to vaccine could be enhanced by coexpression of hIL-2.

2. Materials and Methods

2.1. Cell Lines and Animals. The K562 cell line was obtained from the Institute of Hematology, Jinan University College of Medicine, and it was cultured in RPMI-1640 medium (Gibico-BRL, USA) supplemented with 10% fetal bovine serum (Gibico-BRL, USA) at 37°C in a 5% CO_2 atmosphere.

Male BALB/c mice, 6 to 8 weeks of age, were purchased from the Guangdong Provincial Medical Experimental Animal Center (animal certificate no. SCXK2008-0002), and they were bred at the Experimental Animal Center of Jinan University College of Medicine under controlled conditions and received standard laboratory chow and water according to institutional guidelines. Upon delivery, the mice were allowed to acclimatize for one to two weeks before the start of the experiment. The experiments were approved by the local Animal Ethics Committee and followed international ethical standards of conduct.

2.2. DNA Vaccine Preparation. The 487 bp hIL-2 fragment, which contains four exons expressing the hIL-2 core structure, was amplified as previously described [24]. Amplification of the BCR/ABL fusion gene segment was performed in cDNA from K562 cells by RT-PCR. The primers used in the present study were listed in Table 1. The following is the RT-PCR program file used: 30 cycles at 95°C for 4 min, at 94°C for 1 min, at 60°C for 1 min, and at 72°C for 1 min, one cycle at 72°C for 10 min. Briefly, the BCR/ABL segment with was designed to cover the fusion point of BCR and ABL gene corresponding to $p210^{BCR/ABL}$(b3a2), including part of exon 14 from BCR gene and part of exon 3 and exon 2 from ABL gene (GenBank accession numbers AJ131466.1). The $p210^{BCR/ABL}$ junction region selected contained 110 amino acids (GLYGFLNVIV HSATGFKQSS KALQRPVASD FEPQGLSEAA RWNSKENLLA GPSENDPNLF VALYDFVASG DNTLSITKGE KLRVLGYNHN GEWCEAQTKN GQGWVPSNYI), with lysine of the fusion point in the middle, 20 adjacent amino acids (aa) from the C-terminal of the BCR protein fragment, and 90 adjacent aa from the N-terminal of the ABL protein fragment.

The amplified BCR/ABL-pIRES fragment (354 bp) was inserted into the multiple cloning site (MCS) A using *Xho I* and *EcoR I* restriction sites, and the hIL-2 segment was inserted into the MCS B site of the pIRES eukaryotic expression vector (BD Biosciences Clontech, Palo Alto, CA, USA) using *Sal I* and *Not I* restriction sites. The resulting plasmid was named BCR/ABL-pIRES-hIL-2. The plasmid pIRES-hIL-2, which contained only the hIL-2 gene, and the plasmid BCR/ABL-pIRES, which contained only the BCR/ABL gene, were also prepared.

The nucleotide sequence of the insert was verified by sequencing. Plasmids were maintained and propagated in transformed Top10 *Escherichia coli* bacteria (Pubo Biotech,

Beijing, China) in the presence of ampicillin. Large-scale plasmid production was performed using an EndoFree plasmid Giga kit (Pubo Biotech, Beijing, China) according to the protocol of the manufacturer. Plasmid purification was conducted using PureLink (Invitrogen, Paisley, UK) according to the instructions of the manufacturer, and it was assessed by spectrophotometer (OD_{260}/OD_{280}). All samples were tested by the limulus amebocyte lysate assay (Sigma Chemical Co., St. Louis, MO, USA) to ensure that they were free of endotoxin contamination.

2.3. Immunization. Mice were separated into the following administration groups by random allocation. Five mice per group were used: (1) saline control, (2) pIRES, (3) BCR/ABL-pIRES, (4) BCR/ABL-pIRES-hIL-2, and (5) pIRES-hIL-2. One day before immunization, procaine was injected in the injection sites to enhance vaccine absorption. All mice were intramuscularly administered on one side of a hind leg with 200 μg of purified plasmid. At the second and fourth weeks after the first immunization, all mice groups were boosted with the same plasmid dose i.m. The animals were sacrificed 14 days after the final immunization.

2.4. ELISA. Cytokine production was evaluated *in vitro* in serum samples. The IFN-γ and IL-4 sample concentrations were determined by commercial sandwich ELISA kits (Pubo Biotech Co., Ltd., Beijing, China) following the protocol of the manufacturer. The 450 nm optical density was measured with a BIO-RAD model 450 (BIO-RAD, Hercules, CA, USA) ELISA plate reader. A standard curve was created by plotting the mean absorbance of each standard versus the IFN-γ and IL-4 concentrations. The results were expressed in nanograms per milliliter by reading directly from the standard curve.

2.5. Flow Cytometry. Lymphocyte subset analysis ($CD4^+/CD8^+$ ratio) was conducted by flow cytometry (FCM, Epics Elite ESP, Coulter) for dual-color flow cytometric analysis. Cells collected from mice spleens were immunostained with the FITC-conjugated anti-CD4 and PE-conjugated anti-CD8 antibodies (Pubo Biotech Co., Ltd., Beijing, China). Briefly, 5 μL of the appropriate monoclonal antibody was incubated with 100 μL of splenic cells (1×10^6/mL) for 15 min in the dark before being resuspended in phosphate buffer saline (pH7.4 PBS) and before being analyzed.

2.6. Indirect Immunofluorescence Assay. For detecting anti-BCR/ABL antibodies in mouse serum, the tests were performed. After spreading k562 cells (1×10^6/mL) onto glass slides as target antigen, the slides were incubated with fresh serum for 30 min followed by three 10 min PBS washes. NB4 cells, a BCR-ABL-negative cell line, used as a control. Then, addition of the FITC (fluorescein isothiocyanate) fluorescent-labeled secondary antibody (Sheep anti-Mouse, Pubo Biotech, Beijing, China), the slides were incubated for 30 min, and visualized using a fluorescence microscope.

2.7. Histology and Immunohistochemical Analysis. Muscle samples from all injection sites were fixed in 10% neutral-buffered formalin, embedded in paraffin, sectioned at 5 μm, and processed with standard deparaffinization, rehydrated, and stained with hematoxylin and eosin (HE). For immunohistochemical (IHC) analysis, muscle sample slices without staining were quenched with 3% H_2O_2, blocked with 10% normal rabbit sera, after probed with rabbit anti-c-ABL polyclonal antibody (Pubo Biotech Co., Ltd., Beijing, China), Detection was done using the SuperPicTure Polymer conjugate rabbit Kits (ZYMED, Carlsbad, CA, USA) and the Stable Liquid Substrate DAB System (Tiangen Biotech, Beijing, China), followed by hematoxylin counterstaining.

2.8. RT-PCR. BCR/ABL and hIL-2 mRNA expression analysis was performed by RT-PCR as previously described [24]. RNA was extracted from the injected muscle tissues with standard procedures using the TRIzol reagent (Invitrogen, USA). The PCR products were analyzed in a 2% agarose gel electrophoresis.

2.9. Statistical Analysis. Numerical data are presented as the mean ± SD. Statistical significance of differences between the study groups was analyzed using one-way analysis of variance (ANOVA). A value of $P < 0.05$ was considered statistically significant.

3. Results

3.1. Construction of DNA Vaccines. The hIL-2 gene fragment was inserted into site B of the pIRES and the BCR/ABL-pIRES vectors to make the plasmids pIRES-hIL-2 and BCR/ABL-pIRES-hIL-2. All constructs were confirmed to be identical to published genomic sequences by sequencing.

3.2. IFN-γ and IL-4 Secretion. The mean units of IFN-γ and IL-4 were detected in the sera of five groups of mice immunized with different DNA constructs as shown in Figure 1. The IFN-γ levels of the different groups were 176.59 ± 9.53 pg/mL (saline), 196.16 ± 9.45 pg/mL (pIRES), 240.61 ± 9.54 pg/mL (BCR/ABL-pIRES), 282.55 ± 11.96 pg/mL (BCR/ABL-pIRES-hIL-2), and 214.64 ± 11.44 pg/mL (pIRES-hIL-2). The IL-4 levels of the different groups were 293.04 ± 44.36 pg/mL (saline), 275.12 ± 45.63 pg/mL (pIRES), 263.47 ± 38.19 pg/mL (BCR/ABL-pIRES), 261.27 ± 57.30 pg/mL (BCR/ABL-pIRES-hIL-2), and 294.35 ± 44.05 pg/mL (pIRES-hIL-2). The plasmids encoding BCR/ABL, hIL-2, and BCR/ABL-pIRES-hIL-2 induced a significant enhancement in IFN-γ secretion compared with the empty plasmid-immunized group ($P < 0.01$). The IFN-γ level of mice immunized with BCR/ABL-pIRES-hIL-2 was higher than that of the BCR/ABL-pIRES and pIRES-hIL-2 groups ($P < 0.05$). However, there was no significant difference in the IL-4 secretion level between the different groups ($P = 0.682$).

3.3. CD4/CD8 T Cell Ratio. To assess the composition of the activated T cell subsets, the cell surface markers CD4 and CD8 were detected by FCM. As shown in Figure 2, the $CD4^+/CD8^+$ T cell ratios of the different groups were 2.69 ± 0.06 (saline), 3.08 ± 0.24 (pIRES), 2.32 ± 0.15 (BCR/ABL-pIRES), 2.11 ± 0.09 (BCR/ABL-pIRES-hIL-2), and 2.37 ± 0.04 (pIRES-hIL-2). The $CD4^+/CD8^+$ T cell ratio was lower in the BCR/ABL-pIRES-hIL-2, pIRES-hIL-2, and BCR/ABL-pIRES

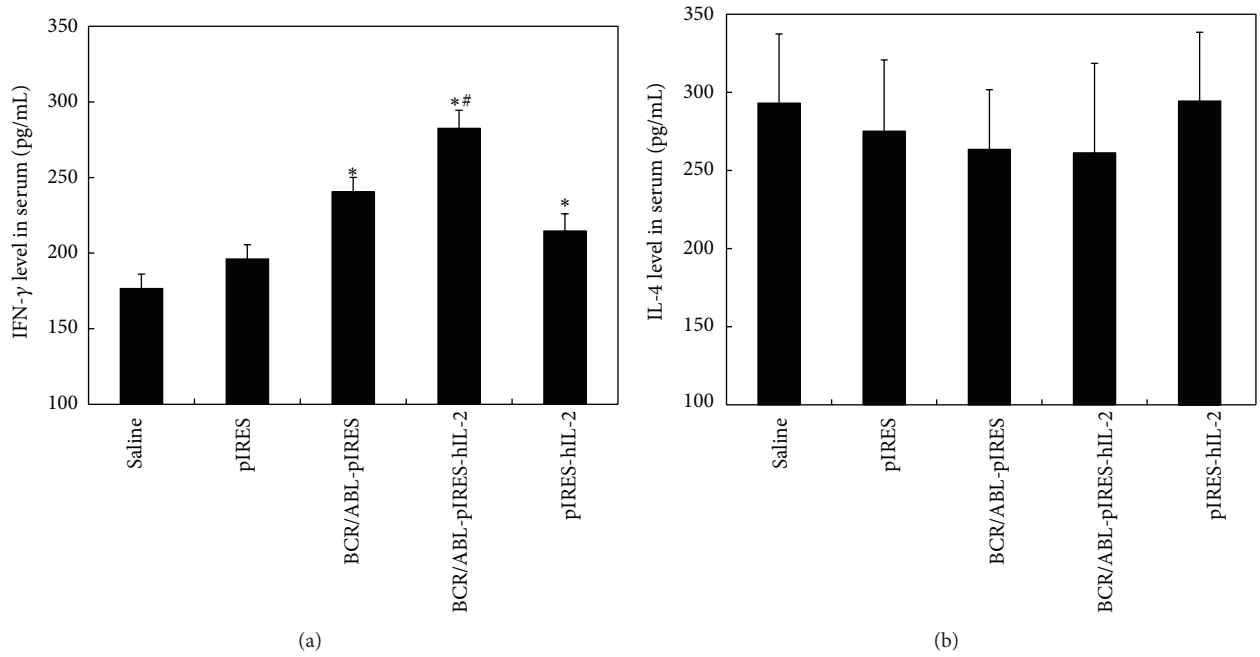

Figure 1: This figure demonstrates the (a) IFN-γ and (b) IL-4 sera secretion results. The mice (n = 5/group) were administered saline, an empty pIRES plasmid, BCR/ABL-pIRES, BCR/ABL-pIRES-hIL-2, and pIRES-hIL-2. The data are shown as mean ± standard deviation. *Compared with the empty plasmid group ($P < 0.01$). #Compared with the BCR/ABL-pIRES group and the pIRES-hIL-2 group ($P < 0.05$). No significant difference in IL-4 secretion was found between the groups.

groups ($P < 0.05$). Additionally, the ratio in mice immunized with BCR/ABL-pIRES-hIL-2 was also lower than those of the BCR/ABL-pIRES and pIRES-hIL-2 groups ($P < 0.05$).

3.4. BCR/ABL Antibody in Sera. Specific antibodies to the BCR/ABL antigen were identified using an indirect immunofluorescence technique. Specific antibodies were only found in the BCR/ABL-pIRES-hIL-2 group (Figure 3). The sera from immunized mice were not reactive with the BCR-ABL-negative NB4 cells. The results showed that BCR/ABL antibody production could be enhanced in mice vaccinated with BCR/ABL-pIRES-hIL-2 plasmid.

3.5. Transcription of DNA Vaccines In Vivo . We detected the mRNA expression of BCR/ABL and hIL-2 genes in mice. The BCR/ABL and hIL-2 mRNA of muscle samples from all injection sites was analyzed using RT-PCR. The results demonstrated that the BCR/ABL and hIL-2 RT-PCR products were the result of mRNA transcribed from the recombinant plasmids in muscle samples. The BCR/ABL gene was expressed in the BCR/ABL-pIRES and BCR/ABL-pIRES-hIL-2 groups (Figure 4).

3.6. Histological Examination of Injection Sites. The inflammatory responses were evaluated in muscle samples from injection sites by the amount of blue (nuclear) staining. The mild-to-moderate infiltrations by inflammatory cells were observed. As shown in Figure 5, mice immunized with the

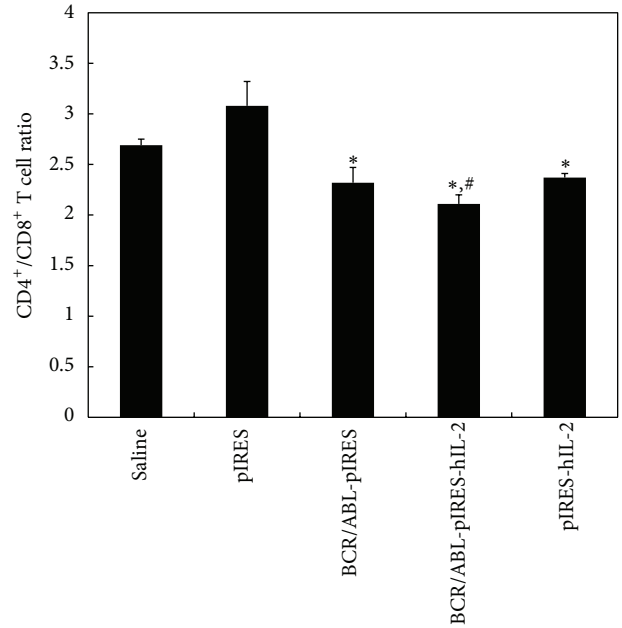

Figure 2: The $CD4^+/CD8^+$ T cell ratio by flow cytometry. The $CD4^+/CD8^+$ T cell ratio was lower in the BCR/ABL-pIRES-hIL-2, pIRES-hIL-2, and BCR/ABL-pIRES groups ($P < 0.05$). Additionally, the ratio of the BCR/ABL-pIRES-hIL-2 group was lower than that of the BCR/ABL-pIRES and pIRES-hIL-2 groups. *Compared with the empty plasmid group ($P < 0.01$). #Compared with the BCR/ABL-pIRES group and the pIRES-hIL-2 group ($P < 0.05$).

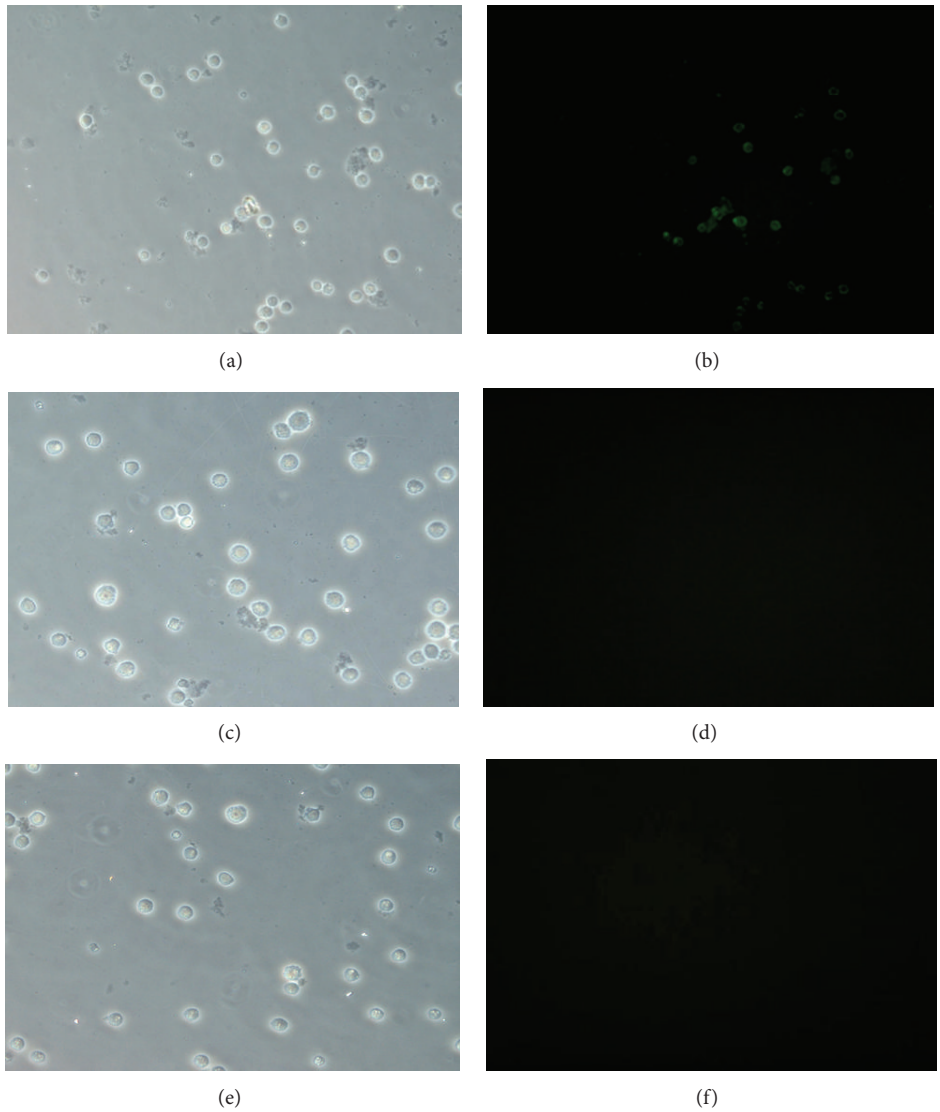

Figure 3: Indirect immunofluorescence of the BCR/ABL antibody in sera. K562 cells were incubated with sera from mice immunized with BCR/ABL-pIRES-hIL-2 (a) and (b), saline (c) and (d), and BCR/ABL-pIRES (e) and (f). Images (a), (c), and (e) were obtained using bright field microscopy, and images (b), (d), and (f) were obtained using fluorescence. The BCR/ABL antibody was shown in Image (b).

BCR/ABL-pIRES-hIL-2 (d) caused moderate cell inflammatory cell infiltration, and those immunized with BCR/ABL-pIRES (c) and pIRES-hIL-2 (e) induced mild cell infiltration. Expression of BCR/ABL was additionally validated by immunohistochemistry. Muscles from immunized mice with the BCR/ABL-pIRES-hIL-2 (g) and BCR/ABL-pIRES (h) showed a predominant staining pattern while the empty plasmid control did not (f).

4. Discussion

DNA-based immunization is an attractive nonviral alternative for cancer immunotherapy. The use of DNA vaccines has demonstrated the feasibility of using DNA vaccines to induce antigen-specific immune responses targeting tumor cells in preclinical and clinical trials [18, 25–27]. After vaccination, plasmid DNA is taken up by host tissue, the encoded antigen epitope binds to MHC class I molecules in the endoplasmic reticulum (ER), and it is presented on the cell surface.

Almost all of the leukemia antigens are intracellular; thus, they are only presented as peptides in the grooves of MHC class I molecules. Only $CD8^+$ T cells, which recognize these peptides, are capable of killing these leukemia cells. Thus, development of DNA vaccines that induce potent $CD8^+$ T cell responses is critical. However, studies in mice have shown that the frequency of antigen-specific CTLs induced by DNA vaccines are approximately ten-fold lower compared to virally induced responses. The responses induced by DNA vaccination differ quantitatively but not qualitatively from those induced by live virus infection [28–30].

Several strategies for increasing the DNA vaccine potency have been developed in the last decade. One of these has focused on the use of various immunostimulatory molecules including cytokines or costimulatory molecules. Although

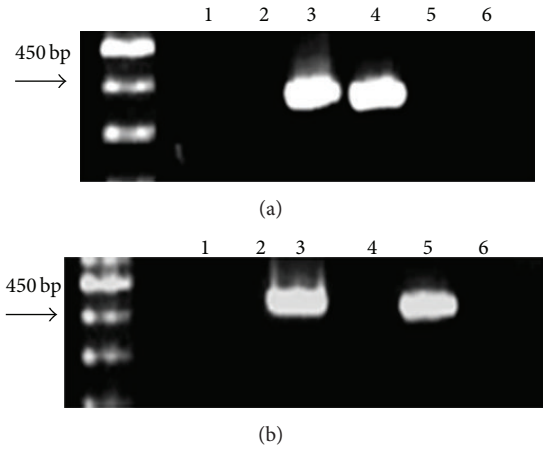

Figure 4: RT-PCR of muscle mRNA from the injection sites. (a) PCR products for the BCR/ABL segment (354 bp); (b) PCR products for the hIL-2 gene (487 bp). Mice were administered with saline (lane 1), the empty plasmid (lane 2), BCR/ABL-pIRES-hIL-2 (lane 3), BCR/ABL-pIRES (lane 4), and pIRES-hIL-2 (lane 5). Control for residual plasmid DNA in the injected muscle (lane 6).

numerous cytokines have been reported to have antitumor effects when administered as single-agent therapy [30–32], several studies have confirmed that the immunogenicity of DNA vaccines can be enhanced by these adjuvants [33, 34]. A panel of cytokines were added as adjuvants following DNA administration, and it was found that rhIL-2, rIL-6, rhIL-7, and rhIL-12 were able to enhance the DNA vaccination-induced therapeutic responses. For example, a plasmid expressing a tumor antigen incorporated in the hIL-2 signal peptide was more effective in protecting mice from tumor challenge [35]. Coexpression of granulocyte-macrophage colony-stimulating factor (GM-CSF) with an antigen in a DNA vaccine has been reported to result in improved immunization [36]. The rationale behind such approaches is based on facilitating T cell priming by providing additional signals through cytokine molecules.

In this study, we chose the hIL-2 gene as an immunostimulatory molecule and cloned the BCR/ABL fusion and hIL-2 genes in the pIRES eukaryotic expression vector based on our previous report [24]. Furthermore, we tested for the presence of BCR/ABL and hIL-2 mRNA by examining the injected muscles of immunized BALB/c mice by RT-PCR and the presence of BCR/ABL expression by IHC. These results show that the plasmid encoding the BCR/ABL fusion and the hIL-2 genes were successfully created.

Cytokine production is one of the principal responses of T cell to antigen recognition. IFN-γ is a homodimeric protein produced by NK, $CD4^+$ Th1, and $CD8^+$ T cells. The functions of IFN-γ are important in cell-mediated immunity by $CD4^+$ Th1, and $CD8^+$ T cells against intracellular antigens. IL-4 is the signature cytokine of the $CD4^+$ Th2 subset and functions as an inducer and effector cytokine in B cells. Therefore, we detected the serum level of IFN-γ and IL-4 by ELISA and the ratio of $CD4^+/CD8^+$ T cells from spleen by FCM in immunized BALB/c mice. The IFN-γ serum level in mice vaccinated with BCR/ABL-pIRES-hIL-2 was significantly higher than that in the BCR/ABL-pIRES or pIRES-hIL-2 groups. This finding is consistent with that of the previous report regarding the use of DNA-based immunizations [18, 24]. The IL-4 serum level was not significantly different among the groups, and the ratio of $CD4^+$-to-$CD8^+$ T cells in mice vaccinated with BCR/ABL-pIRES-hIL-2 was significantly decreased compared to other groups. These results suggest that the BCR/ABL-pIRES-hIL-2 design is capable of inducing a more potent cellular immune response. Neither BCR/ABL nor hIL-2 alone could induce a sufficient immune response. Taken together, it appears that coexpression of the BCR/ABL fusion and hIL-2 genes exerts a synergistic effect, which can be explained by the induced BCR/ABL-specific immune responses and the enhancement in cytokine production levels.

The only BCR/ABL-specific antibodies in BCR/ABL-pIRES-hIL-2 group have been shown by indirect immunofluorescence, which suggests that the low level of BCR/ABL-specific antibodies might be stimulated. BCR-ABL breakpoint epitopes themselves appeared to be weak immunogenes. This is compatible with the previous findings [18, 19]. Possible reason may be related to that the DNA vaccine is processed and presented mainly through MHC class I pathway, which induces the $CD8^+$ T cell response. Hrusková et al. [19] reported that in BALB/c mice VLPs carrying a long fragment covering the fusion zone failed to induce antibodies reactive with that fragment of the BCR-ABL protein. The discrepancy between our data and their data could be explained by that a portion of ABL protein fragment we selected is longer than that reported by Hrusková et al. (90 amino acids to 53 amino acids). The $p210^{BCR/ABL}$ junction region we selected contained 110 amino acids (aa105-aa214), covering lysine 125 of b3a2 breakpoint, and 90 adjacent amino acids from the N-terminal of the ABL protein fragment. Lucansky et al. [18] reported that all of the important epitopes were located in the ABL portion of the $p210^{BCR/ABL}$ protein. Therefore, our results support this conclusion.

Except for $CD8^+$ T cells, CD4 T cell response against b3a2 or b2a2 breakpoint epitopes was also reported in a mouse model and CML patients [15, 37]. In our present study, there was a difficulty to detecting murine cytotoxic T cells, because the recognition of antigens by CTLs in a mouse model is restricted by self class I/II MHC alleles. Further investigation is needed by using humanized NOD/SCID mouse model.

In conclusion, we successfully constructed the BCR/ABL-pIRES-hIL-2 DNA vaccine, which encodes both the BCR-ABL fusion and the human IL-2 genes, and which enhances humoral and cellular immune responses in BALB/c mice in vivo. This approach may provide new perspectives in designing cytokine-adjuvant DNA vaccines for CML clinical applications.

Conflict of Interests

No potential conflict of interests was disclosed.

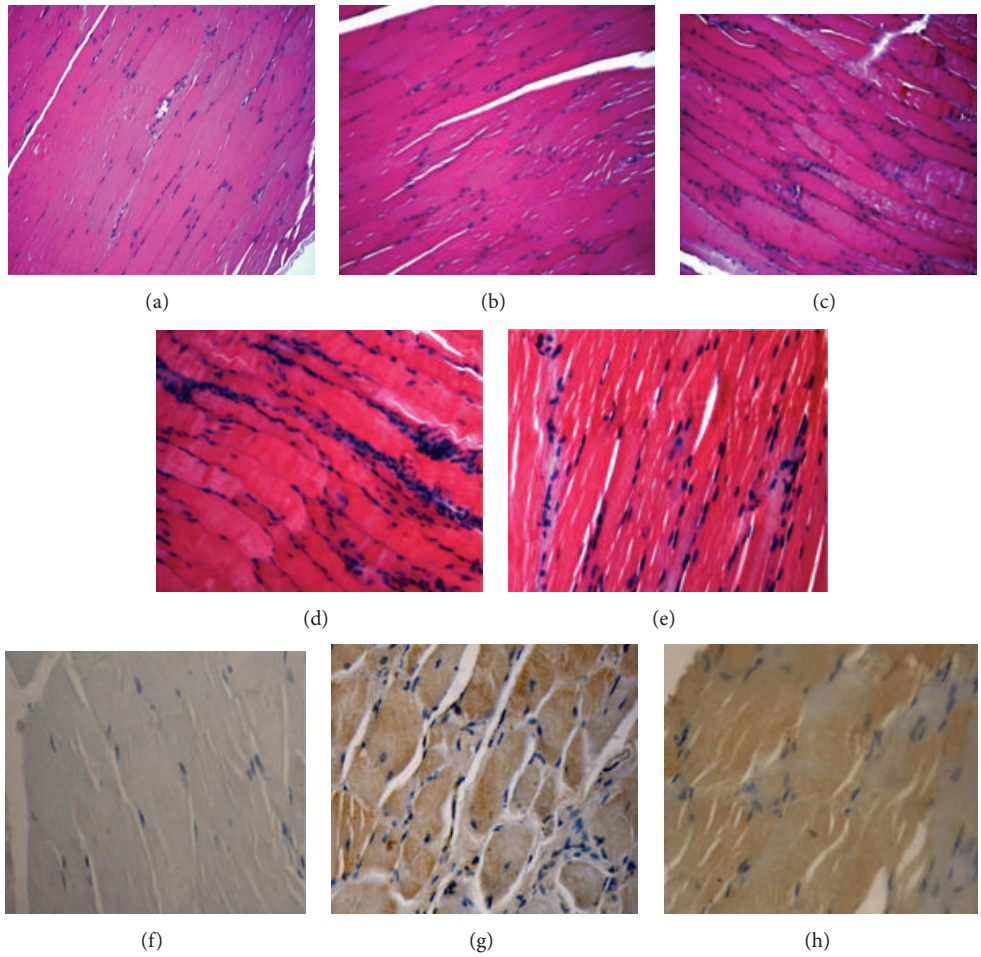

Figure 5: Histological examination of quadriceps muscle at injection sites. Inflammatory cell infiltration was detected by HE stain (10x). Mice were administered with saline (a), empty plasmid (b), BCR/ABL-pIRES (c), BCR/ABL-pIRES-hIL-2 (d), and pIRES-hIL-2 (e). Moderate inflammatory cell infiltration (d), mild inflammation ((c) and (e)). The expressions of BCR/ABL were detected by immunohistochemistry (DAB staining, 10x). Muscle from immunized mice with the BCR/ABL-pIRES-hIL-2 (g) and BCR/ABL-pIRES (h) showed a predominant staining pattern while the empty plasmid did not (f).

Authors' Contribution

Y. Qin, H. Tian, and G. Wang equally contributed to this work. C. Lin and Y. Li contributed with the conception as well as the design and manuscript writing. Y. Qin, H. Tian, and G. Wang provided the study materials and methods besides collecting and assembling the data. Moreover, Y. Qin and C. Lin undertook the data analysis and interpretation. All authors read and approved the final paper.

Acknowledgments

This work was supported by a grant from the Key Project Foundation of the Science and Technology of Guangzhou (2009Z1-E161) and Key Discipline Construction Foundation of Jinan University.

References

[1] M. W. N. Deininger, J. M. Goldman, and J. V. Melo, "The molecular biology of chronic myeloid leukemia," *Blood*, vol. 96, no. 10, pp. 3343–3356, 2000.

[2] D. J. Barnes and J. V. Melo, "Primitive, quiescent and difficult to kill: the role of non-proliferating stem cells in chronic myeloid leukemia," *Cell Cycle*, vol. 5, no. 24, pp. 2862–2866, 2006.

[3] T. Maekawa, E. Ashihara, and S. Kimura, "The Bcr-Abl tyrosine kinase inhibitor imatinib and promising new agents against Philadelphia chromosome-positive leukemias," *International Journal of Clinical Oncology*, vol. 12, no. 5, pp. 327–340, 2007.

[4] E. Weisberg, P. W. Manley, S. W. Cowan-Jacob, A. Hochhaus, and J. D. Griffin, "Second generation inhibitors of BCR-ABL for the treatment of imatinib-resistant chronic myeloid leukaemia," *Nature Reviews Cancer*, vol. 7, no. 5, pp. 345–356, 2007.

[5] S. P. Davies, H. Reddy, M. Caivano, and P. Cohen, "Specificity and mechanism of action of some commonly used protein

kinase inhibitors," *Biochemical Journal*, vol. 351, no. 1, pp. 95–105, 2000.

[6] J. Bain, H. McLauchlan, M. Elliott, and P. Cohen, "The specificities of protein kinase inhibitors: an update," *Biochemical Journal*, vol. 371, no. 1, pp. 199–204, 2003.

[7] A. S. M. Yong, K. Keyvanfar, R. Eniafe et al., "Hematopoietic stem cells and progenitors of chronic myeloid leukemia express leukemia-associated antigens: implications for the graft-versus-leukemia effect and peptide vaccine-based immunotherapy," *Leukemia*, vol. 22, no. 9, pp. 1721–1727, 2008.

[8] R. H. Collins Jr., O. Shpilberg, W. R. Drobyski et al., "Donor leukocyte infusions in 140 patients with relapsed malignancy after allogeneic bone marrow transplantation," *Journal of Clinical Oncology*, vol. 15, no. 2, pp. 433–444, 1997.

[9] P. L. Weiden, N. Flournoy, and E. D. Thomas, "Antileukemic effect of graft-versus-host disease in human recipients of allogeneic-marrow grafts," *The New England Journal of Medicine*, vol. 300, no. 19, pp. 1068–1073, 1979.

[10] L. He, H. Feng, A. Raymond et al., "Dendritic-cell-peptide immunization provides immunoprotection against bcr-abl-positive leukemia in mice," *Cancer Immunology, Immunotherapy*, vol. 50, no. 1, pp. 31–40, 2001.

[11] D. Deeb, X. Gao, H. Jiang, G. Divine, S. A. Dulchavsky, and S. C. Gautam, "Vaccination with leukemia-loaded dendritic cells eradicates residual disease and prevent relapse," *Journal of Experimental Therapeutics and Oncology*, vol. 5, no. 3, pp. 183–193, 2006.

[12] Y. Zeng, H. Feng, M. W. Graner, and E. Katsanis, "Tumor-derived, chaperone-rich cell lysate activates dendritic cells and elicits potent antitumor immunity," *Blood*, vol. 101, no. 11, pp. 4485–4491, 2003.

[13] Y. Osman, M. Takahashi, Z. Zheng et al., "Generation of bcr-abl specific cytotoxic T-lymphocytes by using dendritic cells pulsed with bcr-abl (b3a2) peptide: its applicability for donor leukocyte transfusions in marrow grafted CML patients," *Leukemia*, vol. 13, no. 2, pp. 166–174, 1999.

[14] J. Sun, R. S. Krouse, S. J. Forman et al., "Immunogenicity of a p210BCR-ABL fusion domain candidate DNA vaccine targeted to dendritic cells by a recombinant adeno-associated virus vector in vitro," *Cancer Research*, vol. 62, no. 11, pp. 3175–3183, 2002.

[15] J. Pinilla-Ibarz, K. Cathcart, T. Korontsvit et al., "Vaccination of patients with chronic myelogenous leukemia with bcr-abl oncogene breakpoint fusion peptides generates specific immune responses," *Blood*, vol. 95, no. 5, pp. 1781–1787, 2000.

[16] K. Rezvani, A. S. M. Yong, S. Mielke et al., "Repeated PR1 and WT1 peptide vaccination in montanide-adjuvant fails to induce sustained high-avidity, epitope-specific $CD8^+$ T cells in myeloid malignancies," *Haematologica*, vol. 96, no. 3, pp. 432–440, 2011.

[17] N. Li, Y. Yu, W. Yu, and Z. Sun, "Enhancement of the immunogenicity of DNA replicon vaccine of Clostridium botulinum neurotoxin serotype A by GM-CSF gene adjuvant," *Immunopharmacology and Immunotoxicology*, vol. 33, no. 1, pp. 211–219, 2011.

[18] V. Lucansky, E. Sobotkova, R. Tachezy, M. Duskova, and V. Vonka, "DNA vaccination against bcr-abl-positive cells in mice," *International Journal of Oncology*, vol. 35, no. 4, pp. 941–951, 2009.

[19] V. Hrusková, A. Morávková, K. Babiarová et al., "Bcr-Abl fusion sequences do not induce immune responses in mice when administered in mouse polyomavirus based virus-like particles," *International Journal of Oncology*, vol. 35, no. 6, pp. 1247–1256, 2009.

[20] M. Yu and O. J. Finn, "DNA vaccines for cancer too," *Cancer Immunology, Immunotherapy*, vol. 55, no. 2, pp. 119–130, 2006.

[21] E. Nadal, A. Fowler, E. Kanfer, J. Apperley, J. Goldman, and F. Dazzi, "Adjuvant interleukin-2 therapy for patients refractory to donor lymphocyte infusions," *Experimental Hematology*, vol. 32, no. 2, pp. 218–223, 2004.

[22] A. B. Dietz, M. R. Litzow, P. A. Bulur, and S. Vuk-Pavlović, "Transgenic interleukin 2 secreted by CML dendritic cells stimulates autologous TH1 T cells," *Cytotherapy*, vol. 3, no. 2, pp. 97–105, 2001.

[23] J. R. Greenland and N. L. Letvin, "Chemical adjuvants for plasmid DNA vaccines," *Vaccine*, vol. 25, no. 19, pp. 3731–3741, 2007.

[24] D. Cen, G. Hu, Y. Zhou et al., "Enhancement of specific cellular immune response induced by DNA vaccines encoding PML-RARα and hIL-2 genes," *Hematology*, vol. 15, no. 2, pp. 88–95, 2010.

[25] R. M. Conry, A. F. LoBuglio, F. Loechel et al., "A carcinoembryonic antigen polynucleotide vaccine has in vivo antitumor activity," *Gene Therapy*, vol. 2, no. 1, pp. 59–65, 1995.

[26] A. Roos, M. Pavlenko, J. Charo, L. Egevad, and P. Pisa, "Induction of PSA-specific CTLs and anti-tumor immunity by a genetic prostate cancer vaccine," *Prostate*, vol. 62, no. 3, pp. 217–223, 2005.

[27] J. M. Timmerman, G. Singh, G. Hermanson et al., "Immunogenicity of a plasmid DNA vaccine encoding chimeric idiotype in patients with B-cell lymphoma," *Cancer Research*, vol. 62, no. 20, pp. 5845–5852, 2002.

[28] M. Kwissa, A. Kröger, H. Hauser, J. Reimann, and R. Schirmbeck, "Cytokine-facilitated priming of $CD8^+$ T cell responses by DNA vaccination," *Journal of Molecular Medicine*, vol. 81, no. 2, pp. 91–101, 2003.

[29] D. E. Hassett, M. K. Slifka, J. Zhang, and J. L. Whitton, "Direct ex vivo kinetic and phenotypic analyses of $CD8^+$ T-cell responses induced by DNA immunization," *Journal of Virology*, vol. 74, no. 18, pp. 8286–8291, 2000.

[30] K. L. Komschlies, T. A. Gregorio, M. E. Gruys, T. C. Back, C. R. Faltynek, and R. H. Wiltrout, "Administration of recombinant human IL-7 to mice alters the composition of B-lineage cells and T cell subsets, enhances T cell function, and induces regression of established metastases," *Journal of Immunology*, vol. 152, no. 12, pp. 5776–5784, 1994.

[31] J. J. Mule, M. C. Custer, W. D. Travis, and S. A. Rosenberg, "Cellular mechanisms of the antitumor activity of recombinant IL-6 in mice," *Journal of Immunology*, vol. 148, no. 8, pp. 2622–2629, 1992.

[32] M. J. Brunda, L. Luistro, R. R. Warrier et al., "Antitumor and antimetastatic activity of interleukin 12 against murine tumors," *Journal of Experimental Medicine*, vol. 178, no. 4, pp. 1223–1230, 1993.

[33] S. Pasquini, Z. Xiang, Y. Wang et al., "Cytokines and costimulatory molecules as genetic adjuvants," *Immunology and Cell Biology*, vol. 75, no. 4, pp. 397–401, 1997.

[34] K. R. Irvine, J. B. Rao, S. A. Rosenberg, and N. P. Restifo, "Cytokine enhancement of DNA immunization leads to effective treatment of established pulmonary metastases," *Journal of Immunology*, vol. 156, no. 1, pp. 238–245, 1996.

[35] X. He, T. C. Tsang, T. Zhang, P. Luo, and D. T. Harris, "Antigen epitope-expressing cytokines for DNA immunization," *Vaccine*, vol. 23, no. 16, pp. 1966–1972, 2005.

[36] S. W. L. Seung Woo Lee, J. H. C. Jae Ho Cho, and Y. C. S. Young Chul Sung, "Optimal induction of hepatitis C virus envelope-specific immunity by bicistronic plasmid DNA inoculation with the granulocyte-macrophage colony- stimulating factor gene," *Journal of Virology*, vol. 72, no. 10, pp. 8430–8436, 1998.

[37] W. Chen, D. J. Peace, D. K. Rovira, S.-G. You, and M. A. Cheever, "T-cell immunity to the joining region of p210(BCR-ABL) protein," *Proceedings of the National Academy of Sciences of the United States of America*, vol. 89, no. 4, pp. 1468–1472, 1992.

Hindawi Publishing Corporation
BioMed Research International
Volume 2013, Article ID 230906, 8 pages
http://dx.doi.org/10.1155/2013/230906

Research Article

A Simple Model for Assessment of Anti-Toxin Antibodies

Alex Skvortsov and Peter Gray

HPP Division, Defence Science and Technology Organisation, 506 Lorimer Street, Fishermans Bend, VIC 3207, Australia

Correspondence should be addressed to Alex Skvortsov; alex.skvortsov@dsto.defence.gov.au

Received 21 August 2012; Accepted 20 May 2013

Academic Editor: Nirmal K. Ganguly

The toxins associated with infectious diseases are potential targets for inhibitors which have the potential for prophylactic or therapeutic use. Many antibodies have been generated for this purpose, and the objective of this study was to develop a simple mathematical model that may be used to evaluate the potential protective effect of antibodies. This model was used to evaluate the contributions of antibody affinity and concentration to reducing antibody-receptor complex formation and internalization. The model also enables prediction of the antibody kinetic constants and concentration required to provide a specified degree of protection. We hope that this model, once validated experimentally, will be a useful tool for in vitro selection of potentially protective antibodies for progression to in vivo evaluation.

1. Introduction

Passive immunization using antibodies has been used successfully for treatment and prophylaxis of infectious disease in humans, and there is increasing interest in the use of antibodies for treatment of infectious diseases that may be used as terrorist weapons, but for which the risk is not sufficiently high to justify preventive vaccination of a large civilian population (see [1–4] and references therein). Toxins are an important potential target for designing therapies against these threats and a broad range of approaches have been taken to develop inhibitors that may be of prophylactic or therapeutic use [1, 5].

Antibody engineering techniques allow affinity maturation of antibodies, and these techniques are being exploited to produce inhibitors for a number of toxins [6, 7]. The emphasis of this approach is on producing reagents with high affinity, based on the proposition that higher affinity will provide better protection.

However affinity, by itself, is a poor predictor of protective or therapeutic potential. Antibodies with high in vitro affinity for toxins do not automatically confer protection in vivo [8, 9] and may exacerbate the toxicity [10, 11]. The effects of using multiple antibodies with high affinities may be additive [12] or synergistic [8] or without effect [9]. In addition, epitope specificity [13], antibody titre [14–18], and dissociation rate [19] have been correlated with protection.

Toxins are produced by a number of plants, animals and microorganisms. Toxins may act at the cell surface and either damage the cytoplasmic membrane or bind to a receptor and act via transmembrane signalling subsequent to that binding [20]. Alternatively, toxins may cross the cell membrane and act on intracellular targets [20]. For example, anthrax lethal toxin, ricin and cholera toxin bind to a cell surface receptor and make use of cellular membrane trafficking to enter the cell [21, 22].

The objective of this study is to develop a simple mathematical model that may be used to predict the optimum antibody parameters (kinetic constants and concentration) needed to inhibit the binding of the toxin to its receptor. These predictions may be used to select candidate antibodies for progression to in vivo evaluation and to assess the potential value of affinity enhancement.

This paper is an extension to our previous work [23]. In the model presented in the following we explicitly take into account the process of toxin internalization and diffusive fluxes around the cell.

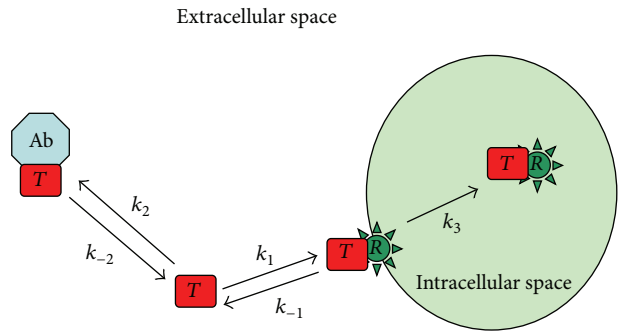

FIGURE 1: Schematic representation of the model for receptor-toxin-antibody interaction.

2. Model

The kinetic model describing the interactions of toxins with cell receptors can be formulated based on the well-known analytical framework for ligand-receptor binding. The models of this process have been studied for many years and a vast amount of literature has accumulated on this subject (see [24–28] and references therein).

When a toxin diffuses in the extracellular environment and binds to the cell surface receptors, the toxin concentration will vary in both space and time. Any rigorous description of this process would entail a system of Partial Differential Equations (PDE), which couples extracellular diffusion with reaction kinetics of the cell surface. The resulting system of PDE is nonlinear and too complex to be treated analytically. This complexity makes any comprehensive study of parameter optimization unfeasible. From another perspective, it is well known that under some rather broad conditions (see [24–28] and references therein) the reaction-diffusion system of the ligand-receptor binding can be well approximated by a system of Ordinary Differential Equations in which the spatial variability of the process is simulated by different concentrations of species in initially predefined spatial domains (called compartments). Although this compartment model is significantly simpler than the initial reaction-diffusion system, it still allows a consistent description of reaction-diffusion transport in underlying system [25, 26, 28]. In the current paper we use the compartment-model approach for our analytical study and numerical simulations.

To begin, we consider the following simple model. The toxin, T, binds reversibly to cell surface receptors, R, with a forward rate k_1 and a reverse rate k_{-1} to form the toxin-receptor complex C_R which is then slowly internalized at a rate k_3. The neutralizing antibody binds competitively to the toxin with on and off rates of k_2 and k_{-2}, respectively. The antibody-toxin complex, C_A, remains in the extracellular space (see Figure 1).

We can easily write an equation for the toxin-receptor binding (namely, without antibody being present). For a spherical cell of radius a with the toxin binding to its surface [24–28],

$$\frac{dC_R}{dt} = k_f^e RT + k_r^e C_R, \tag{1}$$

where C_R is the concentration of the bound receptors (toxin-receptor complexes), R is the concentration of receptors, and T is the bulk toxin concentration (i.e., far from the cell surface) and is assumed to be spatially uniform. The effective forward and reverse rate coefficients are defined by [24–28]

$$k_f^e = \gamma k_1, \qquad k_r^e = \gamma k_{-1}, \tag{2}$$

where k_1, k_{-1} are intrinsic reaction rates, $k_D = 4\pi a D$ is the diffusion rate, D is the diffusivity of toxin in the extracellular space, and $\gamma = 1/(1 + Rk_1/k_D) \leq 1$ [25–27].

The bulk concentration of toxin T is mainly driven by the binding to antibody. Therefore, in this case we can write an equation system similar to (1) but without any "diffusive" modification of the intrinsic rate constants:

$$\frac{dC_A}{dt} = k_2 AT + k_{-2} C_A, \tag{3}$$

where C_A is the concentration of toxin-antibody complexes and A is the concentration of antibody.

The process of toxin internalization is phenomenologically introduced into our model by the following equation:

$$\frac{dT_i}{dt} = k_3 C_R, \tag{4}$$

where T_i is the concentration of internalized toxin. The corresponding term should be included in (1), so we arrive at modified expression for k_r^e

$$k_r^e = \gamma k_{-1} - k_3. \tag{5}$$

The systems (1), (3), and (4) should be supplemented with three conservation laws for concentrations of R, T, and A:

$$R_0 = R + C_R, \tag{6}$$

$$A_0 = A + C_A, \tag{7}$$

$$T_0 = T + C_T + C_A + T_i, \tag{8}$$

where R_0, T_0, and A_0 are the initial concentrations.

Equations (1), (3), (4), and (6)–(8) form a framework for our analysis. This is a system of nonlinear ODE (because of conservation laws (6)–(8) and because effective rates k_f^e, k_r^e are functions of the receptor concentration). It can be easily solved numerically and also allows some analytical progress (see the following). If parameter $\gamma \ll 1$ (and this is the case in many practical situations), then this model can be reduced to the "well-mixed" kinetic model with constant kinetic rates [23].

It is worth emphasizing that the aim of our analytical framework is to develop a simple but scientifically rigorous model that may be used to predict the optimum antibody kinetic properties and concentration required to achieve

Table 1: Kinetic constants used in numerical simulations (the binding of ricin to its receptor and the monoclonal antibody 2B11).

Reaction	Value
k_1	$1.3 \cdot 10^5\ \mathrm{M^{-1}s^{-1}}$
k_{-1}	$1.4 \cdot 10^{-2}\ \mathrm{s^{-1}}$
k_2	$1.25 \cdot 10^5\ \mathrm{M^{-1}s^{-1}}$
k_{-2}	$5.2 \cdot 10^{-4}\ \mathrm{s^{-1}}$
k_3	$3.3 \cdot 10^{-5}\ \mathrm{s^{-1}}$

a desired protective effect rather than develop a detailed, biologically accurate model that captures all the details of the toxin internalization process. Therefore, the model does not take into account the pharmacokinetics of the toxin-antibody complex [11] or receptor internalization and recycling [29, 30]. k_3 is a lumped constant that describes all the processes that result in the appearance of the free toxin in the intracellular space [31]. Wiley and Cunningham [32] and Shankaran et al. [33] have also developed mathematical models of this type of process.

We are particularly interested in the behaviour of the model under conditions most likely to reflect the real biological situation, that is, toxin concentration much lower than the concentration of receptors ($T_0/R_0 \ll 1$).

Testing of the model was carried out using `COPASI` (software application for simulation and analysis of biochemical networks and their dynamics [34]) and the kinetic parameters for the binding of ricin to its receptor and its internalization [35] and competition by the monoclonal antibody 2B11 [8]. The kinetic parameters used are shown in Table 1. The value of k_3 used is that determined by Sandvig et al. [35] to be the rate of irreversible binding of ricin to HeLa cells. For simplicity, the simulation was carried out using all reactions taking place in the same compartment.

To illustrate the model, we used toxin and receptor concentrations based on cell culture studies carried out in our laboratory. These typically use a cell concentration of $1 \cdot 10^4$ cells per 100 μL experiment and a ricin concentration of 10 pM. Assuming $3 \cdot 10^7$ receptors/cell [35], the receptor concentration is approximately 5 nM.

3. Analytical Results

3.1. Cell Surface Binding. Initially we derive some analytical results for toxins that act at the cell surface and are not internalized; that is, we set $k_3 = 0$ in (4). At equilibrium $d/dt = 0$ and from (1) and (3) we can write

$$C_R = \frac{RT}{K_1}, \qquad C_A = \frac{AT}{K_2}, \tag{9}$$

where $K_1 = k_1/k_{-1}$, $K_2 = k_2/k_{-2}$ are the association constants for the toxin binding to the receptor and antibody, respectively. It is worth noting that the parameter γ (diffusive correction of the intrinsic reaction rates) disappears from (9), so in this case the analytical results are identical to ones derived using the "well-mixed" approximation [23].

In order to simplify notations, we denote by z and y the equilibrium concentrations of the toxin-receptor and toxin-antibody complexes; that is,

$$z = [C_R]_{\mathrm{eq}}, \qquad y = [C_A]_{\mathrm{eq}}. \tag{10}$$

From (9) and conservation laws (6)–(8) the following closed equation for z can be derived:

$$(R_0 - z)(T_0 - z - y) - K_1 z = 0, \tag{11}$$

$$y = A_0 \frac{\epsilon z}{R_0 - z(1-\epsilon)}, \tag{12}$$

where $\epsilon = K_1/K_2$.

Equation (11) can be written in a more conventional form of a cubic equation as follows:

$$a_3 z^3 + a_2 z^2 + a_1 z + a_0 = 0, \tag{13}$$

where

$$\begin{aligned} a_3 &= \epsilon - 1, \\ a_2 &= (1-\epsilon) C_0 + \epsilon A_0 + R_0, \\ a_1 &= -R_0 (C_0 + A_0 + (1-\epsilon) T_0), \\ a_0 &= T_0 R_0^2, \end{aligned} \tag{14}$$

and $C_0 = R_0 + K_1$.

It is well known that (13) has a closed-form analytical solution (Cardano's formula [36]), which in our case provides a consistent way to derive exact solutions for the proposed model. Unfortunately these solutions still involve rather cumbersome expressions, which require further simplifications in order to be used in practical situations. In the following we present another approach that explicitly employs the smallness of ratio $T_0/R_0 \ll 1$ and leads to a simple analytical expression for the protective properties of the antibody.

We observe that in the absence of antibody (i.e., $A_0 = 0$), (11) is an elementary quadratic equation that has two roots. If we impose the obvious constraint $z \to 0$ as $T_0 \to 0$, then there is only one solution, which we designate as z_0:

$$z_0 = \frac{C_0}{2}\left[1 - \left(1 - \frac{4R_0T_0}{C_0^2}\right)^{1/2}\right]. \tag{15}$$

Under the condition $T_0/R_0 \ll 1$, this can be simplified to

$$z_0 \approx \frac{R_0 T_0}{C_0}, \qquad C_0 = R_0 + K_1. \tag{16}$$

Let us now evaluate the effect of adding an antibody. From a mathematical point of view this effect (i.e., change of z under condition $A_0 > 0$) is captured entirely by the term y in (11), so our aim is to provide a reasonable analytical estimation of this term.

From (12) and based on our initial assumption of low toxin concentration ($T_0/R_0 \ll 1$), we can deduce the

following simple estimate $y \approx \epsilon z A_0/R_0$. This then leads to a modified form of (11) as follows:

$$(R_0 - z)(T_0 - z) - K_* z = 0, \tag{17}$$

where

$$K_* = K_1 + \epsilon A_0. \tag{18}$$

We can see that this is the same form as the equation for z when $A_0 = 0$, but now with K_1 replaced with K_*. This also implies that the analytical solution (16) is still valid but only with the substitution $K_1 = K_*$.

In order to characterize the effect of an antibody on the binding of a toxin to its receptor, we introduce the nondimensional parameter Ψ, the relative reduction in C_R due to the introduction of an antibody as follows:

$$\Psi \equiv \frac{z(A_0 > 0)}{z(A_0 = 0)}. \tag{19}$$

The analytical results presented previously enable us easily to derive a simple formula for the antibody efficiency parameter Ψ. By using (10), (16), (18), and (19), we can readily deduce the following:

$$\Psi = \frac{1}{1 + \epsilon\lambda}, \qquad \epsilon = \frac{K_1}{K_2}, \qquad \lambda = \frac{A_0}{C_0}. \tag{20}$$

This expression is the main result of the current paper and will be validated with numerical simulations.

To conclude this section let us briefly discuss some additional constraints for the parameters of our model in order for the expression (20) to be valid. As mentioned above the condition of low toxin concentration is always assumed in our study. Another simple condition can be derived from the constraint $C_R + C_A \leq T_0$ and by using (16):

$$\frac{R_0}{C_0}\left(1 + \epsilon\frac{A_0}{C_0}\right) \approx \epsilon\frac{R_0 A_0}{C_0^2} \leq 1, \tag{21}$$

since $R_0/C_0 \leq 1$. This condition could always be checked retrospectively and always hold in our numerical simulations.

3.2. Toxin Internalization. For toxins that are internalized, the effect of antibodies that prevent receptor binding is to reduce the effective rate of internalization. To examine and evaluate this effect, we need to analyze the full systems (1), (3), and (4).

In order to characterize the effect of antibody concentration on the rate of toxin internalization, we introduce a new parameter as follows:

$$G = \frac{T_i(A_0 > 0)}{T_i(A_0 = 0)}, \tag{22}$$

which is a function of time (i.e., $G \equiv G(t)$).

Our aim is to deduce function G based on the kinetic models (1), (3), and (4). It is evident that $G \leq 1$ for $t > 0$ and $G \to 1$ as $t \to \infty$ (since in that case all toxin will be internalized).

For the toxins of interest, while the receptor binding is rapid (time sale $\sim 1/(k_1 C_0)$) [24, 26], the subsequent internalization is much slower (time scale $\sim 1/k_3 \gg 1/(k_1 C_0)$). This coupling of slow and fast processes in our system allows us to develop a simplified model of toxin internalization using the well-known framework of Quasi-Steady-State Approximation (QSSA); see [24–28, 37] and refs therein.

When applied to our system, QSSA elucidates the toxin internalization as a two-stage process. After the initial rapid binding of the toxin to the receptor we can simply set $dC_R/dt = 0$ in (1). The further slow evolution of $T(t)$ (namely, quasi-steady state) is completely determined by the conservation laws (8) and (4) and spans a time scale of the order of the internalization time ($\sim 1/k_3$). In addition, for solving (4) at the initial stage of internalization, we can assume that $T_i \ll T_0$ and write

$$T_i(t) = k_3 z_0 t, \quad t \ll \frac{1}{k_3}, \tag{23}$$

where z_0 is given by expressions (15) and (16). The evolution of $T_i(t)$ for the late stage of internalization can be readily derived from (4) and (6)–(8) by assuming $[T_0 - T_i(t)] \ll T_0$:

$$T_i(t) = T_0\left[1 - \exp(-k_3 t)\right], \quad t \geq \frac{1}{k_3}, \tag{24}$$

so $T_i(t)$ exponentially approaches its saturation limit. A simulation of this process is shown in Figure 5, and the slow linear increase of T_i at the initial stage is clearly visible.

Now, consider the case where $A_0 > 0$. According to (23) the main effect of the introduction of an antibody is to reduce the value of z_0, as described in the previous section. Then, based on (22), (23), and (19) we can conclude that, during the quasi-equilibrium stage, the following approximation holds:

$$G = \frac{T_i(A_0 > 0)}{T_i(A_0 = 0)} \approx \Psi, \tag{25}$$

where Ψ is given by expression (20).

The overall effect of introducing an antibody can be best described in terms of the internalization half-time, τ_i. Without antibody the latter can be estimated from (24) and condition $T_i(\tau_i) = T_0/2$. Thus from (23) we yield

$$\tau_i \approx \frac{T_0}{2k_3 z_0} = \frac{C_0}{2k_3 R_0}. \tag{26}$$

For the internalization time with the presence of antibody we can apply reduced value of z_0 and write the following simple formula:

$$\frac{\tau_i}{\tau_i^0} \approx \frac{1}{\Psi}, \tag{27}$$

where τ_i^0 is the internalization time in the absence of antibody ($A_0 = 0$).

Equations (26) and (27) have a clear interpretation. As described in the previous section, the introduction of an antibody results in a decrease, at $t \ll \tau_i$, in the equilibrium

value of C_R (i.e., in z_0). This can be related, in accordance with (23) and (26), to a corresponding decrease in the concentration of internalized toxin T_i and a consequent increase in the toxin internalization time (since it takes longer to achieve a give level of T_i). Since changes in z_0 can be described comprehensively by means of the parameter Ψ, it still remains the only parameter needed to characterize the influence of an antibody on the concentration of internalized toxin (25), (27).

It is evident that the two main effects described above (reduction of the concentration of internalized toxin at a given time and increase in the time required for the internalized toxin to reach a given concentration) are not independent of each other. The linear relationships (25), (27) allow us to establish a general identity that relates these two effects for any time t.

Let us assume that for $A_0 = 0$, τ_0 is the time taken for the internalized toxin to reach a concentration T_i^0 (i.e., $\tau^0 = T_i^0/(k_3 z_0)$; see (23)). The effect of introducing an antibody is to reduce the internalized toxin concentration to a value $T_i \leq T_i^0$. Then from (25), (27) we can derive the following identity:

$$T_i \tau_i = T_i^0 \tau_i^0, \tag{28}$$

where τ_i is the time required for the internalized toxin to reach T_i^0 when $A_0 > 0$. The identity (28) has no explicit dependency on antibody kinetic parameters or concentration and provides an easy way to calculate any of the parameters $(T_i, T_i^0, \tau_i, \tau_i^0)$ if the other three are known.

4. Numerical Results and Discussion

We have derived an analytical expression for the parameter Ψ, the relative ability of an antibody to reduce the binding of a toxin to its receptor (20). Our derivation is based on the following assumptions:

(1) toxin concentration is much lower than the receptor concentration,

(2) for toxins that are internalized, the internalization rate is much slower than establishment of the receptor-toxin binding equilibrium.

Applying these assumptions, we found that parameter Ψ is independent of the toxin concentration (see (20)); that is, it is determined by the ratio of antibody to receptor concentration and not by the ratio of antibody to toxin concentration as commonly used. For the low toxin/receptor ratios likely to occur in biological situations, the condition (21) can be met by large range of antibody kinetic parameters. From this point of view (20) should be valid for most practical applications.

The implications of our analytical findings are illustrated by simulation of the complete kinetic models ((1),(3), (4), and (6)–(8)) using the kinetic constants for ricin and the anti-ricin antibody 2B11 (Table 1). Figure 2 is a simulation of the effect of the presence of an antibody on the binding of the toxin to its receptor (formation of C_R). The antibody concentration is expressed as the dimensionless parameter $\lambda = A_0/C_0$. In this

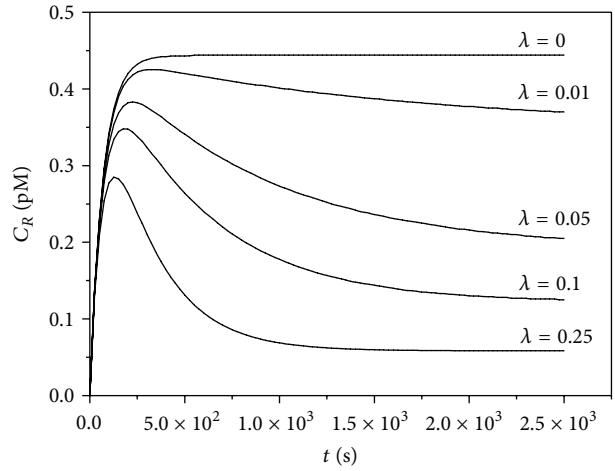

Figure 2: Simulated effect of antibody concentration on formation of toxin-receptor complexes C_R. Parameter $\lambda = A_0/C_0$, $C_0 = R_0 + K_1$. The binding curves were created using the simulation package COPASI and the kinetic constants in Table 1. $R_0 = 5$ nM, $T_0 = 10$ pM, $C_0 = 1.15 \cdot 10^{-7}$.

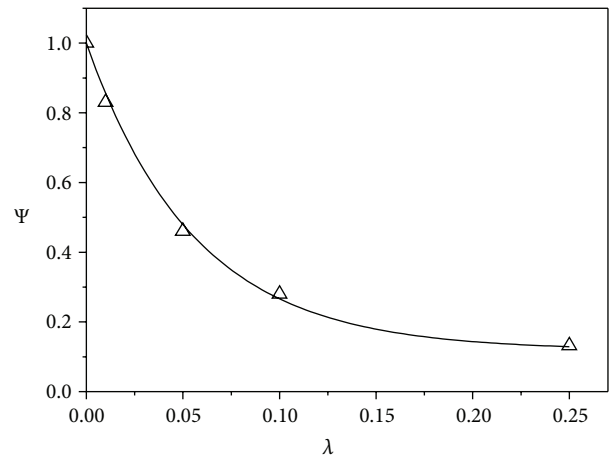

Figure 3: Effect of antibody concentration on protection factor. Parameter Ψ (19) was determined from (20) (solid lines) and by using simulated values of C_R from Figure 2 at 2500 sec (△), $\epsilon = 25.9$.

case, since R_0 and $T_0 \ll K_1$, the parameter $C_0 = R_0 + K_1$ is dominated by K_1 ($1.08 \cdot 10^{-7}$).

Figure 3 shows the effect of increasing antibody concentration on Ψ. There is a good agreement between the values of Ψ determined from (20) and from (19) using the equilibrium values of C_R determined from simulation of the complete kinetic model (Figure 3). For instance, the results predict that, for this toxin and antibody combination, the additional protection provided by increasing the antibody concentration diminishes rapidly when λ exceeds 0.1.

Figure 4 shows the relationship (20) between Ψ, antibody concentration and the toxin/antibody and the ratio of toxin/receptor dissociation constants (ϵ). This plot is valid for all combinations of toxin, receptor, and antibody consistent with the assumptions used to derive (20), principally

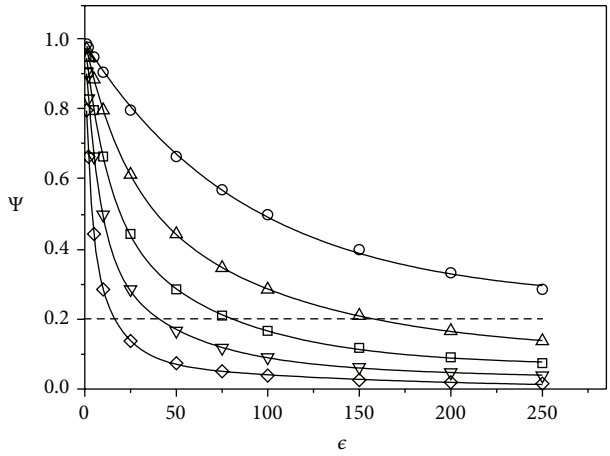

Figure 4: Protection factor Ψ (19) as a function of parameter $\epsilon = K_1/K_2$ and $\lambda = A_0/C_0$ ((20)): $\lambda = 0.01$ (○); 0.025 (△); 0.05 (□); 0.1 (▽); 0.25 (◊). The range of values for λ and ϵ below dashed line corresponds to 80% protection.

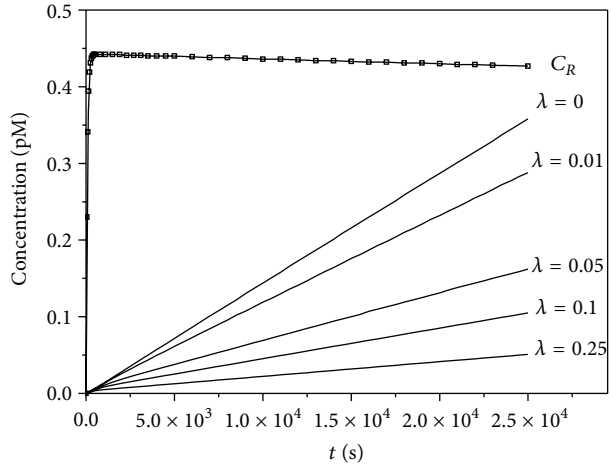

Figure 5: Different time scales for formation of receptor-toxin complex C_R (□) and associated toxin internalization T_i (solid lines). Results of COPASI simulation with kinetic constants from Table 1. $\lambda = A_0/C_0$, $R_0 = 5$ nM, $T_0 = 10$ pM, $C_0 = 1.15 \cdot 10^{-7}$, $\epsilon = 25.9$.

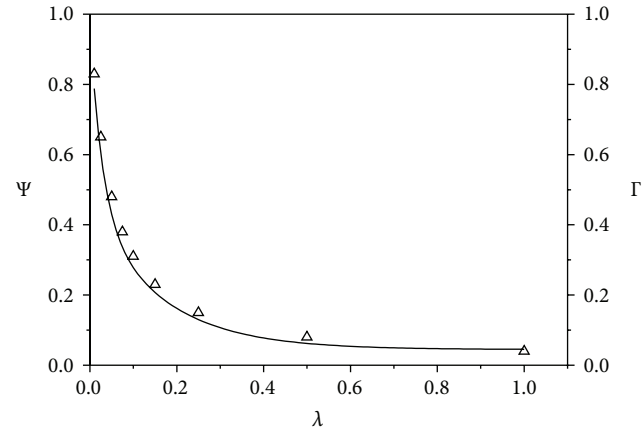

Figure 6: Comparison of parameters Ψ and Γ. Γ (△) was determined using values of T_i and T_i^0 at $t = 10^4$ sec from toxin internalization time courses simulated using COPASI and the kinetic constants in Table 1. Parameter Ψ (solid line) was determined from (20). $R_0 = 5$ nM, $T_0 = 10$ pM, $C_0 = 1.15 \cdot 10^{-7}$, $\epsilon = 25.9$.

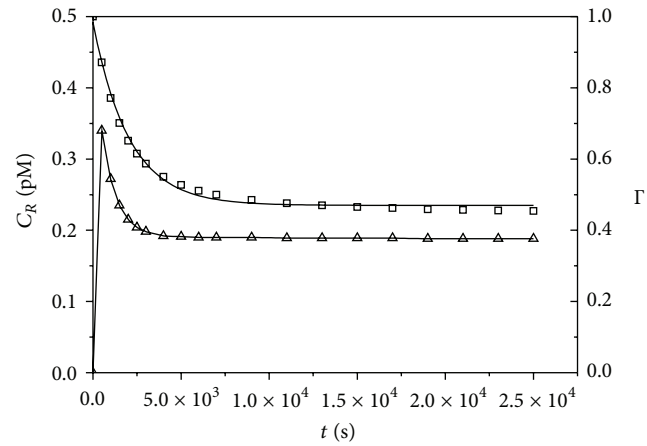

Figure 7: Establishment of the quasi-equilibrium state in the presence of antibody. C_R formation (△) was simulated using COPASI and the kinetic constants in Table 1. Γ (□) was determined using (25) and values T_i and T_i^0 at $t = 10^4$ sec using simulated toxin internalization time courses. $R_0 = 5$ nM, $T_0 = 10$ pM, $C_0 = 1.15 \cdot 10^{-7}$, $\lambda = 0.05$.

$T_0 \ll R_0$. The antibody kinetic parameters and concentration required to provide a specified degree of protection may be determined from this plot. For example, any combination of ϵ and λ falling below the dashed line will reduce either C_R or T_i by 80%.

This, in turn, enables important judgements to be made about antibody selection. For example, if an antibody concentration of $0.25C_0$ ($\lambda = 0.25$) is achievable, then an antibody with an ϵ value of 50 will provide good protection (93% reduction in C_R or T_i). If an antibody concentration of only $0.05C_0$ ($\lambda = 0.05$) is achievable, then an ϵ value of 250 is required to achieve the same level of protection. The structure of (20) is such that a given increase in protection (Ψ or Γ) may be achieved by either an x-fold increase in ϵ or an x-fold increase in λ.

The effect of antibody on toxin internalization is simulated in Figure 5. Rapid equilibration of receptor and toxin is followed by slow accumulation of toxin within the cell. Equation (25) predicts that Ψ is the only parameter needed to characterize the influence of an antibody on toxin internalization. Figure 6 compares Γ calculated using (25), (20) with Γ determined using values of T_i and T_i^0 at $t = 10^4$ sec from this simulated data and shows good agreement between the two values under the condition $T_0 \ll R_0$, although the value of Γ is slightly greater than Ψ. The plot predicts the degree of protection provided by a given concentration of antibody and enables assessment of the value of increasing antibody concentration beyond a certain value. For example,

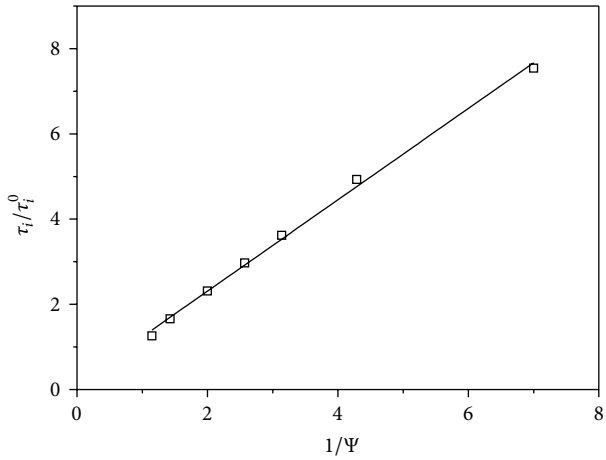

FIGURE 8: Relationship between toxin internalization time τ_i and protection factor Ψ (19). Solid line is formula (27) and (□) is simulation with COPASI. τ_i was determined as the time to internalize $5 \cdot 10^{-14}$ M of ricin. All other parameters are the same as in Figure 7.

to enhance the reduction of T_i from 90% to 95% requires doubling of A_0.

The expression for Ψ, (20), assumes a quasi-equilibrium state in the system. In practice, this state may take significant time to be achieved. Figure 7 shows a simulation of the time taken by the ricin/receptor/2B11 system to reach the quasi-equilibrium state for $\lambda = 0.05$. The value of Γ determined from the toxin internalization profiles (Figure 7) parallels this process; that is, experimental validation of Γ must allow sufficient time to elapse for the quasi-equilibrium state to be established.

The relationship between the internalization time τ_i and Ψ described in (27) is shown in Figure 8. Ψ was determined from simulated toxin internalization time courses (Figure 5) as the time to internalize $5 \cdot 10^{-14}$ M ricin. The slope of the fitted line is 1.07, close to the predicted value of 1.0.

In summary, the protection provided by an antibody against toxins that act either at the cell surface or after binding to the cell surface followed by internalization may be predicted from a simple kinetic model. Protection parameter Ψ is a simple function of antibody, receptor, and toxin concentrations and the kinetic parameters governing the binding of the toxin to the receptor and antibody:

$$\Psi = \frac{1}{1 + (K_1/K_2)(A_0/C_0)}. \quad (29)$$

The calculated value of Ψ matches closely the degree of protection determined from numerical simulation of the binding and internalization reactions and provides a convenient method for predicting the optimum antibody parameters (concentration and dissociation constants) needed to provide effective treatment or prophylaxis for toxins.

Acknowledgments

The authors acknowledge helpful discussions with Dr. Chris Woodruff and Dr. Ralph Leslie.

References

[1] R. B. Reisler and L. A. Smith, "The need for continued development of ricin countermeasures," *Advances in Preventive Medicine*, vol. 2012, Article ID 149737, 4 pages, 2012.

[2] J. Prigent, L. Panigai, P. Lamourette et al., "Neutralising antibodies against ricin toxin," *PLoS ONE*, vol. 6, no. 5, Article ID e20166, 2011.

[3] H. B. Oral, C. Ozakin, and C. A. Akdis, "Back to the future: antibody-based strategies for the treatment of infectious diseases," *Molecular Biotechnology*, vol. 21, pp. 225–239, 2002.

[4] A. F. Kaufmann, M. I. Meltzer, and G. P. Schmid, "The economic impact of a bioterrorist attack: are prevention and postattack intervention programs justifiable?" *Emerging Infectious Diseases*, vol. 3, no. 2, pp. 83–94, 1997.

[5] G. J. A. Rainey and J. A. T. Young, "Antitoxins: novel strategies to target agents of bioterrorism," *Nature Reviews Microbiology*, vol. 2, no. 9, pp. 721–726, 2004.

[6] M. Nehal, C. Michelle, L. Juan et al., "A high-affinity monoclonal antibody to anthrax protective antigen passively protects rabbits before and after aerosolized," *Infection and Immunity*, vol. 73, pp. 795–802, 2005.

[7] A. Razai, C. Garcia-Rodriguez, J. Lou et al., "Molecular evolution of antibody affinity for sensitive detection of botulinum neurotoxin type A," *Journal of Molecular Biology*, vol. 351, no. 1, pp. 158–169, 2005.

[8] C. R. McGuinness and N. J. Mantis, "Characterization of a novel high-affinity monoclonal immunoglobulin G antibody against the ricin B subunit," *Infection and Immunity*, vol. 74, no. 6, pp. 3463–3470, 2006.

[9] H. F. Staats, S. M. Alam, R. M. Scearce et al., "In vitro and in vivo characterization of anthrax anti-protective antigen and anti-lethal factor monoclonal antibodies after passive transfer in a mouse lethal toxin challenge model to define correlates of immunity," *Infection and Immunity*, vol. 75, no. 11, pp. 5443–5452, 2007.

[10] M. Maddaloni, C. Cooke, R. Wilkinson, A. V. Stout, L. Eng, and S. H. Pincus, "Immunological characteristics associated with the protective efficacy of antibodies to ricin," *Journal of Immunology*, vol. 172, no. 10, pp. 6221–6228, 2004.

[11] E. D. Lobo, R. J. Hansen, and J. P. Balthasar, "Antibody pharmacokinetics and pharmacodynamics," *Journal of Pharmaceutical Sciences*, vol. 93, no. 11, pp. 2645–2668, 2004.

[12] M. T. Albrecht, H. Li, E. D. Williamson et al., "Human monoclonal antibodies against anthrax lethal factor and protective antigen act independently to protect against *Bacillus anthracis* infection and enhance endogenous immunity to anthrax," *Infection and Immunity*, vol. 75, no. 11, pp. 5425–5433, 2007.

[13] T. J. Smith, J. Lou, I. N. Geren et al., "Sequence variation within botulinum neurotoxin serotypes impacts antibody binding and neutralization," *Infection and Immunity*, vol. 73, no. 9, pp. 5450–5457, 2005.

[14] S. Reuveny, M. D. White, Y. Y. Adar et al., "Search for correlates of protective immunity conferred by anthrax vaccine," *Infection and Immunity*, vol. 69, no. 5, pp. 2888–2893, 2001.

[15] S. F. Little, B. E. Ivins, P. F. Fellows, M. L. M. Pitt, S. L. W. Norris, and G. P. Andrews, "Defining a serological correlate of protection in rabbits for a recombinant anthrax vaccine," *Vaccine*, vol. 22, no. 3-4, pp. 422–430, 2004.

[16] M. L. M. Pitt, S. F. Little, B. E. Ivins et al., "In vitro correlate of immunity in a rabbit model of inhalational anthrax," *Vaccine*, vol. 19, no. 32, pp. 4768–4773, 2001.

[17] K. K. Peachman, M. Rao, C. R. Alving et al., "Correlation between lethal toxin-neutralizing antibody titers and protection from intranasal challenge with *Bacillus anthracis* ames strain spores in mice after transcutaneous immunization with recombinant anthrax protective antigen," *Infection and Immunity*, vol. 74, no. 1, pp. 794–797, 2006.

[18] N. Mohamed, M. Clagett, J. Li et al., "A high-affinity monoclonal antibody to anthrax protective antigen passively protects rabbits before and after aerosolized *Bacillus anthracis* spore challenge," *Infection and Immunity*, vol. 73, no. 2, pp. 795–802, 2005.

[19] G. A. Papalia, M. Baer, K. Luehrsen, H. Nordin, P. Flynn, and D. G. Myszka, "High-resolution characterization of antibody fragment/antigen interactions using Biacore T100," *Analytical Biochemistry*, vol. 359, no. 1, pp. 112–119, 2006.

[20] J. E. Alouf and M. R. Popoff, *The Comprehensive Sourcebook of Bacterial Protein Toxins*, Elsevier, Amsterdam, The Netherlands, 3rd edition, 2006.

[21] K. Sandvig and B. van Deurs, "Membrane traffic exploited by protein toxins," *Annual Review of Cell and Developmental Biology*, vol. 18, pp. 1–24, 2002.

[22] K. Sandvig and B. van Deurs, "Transport of protein toxins into cells: pathways used by ricin, cholera toxin and Shiga toxin," *FEBS Letters*, vol. 529, no. 1, pp. 49–53, 2002.

[23] A. Skvortsov and P. Gray, "Modeling and simulation of receptor-toxin-antibody interaction," in *Proceedings of the 18th World IMACS Congress and International Congress on Modelling and Simulation (MODSIM '09)*, pp. 185–191, Cairns, Australia, July 2009.

[24] G. A. Truskey and F. Yuan, *Transport Phenomena in Biological Systems*, Prentice Hall, New York, NY, USA, 2nd edition, 2009.

[25] D. A. Lauffenburger, *Receptors: Models for Binding, Trafficking, and Signaling*, Oxford Univercity Press, Oxford, UK, 2nd edition, 1993.

[26] B. Goldstein and M. Dembo, "Approximating the effects of diffusion on reversible reactions at the cell surface: ligand-receptor kinetics," *Biophysical Journal*, vol. 68, no. 4, pp. 1222–1230, 1995.

[27] M. Coppey, A. M. Berezhkovskii, S. C. Sealfon, and S. Y. Shvartsman, "Time and length scales of autocrine signals in three dimensions," *Biophysical Journal*, vol. 93, no. 6, pp. 1917–1922, 2007.

[28] S. Ghosh, M. Gopalakrishnan, and K. Forsten-Williams, "Self-consistent theory of reversible ligand binding to a spherical cell," *Physical Biology*, vol. 4, no. 4, pp. 344–352, 2007.

[29] F. R. Maxfield and T. E. McGraw, "Endocytic recycling," *Nature Reviews Molecular Cell Biology*, vol. 5, no. 2, pp. 121–132, 2004.

[30] D. R. Sheff, E. A. Daro, M. Hull, and I. Mellman, "The receptors recycling pathway contains two distinct populations of early endosomes with different sorting functions," *Journal of Cell Biology*, vol. 145, no. 1, pp. 123–139, 1999.

[31] C. Lamaze and L. Johannes, "Intracellular trafficking of bacterial and plant protein toxins," in *The Comprehensive Sourcebook of Bacterial Protein Toxins*, J. E. Alouf and N. R. Popoff, Eds., pp. 135–153, Elsevier, Amsterdam, The Netherlands, 3rd edition, 2006.

[32] H. S. Wiley and D. D. Cunningham, "A steady state model for analyzing the cellular binding, internalization and degradation of polypeptide ligands," *Cell*, vol. 25, no. 2, pp. 433–440, 1981.

[33] H. Shankaran, H. Resat, and H. S. Wiley, "Cell surface receptors for signal transduction and ligand transport: a design principles study," *PLoS Computational Biology*, vol. 3, no. 6, article e101, 2007.

[34] S. Hoops, R. Gauges, C. Lee et al., "COPASI—a complex pathway simulator," *Bioinformatics*, vol. 22, no. 24, pp. 3067–3074, 2006.

[35] K. Sandvig, S. Olsnes, and A. Pihl, "Kinetics of binding of the toxic lectins abrin and ricin to surface receptors of human cells," *The Journal of Biological Chemistry*, vol. 251, no. 13, pp. 3977–3984, 1976.

[36] A. D. Polyanin and A. V. Manzhirov, *Handbook of Mathematics for Engineers and Scientists*, CRC Press, New York, NY, USA, 2007.

[37] A. R. Tzafriri and E. R. Edelman, "On the validity of the quasi-steady state approximation of bimolecular reactions in solution," *Journal of Theoretical Biology*, vol. 233, no. 3, pp. 343–350, 2005.

Hindawi Publishing Corporation
BioMed Research International
Volume 2013, Article ID 472626, 11 pages
http://dx.doi.org/10.1155/2013/472626

Research Article

Characterization of Antibiotic-Loaded Alginate-Osa Starch Microbeads Produced by Ionotropic Pregelation

Gizele Cardoso Fontes,[1] Verônica Maria Araújo Calado,[1] Alexandre Malta Rossi,[2] and Maria Helena Miguez da Rocha-Leão[1]

[1] *Escola de Química, Universidade Federal do Rio de Janeiro, 21949-900 Rio de Janeiro, RJ, Brazil*
[2] *Centro Brasileiro de Pesquisas Físicas, Rua Dr. Xavier Sigaud 150, 22290-180 Urca, RJ, Brazil*

Correspondence should be addressed to Gizele Cardoso Fontes; gizelecf@yahoo.com.br

Received 22 October 2012; Accepted 2 May 2013

Academic Editor: Subrata Sinha

The aim of this study was to characterize the penicillin-loaded microbeads composed of alginate and octenyl succinic anhydride (OSA) starch prepared by ionotropic pregelation with calcium chloride and to evaluate their *in vitro* drug delivery profile. The beads were characterized by size, scanning electron microscopy (SEM), zeta potential, swelling behavior, and degree of erosion. Also, the possible interaction between penicillin and biopolymers was investigated by differential scanning calorimetry (DSC), powder X-ray diffraction (XRD), and Fourier transform infrared (FTIR) analysis. The SEM micrograph results indicated a homogeneous drug distribution in the matrix. Also, based on thermal analyses (TGA/DSC), interactions were detected between microbead components. Although FTIR spectra of penicillin-loaded microbeads did not reveal the formation of new chemical entities, they confirmed the chemical drug stability. XRD patterns showed that the incorporated crystalline structure of penicillin did not significantly alter the primarily amorphous polymeric network. In addition, the results confirmed a prolonged penicillin delivery system profile. These results imply that alginate and OSA starch beads can be used as a suitable controlled-release carrier for penicillin.

1. Introduction

Benzathine penicillin G (PenG) and its semisynthetic derivatives comprise one of the main groups of antimicrobials used in the treatment of major infectious diseases [1]. Since its discovery in the 1920s, penicillin has been administered through injection. The discomfort and inconvenience associated with this type of administration have led patients with rheumatic fever to neglect and even stop the therapy [2]. For this reason, alternative procedures of PenG administration using polymeric matrices for controlled release systems, such as poly-D,L-lactic acid-co-glycolic acid polymer (PLGA) [3], polyethylene glycol polyamidoamine (PEG-PAMAM) star polymer [4], polybutyl adipato (PBA) [5], and polyacrylate [6], have been proposed.

The use of natural polymers in the design of drug delivery formulations has received much attention because of their excellent biocompatibility and biodegradability. Among them, alginate and starch are very promising and have been exploited in the pharmaceutical industry for controlled drug delivery.

Alginates are composed of (1-4)-linked β-D-mannuronic acid (M units) and α-L-guluronic acid (G units) monomers, which vary in amount and sequential distribution along the polymer chain depending on the source of alginate [7]. Divalent cations, such as Ca^{2+}, cooperatively bind between the G-blocks of adjacent alginate chains, producing the so-called "egg-box" structure and creating ionic interchain bridges, which cause gelling of aqueous alginate solutions [8].

Another potential biopolymer for drug delivery is starch. Starch is regenerated from carbon dioxide and water by photosynthesis in plants. Owing to its complete biodegradability, low cost, and renewability, starch is considered a promising candidate for developing sustainable materials [9]. Octenyl succinic anhydride (OSA) starch is a modified starch developed by the National Starch and Chemical Corporation in the

United States. This modification consists of the addition of a lipophilic component (octenyl-succinate), which increases the emulsion stability in formulations [10]. Furthermore, it is a polymer applied widely in controlled release systems because it can lead to the formation of less porous materials.

Mixtures of alginate and OSA starch have been studied as coating materials for ascorbic acid edible film [10]. This application was the first example in which a calcium alginate-OSA starch mixture was made to obtain microbeads containing antibiotic with potential for biomedical applications. This combination is noteworthy because the calcium alginate forms a reticulate polymer and the OSA starch may contribute to decreasing the pore size of this polymeric matrix to allow the retention of many amphipathic components within the material, such as PenG, because of its both hydrophilic and hydrophobic nature.

Fontes et al. [11] developed and optimized PenG microencapsulation from alginate and OSA starch biopolymers, obtaining a high retention percentage of antibiotic in the microbeads. Thus, in the present work, we have performed an in-depth characterization of microbeads developed by Fontes et al. [11] for future application in subdermal implants using several different techniques. Understanding both the correlation between physical and chemical properties of the structural characteristics and the drug release kinetics are of crucial importance for the development of new products.

We have analyzed the thermal and structural properties and drug release kinetics of the microspheres and biopolymers in an attempt to gain a better understanding of the structure-function relationship. The thermal properties were characterized using thermogravimetric analysis (TGA) and differential scanning calorimetry (DSC). The structure of the beads was studied using scanning electron microscopy and X-ray diffraction (XRD). The chemical propriety was analyzed by FTIR studies. The swelling and erosion behaviors were also evaluated because of their effects on the diffusion and release of drugs when microspheres are applied in drug delivery systems. Comprehensive knowledge of the material properties of a product in production and its application conditions is critical for a product success.

2. Materials and Methods

2.1. Materials. Sodium alginate was obtained from Keltone LV. The ratio of mannuronic acid to guluronic acid residues (M/G) ranged from 0.4 to 1.9. Octenyl succinic anhydride (OSA) starch was obtained from National Starch, and $CaCl_2 \cdot H_2O$ was obtained from Vetec. Penicillin G sodium salt was purchased from Sigma-Aldrich (Fluka and Science Lab, USA).

2.2. Sample Preparation. The beads containing PenG were prepared in triplicate by the extrusion method (dripping method) as described by Fontes et al. [11]. Sodium alginate (4,5%, w/v) with OSA starch (2%, w/v) and PenG (10%, w/v) was dissolved in distilled water. The solution was stirred thoroughly for 30 minutes to ensure complete mixing of the drug. The mixture was dropped into calcium chloride solution (2%, w/v). After gelation, the beads remained in the $CaCl_2$ solution for 10 min. The beads were then removed, washed with Milli-Q water, and dried in the oven at 35°C for 12 h.

2.3. Retention Percentage of PenG Entrapment in Beads. The retention percentage of PenG was determined by HPLC analysis (γ = 220 nm, Waters). The alginate-OSA starch beads loaded with PenG were completely dissolved in phosphate buffer pH 7.4 and measured by HPLC. Preliminary UV studies showed that the presence of dissolved polymers did not interfere with the absorbance of the drug at 220 nm. HPLC analysis of PenG was performed using a Waters 1525 HPLC system with an analytical 4.6 × 150 mm (5 μm) RPC18 YMC-Pack ODS-AQ column, a flow rate of 1 mL/min, and a detector wavelength of 220 nm (Waters 2414). Samples (15 μL) were injected and eluted using A (0.025 M KH_2PO_4 in water (pH = 3)) and B (acetonitrile) as the mobile phase with an isocratic method (67% of A). PenG showed a retention time of 4.5 ± 0.17 min, and its detection limit was 0.1 μg/mL. The retention percentage (%) of entrapment PenG was calculated using the following equation:

$$\text{Retention (\%) of entrapment} = \frac{\text{mass of penicillin present in beads}}{\text{mass of penicillin present in the formulation}} \times 100. \quad (1)$$

2.4. In Vitro PenG Release Studies. The *in vitro* PenG release profiles of the beads were followed in 20 mL of Milli-Q water for 800 h. without mechanical stirring at 37°C. At predetermined time intervals, 0.7 mL of the samples was withdrawn and replaced with fresh medium. The PenG content was determined by HPLC at 220 nm. The unloaded OSA starch alginate beads (without PenG) were taken as reference. Each experiment was done in triplicate.

2.4.1. Analysis of Release Data. To analyze the *in vitro* release data, various kinetic models were used. The zero-order rate equation (2) describes the systems where the drug release rate is independent of its concentration [12]. The first-order equation (3) describes the release from the system where the release rate is concentration dependent [13]. Higuchi [14] described the release of drugs from an insoluble matrix as the square root of the time-dependent process based on Fickian diffusion (4). The Baker-Lonsdale model (5) describes the drug release from spherical matrices [15]. Korsmeyer et al. [16] derived a simple relationship that described drug release from a polymeric system equation (6). The adjusted coefficient of determination (R^2_{adjusted}) value was

used as a criterion to choose the best model to describe drug release:

$$\frac{Q_t}{Q_\infty} = K_0 t + Q_0, \quad (2)$$

$$\log Q_t = \log Q_0 - \frac{K_1 t}{2,303}, \quad (3)$$

$$\frac{Q_t}{Q_\infty} = K_h \sqrt{t}, \quad (4)$$

$$\left(\frac{3}{2}\right)\left[1 - \left(1 - \left(\frac{Q_t}{Q_\infty}\right)\right)^{2/3}\right] - \left(\frac{Q_t}{Q_\infty}\right) = K_b t, \quad (5)$$

$$\frac{Q_t}{Q_\infty} = K_k t^n + Q_0, \quad (6)$$

where Q_t/Q_∞ is the amount of drug released in time t, Q_0 is the initial amount of the drug, K_0 is the zero-order rate constant, K_1 is the first order constant, K_h is the rate constant for Higuchi, K_b is the rate constant for Baker-Lonsdale, and K_k is the rate constant for Korsmeyer Peppas.

2.5. Characterization

2.5.1. Swelling Behavior. Swelling studies were conducted using both wet and dry beads. The term wet refers to the state of the beads immediately after the preparation, and the term dry refers to beads that were left to dry for 24 h. at 37°C in air. Swelling studies of alginate-OSA starch-PenG beads were carried out in Milli-Q water media. The samples were placed in water, and the weight of the swollen samples was measured over time after the excess surface water was removed by gently tapping the surface with a dry piece of filter paper. The degree of swelling (S_W) for the beads sample at time t was calculated using (7):

$$S_W\,(\%) = \left(\frac{W_S - W_i}{W_i}\right) \times 100, \quad (7)$$

where W_S is the weight of the beads in the swollen state and W_i is the initial weight of the dry beads.

2.5.2. Erosion Determination. The degree of erosion was determined after the immersion of dry beads in 20 mL of Milli-Q water. After a selected time interval, the beads were withdrawn and dried in an oven at 110–120°C for a 24 h time period, allowed to cool in a desiccator, and finally weighed until constant weight was achieved (final dry weight). Three different samples were measured for each time point, and fresh samples were used for each individual time point. The percentage erosion (E) was estimated as follows:

$$E\,(\%) = \frac{W_i - W_f}{W_i} \times 100, \quad (8)$$

where W_i is the initial starting dry weight and W_f is the final weight of the same dried and partially eroded sample. All experiments were done in triplicate.

2.5.3. Scanning Electronic Microscopy and Zeta Potential. The microstructures of the beads were studied by scanning electron microscopy (SEM). Randomly selected dry beads were deposited on double-coated carbon conductive tape previously adhered to SEM aluminum stubs. The bead samples were then sputter-coated with a thin gold layer using a coating unit (Balzers Union model FL 9496) and analyzed in a JEOL JSM 5310 operated at 15 or 20 kV. For the surface morphology observation, beads with and without PenG addition were utilized.

The surface charge of beads was evaluated as a function of pH by zeta potential (Dispersion Technology DT 1200).

2.5.4. X-Ray Diffraction (XRD). X-diffraction patterns of the individual biomaterials, physical mixtures, and beads were obtained with an X-ray diffractometer (PANalytical, model X'Pert PRO) using a KαCu radiation wavelength of 1.54184 Å [17].

2.5.5. FT-Infrared Spectroscopy. Individual beads/samples were crushed in a mortar with a pestle. The crushed material was mixed with potassium bromide in a 1 : 100 proportion and dried at 40°C. The mixture was compressed to a 12 mm semitransparent disk by applying a pressure of 10 tons for 2 minutes. The FTIR spectra over the wavelength range from 4100 to 500 cm^{-1} were recorded using an FTIR spectrometer (Prestige 21-Shimadzu).

2.5.6. Thermal Analysis

Differential Scanning Calorimetry (DSC). The DSC of PenG, sodium alginate, OSA starch, as well as unloaded alginate/OSA starch beads, and PenG/sodium alginate/OSA starch beads were evaluated. The test was carried out by using a thermal analysis system (Perkin-Elmer, Diamond) calibrated with indium as the standard and operated in the temperature range of 30–400°C. The bead sample (5 mg) was heated at a rate of 10°C min^{-1} in an aluminum pan under a nitrogen atmosphere using an empty pan as the reference. The onsets of melting point and enthalpy of fusion were automatically computed.

Thermogravimetric Analysis (TGA). Degradation temperatures were performed in a TGA (Perkin-Elmer, Pyris 1) using a sample mass of *ca.* 7 mg and an platinum sample holder at a heating rate of 10°C min^{-1} under a dynamic nitrogen atmosphere flowing at 20 mL min^{-1}.

3. Results and Discussion

3.1. Morphological Characterization, Size, and Surface Charge. In this study, microbead drug delivery systems were prepared using alginate and OSA starch as wall materials for PenG microencapsulation. Because both PenG and alginate are electronically negative and Ca^{2+} is electronically positive, polyelectrolyte complexes can be formed between PenG/alginate and Ca^{2+} via electrostatic interactions during the microparticle preparation. Furthermore, the interactions

between PenG and OSA starch are favorable, as PenG has a hydrophobic portion that can interact with the octenylsuccinate lipophilic component of OSA starch. The dripping technique produced spherical droplets that, after falling into the $CaCl_2$ solution, resulted in spherical thermostable gel particles because of the ionic interactions between guluronate blocks formed from alginate and Ca^{2+} ions.

The results showed a high retention percentage of PenG (95.4%) when alginate and OSA starch were used as the wall materials [11].

PenG-loaded alginate/OSA starch beads showed a spherical geometry (1 ± 2 mm diameter) and a compact structure as evidenced by the SEM analysis reported in Figure 1.

The surface of the beads exhibited a homogeneous microstructure with several wrinkles. The arrangement of the particles formed a surface porosity with pores of a few micrometers in diameter. Figure 1(b) shows a section near the surface of the bead. Some crystals of PenG were observed at the surface of the beads. Figure 1(d) shows pure PenG micrographs. The image reveals the existence of elongated and radially oriented crystals.

Figure 1(c) represents the surface micrographs for beads without PenG, in which a cohesive and compact surface arrangement was observed with irregularities that include peaks and troughs. The irregularities can be attributed to the drying process and the cohesions may be because of the ionic and electrostatic interactions between the components of the beads. The morphology observed is typical of drug-loaded alginate beads, similar to that observed by Rajendran and Basu [17] and Liu et al. [18].

The surface charge of the beads was evaluated as a function of pH (Figure 2). The results from the zeta potential evaluation showed that the surface potential of the microbeads was negatively charged. A greater negative value of the zeta potential was obtained upon an increase in pH, which changed regularly from −3 to −35 mV. In the low pH region (pH 2), most of the carboxylic acid groups in the alginate and OSA starch were in the form of –COOH because the pKa of alginate is in the range of 3.4 to 4.4 [19] and OSA starch is approximately 4.76 [20].

When the pH of the medium was increased, the carboxylic acid groups became ionized, resulting in the increase of negative charge. The PenG alginate/OSA starch beads presented higher negative values of zeta potential than the unloaded beads. This observation may be attributed to the negativelycharged PenG on the alginate/OSA starch microbeads, which caused a decrease in zeta potential. This result shows that beads can make ionic interactions with other biomacromolecules that have a positive charge, such as chitosan and polylysine.

3.2. Swelling Behavior and Erosion Determination. When hydrophilic polymers come into contact with a liquid hydrate, a gel layer is formed. The formation of the gel layer is essential for sustaining and controlling drug release from polymer solid dosage forms. The thickness of this hydrated layer determines the diffusion of the drug molecules through the polymer mass into the liquid medium, but diffusion is not the only mechanism controlling drug release. The rate and extent of drug release also depend on the swelling and erosion of the hydrated polymer preparation [21].

Figure 3(a) shows the beads immediately after preparation, and Figure 3(b) shows the dry bead. In comparison with the size of the wet beads, which was measured to be 3.0 ± 0.2 mm, dried beads were shrunken and their diameter was found to be 1.2 ± 0.09 mm. The maximum degree of swelling calculated is 637.75%. The swelling behavior can be explained by the fact that wet beads tend to absorb water (free or bulk water) in order to fill the empty regions of the polymer network within the beads until they reach the equilibrium state [22].

Figure 4 shows the swelling behavior of dry beads in water. The results obtained using dry beads varied substantially when compared to the wet beads in terms of maximum swelling degree, which was lower by approximately one order of magnitude. The swelling of the beads reached 25% in the first 24 hours and then remained constant until 960 hours. The swelling of the dry beads is mainly attributed to the hydration of the hydrophilic groups of alginate [23]. In this case, free water penetrates inside the beads to fill the inert pores among the polymer chains, which contributes to the degree of swelling. In the literature, different swelling degrees (from 80% to 220%) were observed when alginate was used as the wall material. The lower swelling degree observed in the present work was mainly due to the intrinsic rigidity of the polysaccharide as well as the extent of cross-linking between the carboxyl groups of alginate, Ca^{2+}, and OSA starch. When dried, the alginate network shrinks and collapses, and egg-box junctions move close enough to form side-by-side aggregations under the mediation of free calcium ions. This process is equal to the increasing cross-linking density and makes the dried alginate gel structure extremely dense, which is the reason that the alginate gel beads barely swelled in pure water, as shown in Figure 4.

According to Davidovich-Pinhas and Bianco-Peled [23], the degree of swelling diminishes considerably as calcium concentration increases. An increase of calcium concentration probably increases the number of alginate strands creating a thicker "egg-box" model, which results in a stronger network and hinders water absorption [24]. Therefore, the cross-linking conditions used in this work (previously optimized by Fontes et al. [11]) were sufficient to promote considerable cohesion between the polymers, avoiding a higher water uptake.

The beads did not show any visual sign of disintegration in the media over a period of 30 days. Figure 5 presents the scanning electron micrographs of the beads after 30 days of immersion in water. There was a change in the morphology of the beads, as seen in Figure 5. The surface of the beads was smoother as compared to the micrographs shown in Figure 1. Irregular pores and cracks were observed on the beads, probably due to erosion of the polymer matrix.

Another parameter evaluated was the degree of bead erosion. A decrease in the weight of the beads occurred after 24 hours of water immersion when the maximum degree of hydration was reached. The hydration probably caused the removal and solubilization of the polymer chains with a slight

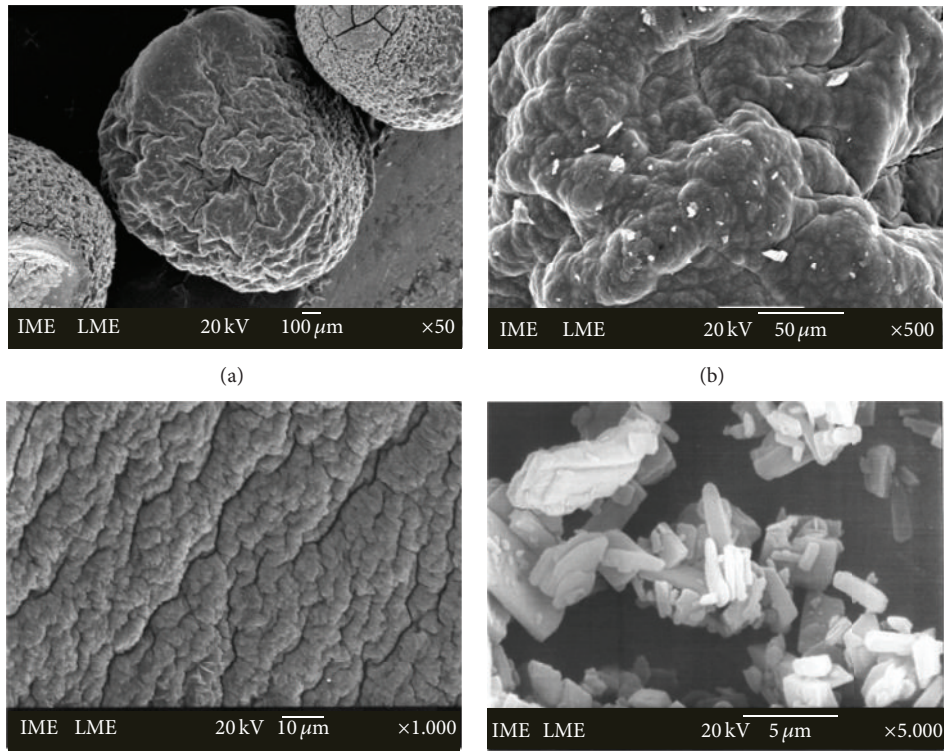

Figure 1: SEM photomicrographs of OSA starch/alginate containing PenG (a), a section near the surface of the bead (b), beads without PenG (c), and pure PenG (d).

Table 1: Release parameters (K) of PenG sustained release and adjusted coefficient of determination (R^2) values in various kinetic models tested.

Zero order Cumulative release % versus time (day)		First order log % drug remaining versus time (day)		Higuchi Cumulative % drug release versus square root of time (day)		Baker-Lonsdale		Korsmeyer Peppas log % cumulative versus log time (day)		
R^2	K	R^2	K	R^2	K	R^2	K	R^2	n value	K
0.99	3.55 ± 0.07	0.83	0.12 ± 0.012	0.97	12.60 ± 0.39	0.92	0	0.96	0.82	5.63 ± 0.71

loss in the weight of the polymers. The maximum erosion degree of the beads was 5% over 30 days of experiments.

3.3. In Vitro Drug Release Kinetics. The release behavior of PenG-loaded beads is presented in Figure 6. The purpose of these drug delivery systems is to implant the microbeads subcutaneously. For that reason, water was chosen as the release medium instead of simulated gastric fluid or even a phosphate buffer, which has an affinity for calcium and could influence the PenG release by alginate erosion. The release of PenG from alginate beads in Milli-Q water was monitored periodically until its concentration in the solution reached a constant value. It was verified (Figure 6) that the PenG release occurs in at least two steps: first, a fast release of about 5% in the first hour of the assay, which corresponds to PenG being physically entrapped in the bead's external layer, and second, the PenG being gradually released, reaching 65% in 432 hours. This second stage can be attributed to the diffusion of the antibiotic from the bead's interior to the outside. After 432 h of assay in this experiment, the PenG concentration was constant until the end (~960 h). This multistage release pattern is due to the complexity of the bead's microstructure, as presented earlier.

The kinetics of PenG release in alginate and OSA starch beads was also evaluated in a 0.35 M calcium chloride solution in order to investigate whether increasing ionic strength by the presence of calcium ions would influence the release of PenG. Figure 6 shows that there is no difference in the release profile when a different medium released is used.

In order to understand the kinetics and mechanism of drug release, the *in vitro* release data were studied using various kinetic models to predict the drug release kinetic mechanism. Table 1 shows the release parameters of PenG sustained release and adjusted coefficient of determination (R^2) values in various kinetic models tested. The release kinetics of PenG was found to be better described by the

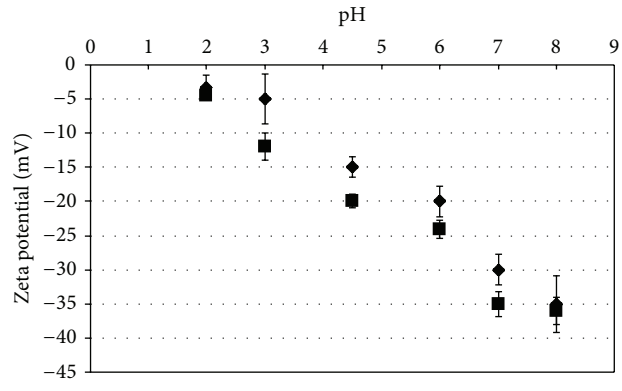

FIGURE 2: Zeta potential of unloaded alginate/OSA starch beads (♦) and PenG alginate/OSA starch beads (■) as a function of pH.

zero-order equation, which provided good linearity and the best fit line ($R^2_{\text{adjusted}} = 0.99$).

According to Kiortsis et al. [25], for the controlled release under investigation and a hydrophilic polymer, the release should follow three steps. The first step is the penetration of the dissolution medium in the matrix (hydration). The second step is the swelling with concomitant or subsequent dissolution or erosion of the matrix. The third step is the transport of the dissolved drug, either through the hydrated matrix or from the parts of the eroded tablet, to the surrounding dissolution medium.

By incorporating the first 60% of release, data mechanism of release can be indicated according to Korsmeyer, where n is the release exponent, indicative of mechanism of drug release. For the case of sphere shape, $0.43 \leq n$ corresponds to Fickian diffusion mechanism, $0.43 < n < 0.85$ to anomalous (non-Fickian) transport, $n = 0.85$ to Case II (relaxation) transport, and $n > 0.85$ to super Case II transport (Siepmann and Peppas, 2001). The value of the release exponent in PenG sustained release obtained was 0.82. This indicates that PenG release from alginate-OSA starch beads followed anomalous transport. In the anomalous processes of drug release, Fickian diffusion through the hydrated layers of the matrix and polymer chain relaxation/erosion are both involved [26].

For predictive completion of release, the drug release data of PenG obtained from dissolution is plotted as concentration ($\text{mg}\cdot\text{L}^{-1}$) versus time ($h$). Linear regression analysis of the data yields the equation of best line as $c = 6.45t + 190.67$ and $R^2 = 0.99$.

According to (2), the slope of line corresponds to the zero-order rate constant. Therefore, the rate of dissolution is $k_0 = 6.45\ \text{mg}\cdot\text{L}^{-1}\ \text{h}^{-1}$. The rate of release in terms of amount of PenG dissolved or released per unit time can be obtained as follows:

$$k_0 \times V, \tag{9}$$

where V is volume of dissolution medium (L).

The rate of release calculated from (9) is $0.13\ \text{mg}\cdot\text{h}^{-1}$. Assuming that this rate of release remains constant throughout the release process, the duration of release is calculated as 769.23 h (32 days) using 100 mg. Hence, the formulation allows a gradual release of the antibiotic from the beads. PenG diffuses through an outer gel layer, which erodes and allows the aqueous medium to penetrate further into the core.

3.4. The X-Ray Diffraction. The X-ray diffraction patterns of the individual polymers, physical mixtures of the polymers, PenG alone, and the PenG-loaded beads are displayed in Figure 7. The diffractogram of alginate consisted of three crystalline peaks at $2\theta = 13.7^\circ$, 23.0°, and 40°. However, according to Wang et al. [27] and Yang et al. [28], the alginate X-ray diffraction consisted of only two crystalline peaks at $2\theta = 13.7^\circ$ and 23.0°. This difference may be because of the amounts of guluronic and manuronic acid present in the different alginate samples. OSA starch also showed three crystalline peaks at $2\theta = 16^\circ, 18^\circ$, and 22°. It presented a typical semicrystalline structure because of its close molecular packing and regular crystallization. Also, Tukomane et al. [29] state that the starch crystalline region is an ordered arrangement of double helical amylopectin structures. Amylose is associated with the amorphous regions and is responsible for water uptake, which occurs more readily at temperatures below that of gelatinization temperature. Pure PenG showed a typical diffractogram of the crystalline substance, with intensive peaks between 17° and 40°. The degree of PenG crystallinity decreased as observed in the X-ray diffraction patterns of the PenG-loaded beads. This decrease can be explained by the possibility of the drug distribution over the polymeric matrix. It is believed that the drug presents some molecular mobility capacity among the polymeric chains, characterizing the observed semiamorphous state of mixture. In addition, the crystallinity of OSA starch was not observed in the beads due to the strong interaction between alginate and OSA starch. This interaction destroyed the close packing of the polymer molecules required for the formation of regular crystallites. Similar results were observed by Wang et al. [27] when alginate and starch were mixed for fiber production.

The X-ray diffraction patterns of the physical mixtures of polymers and beads showed new peaks of crystallinity at $2\theta = 32^\circ$ and 46°. The regularity of the crystal structure may be because of the egg-box regions along the direction of the alginate chain and its aggregating direction.

3.5. Thermal Analysis. Thermal analysis is the most common approach to study physicochemical interactions of a two- or more component system [30]. Table 2 presents the endothermic and exothermic peaks and enthalpies associated with each peak for alginate, OSA starch, unloaded alginate/OSA starch beads, PenG, and PenG/alginate/OSA starch beads by DSC.

Alginate and OSA starch presented one endothermic peak, which is probably due to the melting point. The exothermic peaks of alginate at 237°C resulted from the decomposition of biopolymer because of depolymerization reactions, which are likely owing to the partial decarboxylation of the protonated carboxylic groups and oxidation reactions of the polyelectrolytes [31].

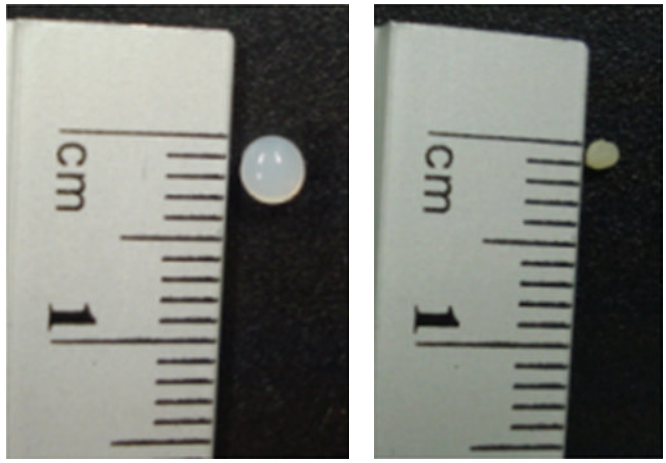

(a) (b)

Figure 3: Photograph of wet beads taken after preparation (a) and dry beads (b).

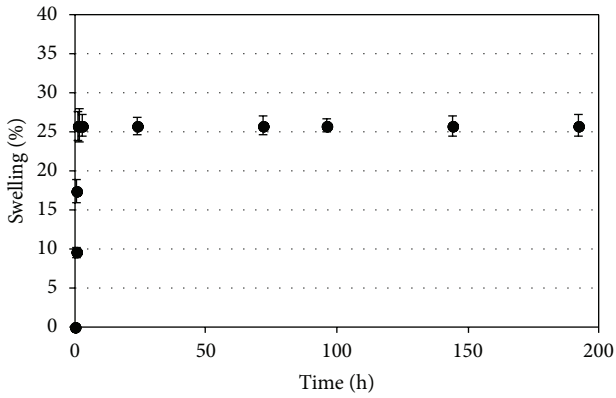

Figure 4: Swelling profiles of dry beads in water. Values are expressed as mean ± standard deviation (S.D.) of three experiments.

Table 2: Peak temperatures and enthalpy changes in the DSC thermograms collected from alginate, OSA starch, unloaded alginate/OSA starch beads, PenG, and PenG-alginate-OSA starch beads.

Sample	Temperature (°C)			ΔH (J/g)	T_g
	Onset	Peak	Endset		
Alginate	161.40	163.26	170.33	332.98	52.10
	209.59	237.36	263.35	−359.40	
OSA starch	182.65	184.31	189.55	125.03	67.06
Unloaded alginate/OSA starch beads	145.57	196.08	220.65	661.07	51.21
Penicillin	189.31	210.52	224.82	−70.69	—
	224.82	226.63	250.00	226.63	
Penicillin/alginate/OSA starch beads	—	—	—	—	80.51

The PenG thermograms presented two exothermic peaks, which are possibly attributed to oxidation.

When alginate was mixed with OSA starch for the production of beads by ionotropic gelation, the thermogram also showed one endothermic peak. The endothermic peak shifted to a higher temperature (196.08°C). This shift corresponded to the interaction of alginate with OSA starch and calcium ions, which showed higher stability of the complexes. The degradation exothermic peak of sodium alginate was absent in the beads; thus, no decomposition event was observed up to 350°C. The thermograms of the PenG-loaded alginate-OSA starch beads did not present any peak during analyses. These results indicate good interaction between both components.

The glass transition temperatures (T_g) were also determined. This parameter can be used as a measurement for the mobility of the macromolecules and the evaluation of the solid-to-liquid transition [32]. The T_g of alginate and OSA starch were 52.10, 67.06°C, respectively (Table 2). Segura-Campos et al. [32] reported that OSA starch T_g was 64.6°C. Similar alginate T_g values were found in the literature [33]. The T_g value of unloaded beads is similar to altinate T_g value due to higher amount of alginate in the beads. PenG did not present T_g, which is likely explained by its structure crystalline. The antibiotic alginate/OSA starch beads show a higher T_g value (80.51°C), which indicates a predominant energetic interaction between the biopolymers and the antibiotic. This effect causes an increase of the glass transition due to the denser packing in the mixture because of the decreasing mobility and the free volume caused by the local ordering effect of heterocontact formation [34].

Brekner et al. [35] have suggested that the glass transition temperature of compatible polymer mixtures depends on the free volume distribution and the related conformational mobility, which is controlled by the probability of heteromolecular contact in the mixture due to specific interactions of the components.

Another analysis carried out was thermogravimetry (TGA). TGA has been proved to be a suitable method to investigate the thermal stability of polymeric systems.

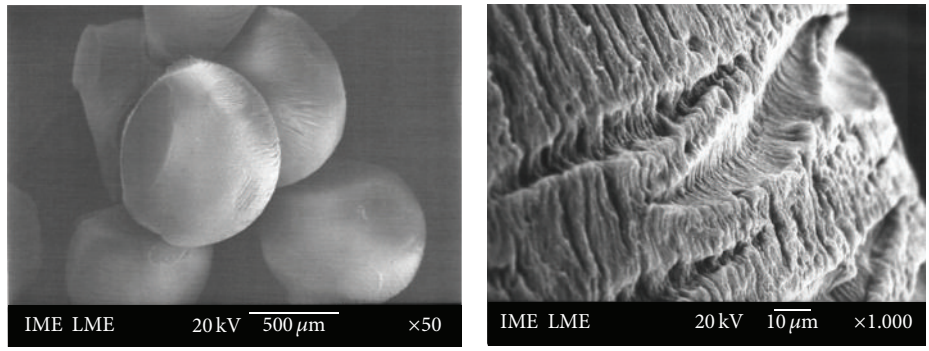

(a) (b)

Figure 5: SEM photomicrographs of OSA starch/alginate beads taken after 30 days of water immersion.

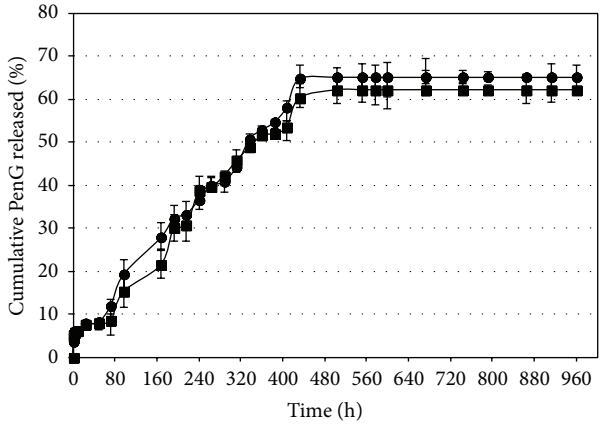

Figure 6: PenG release from alginate and OSA starch beads in Milli-Q water (●) and (■) 0.35 M calcium chloride without mechanical stirring at 37°C.

The knowledge of the threshold decomposition temperature and mode of decomposition upon heating is recommended to determine the highest processing temperature that can be used [36]. The TGA results of the studied materials are shown in Figure 8.

The alginate TG curve presents an initial dehydration process followed by decomposition in two overlapping steps under nitrogen, which is in agreement with DSC data. Similar behavior was observed by Soares et al. [33]; the decomposition product around 400°C was characterized as a carbonaceous material.

The initial weight loss of OSA starch that began just above room temperature corresponds to water desorption. This process was not observed in the mixtures, an indication that a small quantity of water is adsorbed in their structures. OSA starch shows a single degradation step at 250°C.

The unloaded alginate/OSA starch beads showed a two-step degradation inherent to both biopolymers. PenG TGA curves show that weight loss occurred only after 200°C in a single-step degradation.

The OSA starch, alginate, and PenG exhibited 84.92, 68.2, and 73.49% of weight loss at 500°C, while the unloaded alginate-OSA starch beads and PenG/alginate/OSA starch beads presented 53.55% of weight loss at 500°C. The lower weight loss of the beads could be the result of strong interactions between the components of the beads. The thermal stability at 100–120°C (the temperature used in the microbead preparation) shows that both samples were stable during the preparation of the beads, indicating the viability of the implant preparation method developed.

3.6. The Fourier Transform Infrared Spectroscopy (FTIR) Characterization. The possibility of chemical interactions was evaluated by FTIR. Figure 9 shows the infrared spectra of PenG, unloaded alginate/OSA starch beads, and PenG-loaded alginate/OSA starch beads.

The FTIR spectra of unloaded alginate/OSA starch beads provide evidence of both alginate and OSA starch structure information. For the alginate, characteristic functional groups (COO^- stretching) were present, with a broad asymmetrical band at 1610 cm^{-1} and a narrower symmetrical band at 1418 cm^{-1}. An even broader absorption was observed near 1030 cm^{-1}, which can be attributed to COH stretching. OSA starch has similar profiles. In the fingerprint region, there are several discernible absorbances at 1155, 1080, 1021, and 930 cm^{-1}, which were attributed to CO bond stretching [37]. The band at 2928 cm^{-1} is characteristic of the CH stretching vibration. An extremely broad band resulting from vibration of the hydroxyl groups (OH) appeared at 3390 cm^{-1}. These results were confirmed by FTIR spectra obtained from both pure alginate and OSA starch (data not shown) and by the previously reported literature [38].

The FTIR spectra of PenG alone showed major peaks in the wave number ranging from 800 to 1500 cm^{-1}, indicating the presence of carboxyl and carboxylate group stretching. The band at 3350 cm^{-1} was assigned to the NH stretching. The mode oxazolone showed one characteristic band at 1790 cm^{-1} for the carbonyl group. The thiazolidine structure in PenG displayed the carbonyl band at 1622 cm^{-1}. The bands at 1502 and 1701 cm^{-1} are characteristic of primary amide and secondary amide structures, respectively [39].

In FTIR spectra of PenG-loaded alginate/OSA starch beads, no extra bindings or chemical shifts were observed,

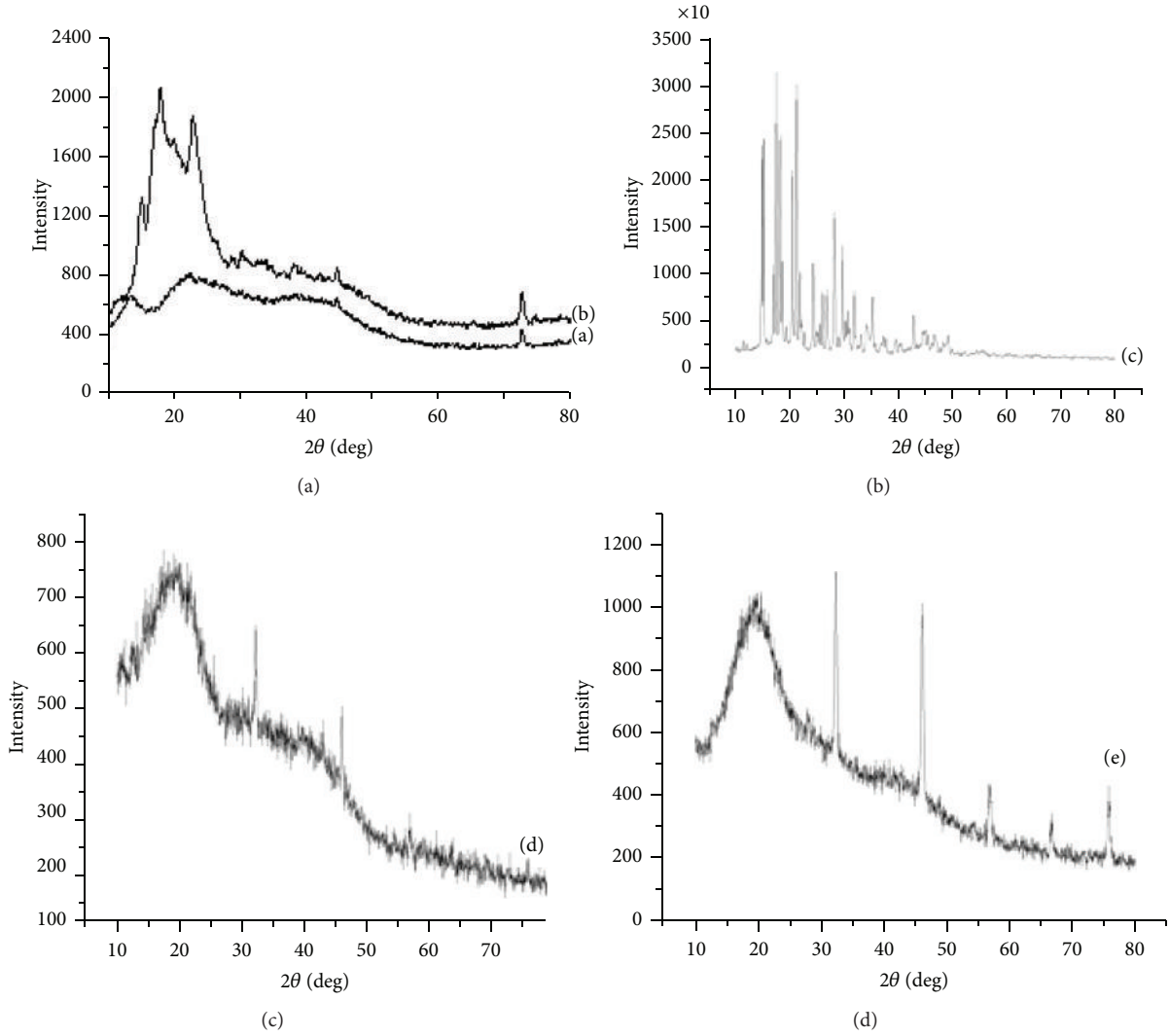

Figure 7: X-ray powder diffraction patterns of sodium alginate (a), OSA starch (b), PenG (c), physical mixture of OSA starch with sodium alginate (d), and PenG-loaded alginate/OSA starch beads (e).

indicating that there is no strong chemical interaction between polymer and drug into the polymer/drug network. Although DSC data show that there are physical interactions, as mentioned earlier, between the polymer and drug, the FTIR spectra did not reveal the formation of new chemical entities. These results confirm the drug's chemical stability, the permanence of its biological activity, and the possibility of a sustained drug delivery system profile.

4. Conclusions

In the present work, antibiotic-loaded alginate/OSA starch microbeads were successfully characterized using several different techniques. The morphological characterization showed that the homogeneous microbeads had negative surface charge. We have shown, by XRD, PenG distribution onto the polymeric matrix. These findings were confirmed by DSC. Shifts of the endothermic and exothermic peaks observed between individual biopolymers and final microbead carriers were interpreted as interactions with different thermal properties. Also, FTIR analysis showed the absence of detectable chemical interactions between the drug and polymer and the presence of PenG in structural biological activity. The *in vitro* release studies proved the capacity of the microbeads to release the drug in a prolonged profile, and the release kinetics of PenG was found to be better described by the zero-order equation. In summary, the delivery system developed and fully characterized in the present work can be applied as a subdermal implant for the treatment of rheumatic fever and other antimicrobial treatments in the future.

Conflict of Interests

None of the listed authors of this paper had any direct financial relation with the commercial identity mentioned in the paper that might lead to a conflict of interests.

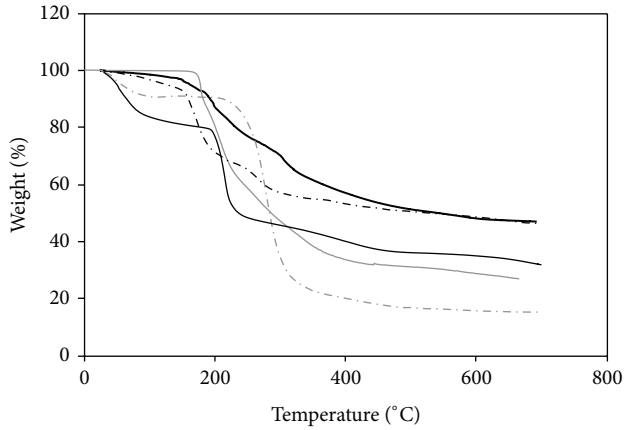

Figure 8: Thermogravimetric curves of alginate (—), OSA starch (dashed grey line), PenG (grey line), alginate/OSA starch microspheres (dashed black line), and PenG/alginate/OSA starch microbeads (black line).

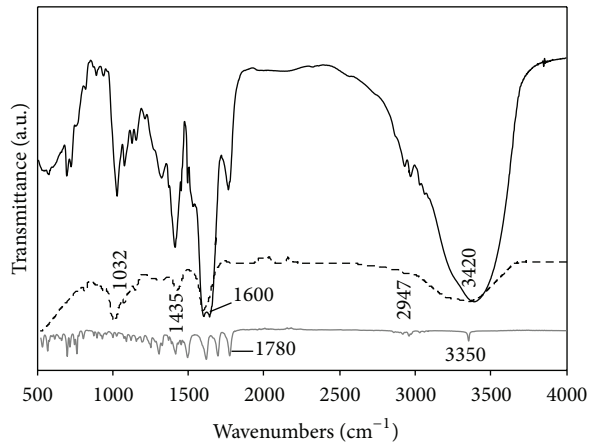

Figure 9: The FTIR spectroscopy of unloaded alginate/OSA starch beads (dashed line), PenG (grey line), and PenG/alginate/OSA starch microspheres (black line).

Acknowledgments

The authors kindly acknowledge the financial aid and research scholarships given by Conselho Nacional de Desenvolvimento Científico e Tecnológico (CNPq) and Fundação Carlos Chagas Filho de Amparo à Pesquisa do Estado do Rio de Janeiro (FAPERJ).

References

[1] C. Barreiro, J. F. Martín, and C. Garcia-Estrada, "Proteomics shows new faces for the old penicillin producer Penicillium crrysogenum," *Journal of Biomedicine and Biotechnology*, vol. 2012, pp. 1–15, 2012.

[2] Z. M. A. Meira, E. M. A. Goulart, E. A. Colosimo, and C. C. C. Mota, "Long term follow up of rheumatic fever and predictors of severe rheumatic valvar disease in Brazilian children and adolescents," *Heart*, vol. 91, no. 8, pp. 1019–1022, 2005.

[3] N. S. Santos-Magalhães, A. Pontes, V. M. W. Pereira, and M. N. P. Caetano, "Colloidal carriers for benzathine penicillin G: nanoemulsions and nanocapsules," *International Journal of Pharmaceutics*, vol. 208, no. 1-2, pp. 71–80, 2000.

[4] H. Yang and S. T. Lopina, "Penicillin V-conjugated PEG-PAMAM star polymers," *Journal of Biomaterials Science, Polymer Edition*, vol. 14, no. 10, pp. 1043–1056, 2003.

[5] S. Khoee and M. Yaghoobian, "An investigation into the role of surfactants in controlling particle size of polymeric nanocapsules containing penicillin-G in double emulsion," *European Journal of Medicinal Chemistry*, vol. 44, no. 6, pp. 2392–2399, 2009.

[6] E. Turos, G. S. K. Reddy, K. Greenhalgh et al., "Penicillin-bound polyacrylate nanoparticles: restoring the activity of β-lactam antibiotics against MRSA," *Bioorganic and Medicinal Chemistry Letters*, vol. 17, no. 12, pp. 3468–3472, 2007.

[7] J. M. López-Cacho, P. L. González-R, B. Talero, A. M. Rabasco, and M. L. González-Rodrigues, "Robust optimization of alginate-carbopol 940 bead formulations," *The Scientific World Journal*, vol. 2012, pp. 1–15, 2012.

[8] M. Davidovich-Pinhas and H. Bianco-Peled, "Physical and structural characteristics of acrylated poly(ethylene glycol)-alginate conjugates," *Acta Biomaterialia*, vol. 7, no. 7, pp. 2817–2825, 2011.

[9] D. R. Lu, C. M. Xiao, and S. J. Xu, "Starch-based completely biodegradable polymer materials," *Express Polymer Letters*, vol. 3, no. 6, pp. 366–375, 2009.

[10] D. S. Bastos, K. G. L. Araújo, and M. H. M. Rocha-Leão, "Ascorbic acid retaining using a new calcium alginate-Capsul based edible film," *Journal of Microencapsulation*, vol. 26, no. 2, pp. 97–103, 2009.

[11] G. C. Fontes, P. V. Finotelli, A. M. Rossi, and M. H. M. Rocha-Leão, "Optimization of penicillin G microencapsulation with OSA starch by factorial design," *Chemical Engineering Transactions*, vol. 27, pp. 85–90, 2012.

[12] T. P. Hadjiioannou, G. D. Christian, M. A. Koupparis, and P. E. Macheras, *Quantitative Calculations in Pharmaceutical Practice and Research*, VCH Publishers, New York, NY, USA, 1993.

[13] D. W. Bourne, *Pharmacokinetics, in Modern Pharmaceutics*, Marcel Dekker, New York, NY, USA, 4th edition, 2002.

[14] T. Higuchi, "Mechanism of sustained-action medication. theoretical analysis of rate," *Journal of Pharmaceutical Sciences*, vol. 52, pp. 1145–1149, 1963.

[15] R. W. Baker and H. S. Lonsdale, "Controled release: mechanisms and rates," in *Controlled Release of Biologically Active Agents*, A. C. Taquary and R. E. Lacey, Eds., pp. 15–17, Plenum Press, New York, NY, USA, 1974.

[16] R. W. Korsmeyer, R. Gurny, and E. Doelker, "Mechanisms of solute release from porous hydrophilic polymers," *International Journal of Pharmaceutics*, vol. 15, no. 1, pp. 25–35, 1983.

[17] A. Rajendran and S. K. Basu, "Alginate-chitosan particulate system for sustained release of nimodipine," *Tropical Journal of Pharmaceutical Research*, vol. 8, no. 5, pp. 433–440, 2009.

[18] X. Liu, W. Xue, Q. Liu et al., "Swelling behaviour of alginate-chitosan microcapsules prepared by external gelation or internal gelation technology," *Carbohydrate Polymers*, vol. 56, no. 4, pp. 459–464, 2004.

[19] U. A. Shinde and M. S. Nagarsenker, "Characterization of gelatin-sodium alginate complex coacervation system," *Indian Journal of Pharmaceutical Sciences*, vol. 71, no. 3, pp. 313–317, 2009.

[20] K. C. Huber and J. N. BeMiller, "Modified starch," in *Starches: Characterization, Properties, and Applications*, A. Bertolini, Ed., pp. 145–203, CRC Press, New York, NY, USA, 2009.

[21] G. Pasparakis and N. Bouropoulos, "Swelling studies and in vitro release of verapamil from calcium alginate and calcium alginate-chitosan beads," *International Journal of Pharmaceutics*, vol. 323, no. 1-2, pp. 34–42, 2006.

[22] A. S. Hoffman, "Hydrogels for biomedical applications," *Advanced Drug Delivery Reviews*, vol. 43, pp. 3–12, 2002.

[23] M. Davidovich-Pinhas and H. Bianco-Peled, "A quantitative analysis of alginate swelling," *Carbohydrate Polymers*, vol. 79, no. 4, pp. 1020–1027, 2010.

[24] E. M. Zactiti and T. G. Kieckbusch, "Potassium sorbate permeability in biodegradable alginate films: effect of the antimicrobial agent concentration and crosslinking degree," *Journal of Food Engineering*, vol. 77, no. 3, pp. 462–467, 2006.

[25] S. Kiortsis, K. Kachrimanis, T. Broussali, and S. Malamataris, "Drug release from tableted wet granulations comprising cellulosic (HPMC or HPC) and hydrophobic component," *European Journal of Pharmaceutics and Biopharmaceutics*, vol. 59, no. 1, pp. 73–83, 2005.

[26] B. Saša, P. Odon, S. Stane, and K. Julijana, "Analysis of surface properties of cellulose ethers and drug release from their matrix tablets," *European Journal of Pharmaceutical Sciences*, vol. 27, no. 4, pp. 375–383, 2006.

[27] Q. Wang, X. Hu, Y. Du, and J. F. Kennedy, "Alginate/starch blend fibers and their properties for drug controlled release," *Carbohydrate Polymers*, vol. 82, no. 3, pp. 842–847, 2010.

[28] G. Yang, L. Zhang, T. Peng, and W. Zhong, "Effects of Ca^{2+} bridge cross-linking on structure and pervaporation of cellulose/alginate blend membranes," *Journal of Membrane Science*, vol. 175, no. 1, pp. 53–60, 2000.

[29] T. Tukomane, P. Leerapongnun, S. Shobsngob, and S. Varavinit, "Preparation and characterization of annealed-enzymatically hydrolyzed tapioca starch and the utilization in tableting," *Starch/Staerke*, vol. 59, no. 1, pp. 33–45, 2007.

[30] A. Schoubben, P. Blasi, S. Giovagnoli, C. Rossi, and M. Ricci, "Development of a scalable procedure for fine calcium alginate particle preparation," *Chemical Engineering Journal*, vol. 160, no. 1, pp. 363–369, 2010.

[31] T. Mimmo, C. Marzadori, D. Montecchio, and C. Gessa, "Characterisation of Ca- and Al-pectate gels by thermal analysis and FT-IR spectroscopy," *Carbohydrate Research*, vol. 340, no. 16, pp. 2510–2519, 2005.

[32] M. Segura-Campos, L. Chel-Guerrero, and D. Betancur-Ancona, "Synthesis and partial characterization of octenylsuccinic starch from Phaseolus lunatus," *Food Hydrocolloids*, vol. 22, no. 8, pp. 1467–1474, 2008.

[33] J. P. Soares, J. E. Santos, G. O. Chierice, and E. T. G. Cavalheiro, "Thermal behavior of alginic acid and its sodium salt," *Ecletica Quimica*, vol. 29, no. 2, pp. 57–63, 2004.

[34] H. A. Schneider, "Conformational entropy contributions to the glass temperature of blends of miscible polymers," *Journal of Research of the National Institute of Standards and Technology*, vol. 102, no. 2, pp. 229–248, 1997.

[35] M. J. Brekner, H. A. Schneider, and H. J. Cantow, "Approach to the composition dependence of the glass transition temperature of compatible polymer blends: 1," *Polymer*, vol. 29, no. 1, pp. 78–85, 1988.

[36] J. F. Mano, D. Koniarova, and R. L. Reis, "Thermal properties of thermoplastic starch/synthetic polymer blends with potential biomedical applicability," *Journal of Materials Science*, vol. 14, no. 2, pp. 127–135, 2003.

[37] J. M. Fang, P. A. Fowler, C. Sayers, and P. A. Williams, "The chemical modification of a range of starches under aqueous reaction conditions," *Carbohydrate Polymers*, vol. 55, pp. 283–289, 2004.

[38] X. Song, G. He, H. Ruan, and Q. Chen, "Preparation and properties of octenyl succinic anhydride modified early indica rice starch," *Starch/Staerke*, vol. 58, no. 2, pp. 109–117, 2006.

[39] P. S. Kalsi, *Spectroscopy of Organic Compounds*, John Wiley & Sons; Asia, 1995.

Hindawi Publishing Corporation
BioMed Research International
Volume 2013, Article ID 242671, 6 pages
http://dx.doi.org/10.1155/2013/242671

Research Article

Effect of Curcumin on the Increase in Hepatic or Brain Phosphatidylcholine Hydroperoxide Levels in Mice after Consumption of Excessive Alcohol

Chang Won Pyun,[1] Kyu-Ho Han,[2] Go Eun Hong,[1] and Chi Ho Lee[1]

[1] *Department of Food Science and Biotechnology of Animal Resources, College of Animal Bioscience and Biotechnology, Konkuk University, Seoul 143-701, Republic of Korea*
[2] *Department of Food Science, Obihiro University of Agriculture and Veterinary Medicine, Obihiro, Hokkaido 080-8555, Japan*

Correspondence should be addressed to Chi Ho Lee; leech@konkuk.ac.kr

Received 27 July 2012; Accepted 7 March 2013

Academic Editor: Lalji Singh

Curcumin is a bright yellow compound found in *Curcuma longa* L., a member of the family Zingiberaceae. In the present study, we determined whether curcumin protects against oxidative stress in liver and brain in mice fed excessive alcohol. BALB/c mice were administered 20% alcohol (16 g/kg body weight) with or without curcumin (0.016% in diet) for 12 weeks. The concentrations of phosphatidylcholine hydroperoxide (PC-OOH) in liver and brain samples were determined using chemiluminescence high-performance liquid chromatography. Mice treated with ethanol and curcumin significantly ($P < 0.05$) showed a lower hepatic PC-OOH level compared to mice treated with only ethanol. However, there was no significant difference in the brain PC-OOH level among all mice. Our finding indicates that the dosage of alcohol might increase the lipid peroxide level of liver but not of brain, and daily curcumin consumption might be protective for liver against alcohol-related oxidative stress in mice.

1. Introduction

The generation of reactive oxygen species (ROS) by alcohol consumption increases oxidative stress in the body [1]. Excessive alcohol consumption causes various diseases such as alcoholic fatty liver, hepatitis, and cirrhosis [2]. Furthermore, chronic exposure to alcohol-induced oxidative stress may promote carcinogenesis of liver tissue leading to cancer [1, 3]. In addition, dementia is an another major alcohol-related syndrome [4]. Although the mechanisms underlying alcohol-related brain disease and Alzheimer' disease are different, the affected part of the brain and the associated symptoms are similar [5, 6]. Oxidative damage is an early feature of Alzheimer' disease in mild cognitive impairment brains [7]. It might be possible that the oxidative stress might also affect an alcohol-related brain disease.

Lipid peroxide in tissues has been used as a tool for impaired function of tissue or cell biomembrane [8–10]. Particulary, phosphatidylcholine (PC) is a major constituent of cell membranes, and the form of its hydroperoxide, phosphatidylcholine hydroperoxide (PC-OOH), provides a very sensitive and specific marker for oxidative stress in *in vivo* studies [11–13]. For example, the method for measuring PC-OOH level in animal tissue has been developed by using chemiluminescence analyzer-high-performance liquid chromatography (CL-HPLC) system and that has proven useful in many studies (Figure 1) [11]. Indeed, PC-OOH level in plasma or hepatic has been suggested to be available for a hepatic damage indicator [12]. Furthermore, Adachi et al. [13] found that alcohol consumption increases a plasma PC-OOH level, which might be also considered as a marker of oxidative stress caused by alcohol consumption.

Turmeric (*Curcuma longa* L.) is a popular spice in India, and curcumin is bright yellow pigment found in turmeric. It is a member of the family Zingiberaceae and has been used as a folk remedy in some cultures. The positive effects of purified curcuminoid on human diseases have been studied, including cancer [14], inflammatory [15], and Alzheimer's disease

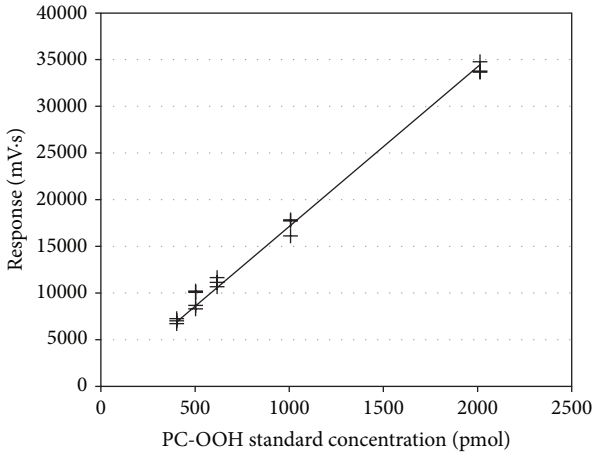

Figure 1: Calibration curve for phosphatidylcholine hydroperoxide (PC-OOH) obtained using the chemiluminescence high-performance liquid chromatography system.

[16, 17]. For example, *in vitro* studies indicate that curcumin protects cells and tissues against oxidative stress by inhibiting generation of ROS [18–20]. In particular, Thong-Ngam et al. [21] reported that curcumin consumption protects liver against alcohol-induced oxidative stress through inhibition of NF-κB activation. However, no information is available for the effect of dietary curcumin on alcohol-related PC-OOH level as oxidative stress maker in the liver and brain in mice.

Therefore, the present study was aimed to investigate the effect of curcumin on alcohol-induced oxidative stress by measuring PC-OOH level in liver and brain of mice. Additionally, we studied the effect of curcumin on alcohol-altered lipid composition in liver and brain.

2. Materials and Methods

2.1. Animals and Diet. 8-week-old male BALB/c mice were purchased from Central Lab Animal Inc. (Seoul, Korea). All mice were daily fed a 4.5 g of AIN-93G modified diet [22] (in g/kg): 239 casein, 185 corn starch, 60 sucrose, 158 dextrose, 60 cellulose, 30 soybean oil, 207 lard, 42 mineral mixture, 12 vitamin mixture, 4 L-cystine, 3 choline bitartrate, and 0.14 tert-butyl hydroquinone. The diet composition was designed by the previous research [21, 23]. The mice were randomly divided into 3 groups ($n = 5$) as follows. ALC group was orally administered 20% ethanol daily, CUR group was orally fed a 0.016% curcumin (Sigma-Aldrich, Saint Louis, MO, USA) in diet after administering 20% ethanol [24, 25], and CON group was administered a volume of saline (0.85% sodium chloride) as equal to that of the alcohol administered to the other 2 groups. The dose of administered alcohol was 16 g/kg body weight to induce alcoholic diseases for 12 weeks, which was based on a long-term consumption as previous studies [26]. Mice were kept in house maintained a 12 h light/12 h dark cycle with 60% humidity and 25°C. After 12 weeks, the mice were anesthetized by intraperitoneal injection of Zoletil (Zoletil 50, Virbac, Carros, France), blood was collected from the abdominal aorta, and livers and brains were quickly removed and weighed before freezing for storage at −80°C.

2.2. Total Lipids, Triglyceride, and Cholesterol. Total lipid in the liver or brain was extracted by a modified method of Folch et al. [27]. First, 300–400 mg of tissue sample was homogenized with 2 mL of saline using a Teflon-glass overhead stirrer, and the homogenate was transferred to a conical tube. Next, 4 mL of chloroform-methanol solution (2 : 1, v/v) containing 0.002% butylated hydroxytoluene was added, and the solution was mixed vigorously using a vortex mixer for 1 min, and then centrifuged at 3000 ×g for 10 min. The lower layer was collected and transferred to another conical tube. The extraction process was repeated 3 times, and the lipid content was then determined gravimetrically after completely evaporating the chloroform with a stream of nitrogen gas. The extract was mixed with 2 mL of chloroform containing 2% triton X-100, and the organic phase was evaporated with stream of nitrogen gas, and the residue was diluted with 2 mL of distilled water. This solution was used for triglyceride (TG) and total cholesterol (TC) using commercial assay kit (Asan Pharmaceutical Co. Ltd., Seoul, Korea).

2.3. PC-OOH Standard. A photoirradiation method was used to synthesize a standard solution of PC-OOH for CL-HPLC analysis (Figure 2). Phosphatidylcholine (PC, from bovine heart, Sigma-Aldrich) was dissolved in methanol containing 0.01 mM methylene blue. The solution was exposed to a UV lamp (50 W) for 8 hr. Oxidant was cleaned up by using Supelclean LC-Si SPE tube (Supelco, Bellefonte, PA, USA) to remove methylene blue. The amount of peroxide in the standard solution was determined by method of the American Oil Chemist's Society [28]. As a result, the hydroperoxide concentration of the photooxidized PC was 19.1 μmol hydroperoxide-O_2 per g of PC.

2.4. Assay of PC-OOH. The PC-OOH level of total lipid extracts in a chloroform-methanol (2 : 1, v/v) solution was measured by using a CL-HPLC system [11]. The analytical system conditions were as follows: a Zorbax NH_2 (4.6 × 250 mm, 5 μm, Agilent Technologies, Wilmington, DE, USA) column was used for separation. The mobile phase consisted of 2-propanol-methanol-water (135 : 45 : 20, v/v/v), and the flow rate was 1 mL/min. The chemiluminescence analyzer (CLD-1100, Tohoku Electronic Industrial Co., Sendai, Japan) reaction temperature was 40°C, and the luminescence reagent was prepared by dissolving 10 mg/L of cytochrome c (from bovine heart, Sigma-Aldrich) and 2 mg/L of luminol (for chemiluminescence analysis, Wako pure chemical, Osaka, Japan) in 50 mM borate buffer (pH 10.0). This reagent was inserted into the sample chamber of the chemiluminescence analyzer by using a peristaltic pump at a flow rate of 1.0 mL/min [11, 13]. To calculate the recovery rate of this procedure, 3 different concentrations of the standard were produced as described above, and the peak areas of the prepreparative solution and postpreparative solutions were compared. The calculated recovery rate was 94.4% ± 4.7% (mean ± standard deviation) (SD)).

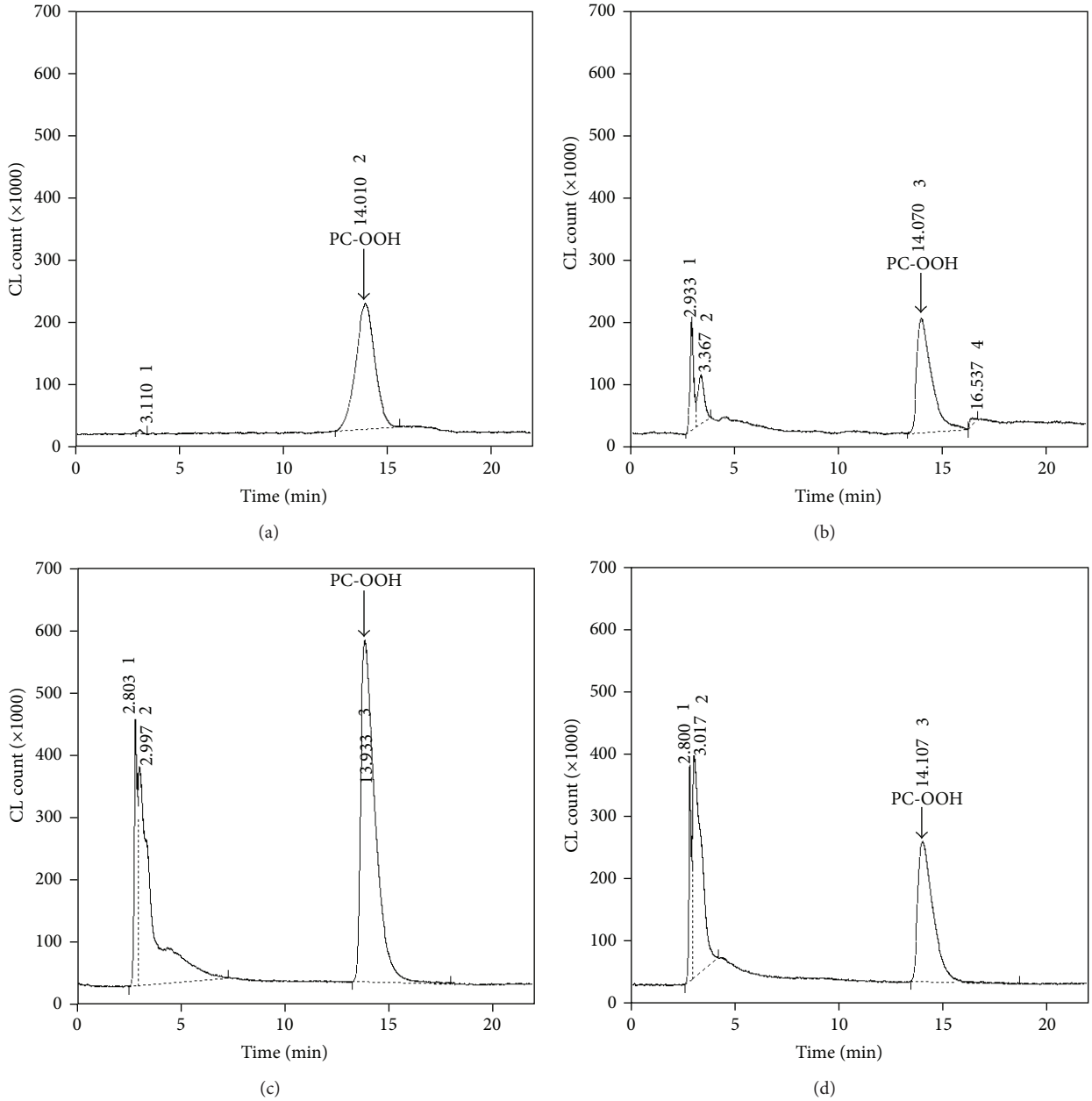

Figure 2: Representative chromatograms of the PC-OOH standard (402.8 pmol) (a), hepatic lipid extracts for the control (CON) (b), ethanol-treated (ALC) (c), and ethanol + curcumin-treated (CUR) (d) groups.

2.5. Statistical Analysis. All data are presented as mean ± SD values. Differences between the groups were calculated using Duncan's multiple range test ($P < 0.05$). All statistical analyses were performed using the Statistical Analysis Software (Statistics Analytical System Institute, Cary, NC, USA).

3. Results and Discussion

3.1. Body and Organ Weights. The body weights of ALC and CUR mice were significantly ($P < 0.05$) higher than those of CON mice (Table 1). This finding may be attributable to the effect of the extra calories contributed by excess ethanol consumption [29]. A similar pattern was observed for the spleen. We assume that reduced functioning of the liver caused by alcohol-related oxidative stress induced enlargement of the spleen [30]. Interestingly, the mean spleen weight of the CUR group was lower than that of the ALC group, but the difference was not significant. The kidney and brain weights of the alcohol-treated groups (ALC and CUR) were significantly ($P < 0.05$) lower than those of the CON group, suggesting that excessive alcohol consumption

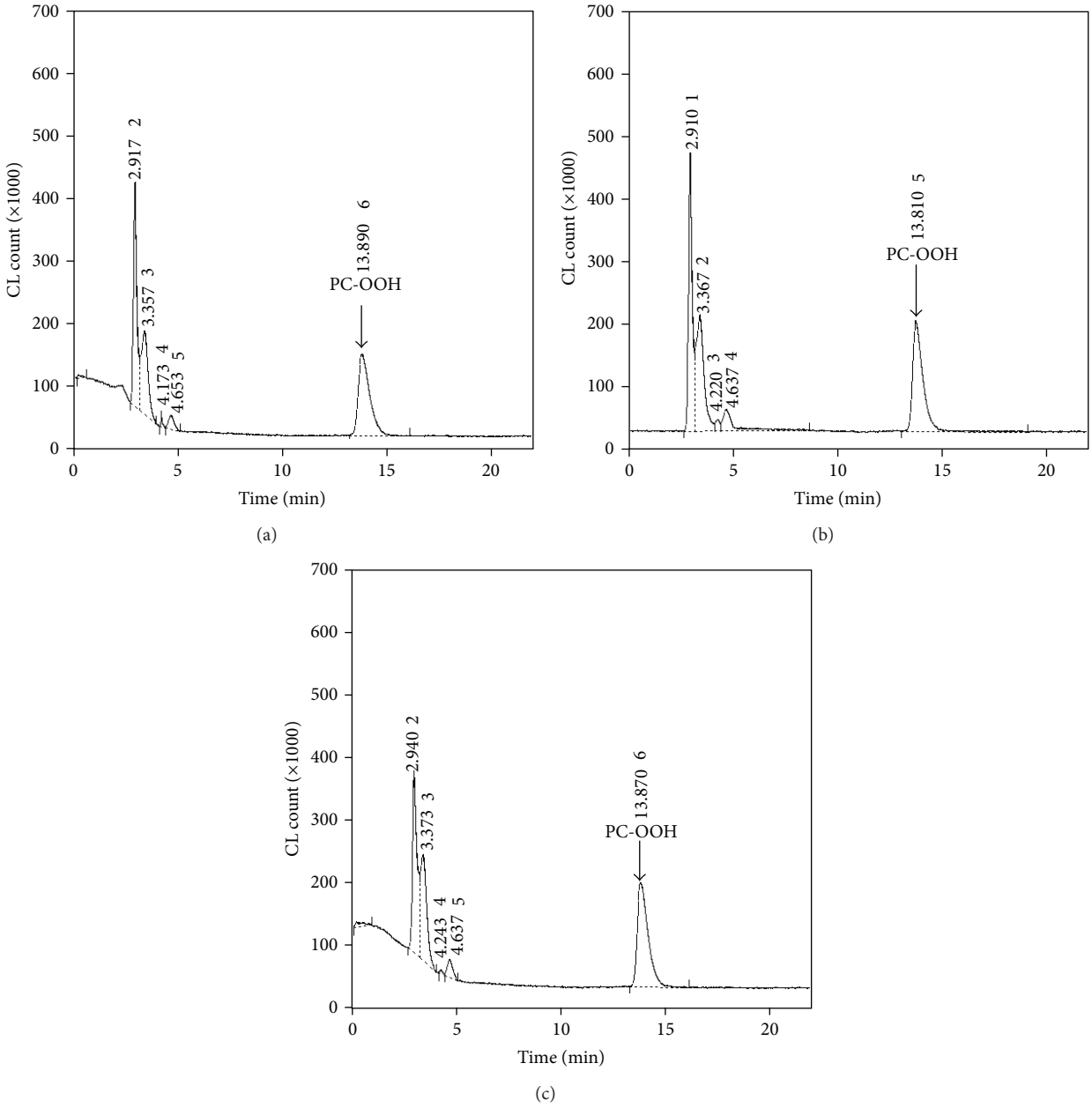

Figure 3: Representative chromatograms of brain lipid extracts for the CON (a), ALC (b), and CUR (c) groups.

may affect the kidney and brain weights. However, the liver weights among all groups were not significantly different.

3.2. Lipid Content of the Liver and Brain. The total lipid contents of the livers and brains of the three groups of mice are shown in Table 2. It was shown that hepatic total lipid and TG levels in the ALC group were significantly ($P < 0.05$) higher than the CON group. These results suggest that an alcohol-treated mouse develops fatty liver due to excessive alcohol consumption [31]. Although the lipid content of the livers of both ethanol-treated groups was high, the content in the CUR group was slightly lower than that of the ALC group, suggesting that steady consumption of curcumin inhibits the development of fatty liver to some extent. The most remarkable findings were that the hepatic TG and TC levels in the CUR group were significantly ($P < 0.05$) lower than those of the ALC group. This result suggests that daily consumption of even a small amount of curcumin may inhibit the development of alcohol-induced fatty liver and regulate hepatic cholesterol content. However, further investigation of these effects is required. No significant differences were observed between the brain lipid content ($P < 0.05$) of each group

Table 1: Organ weights.

	CON	ALC	CUR
Final body weight (g)	20.8 ± 2.2^{b}	26.6 ± 1.7^{a}	25.2 ± 1.1^{a}
Liver (g/kg body weight)	32.6 ± 3.3	34.6 ± 1.3	34.4 ± 1.2
Kidney (g/kg body weight)	17.0 ± 0.8^{a}	14.4 ± 0.8^{b}	14.8 ± 0.8^{b}
Spleen (g/kg body weight)	2.65 ± 0.37^{b}	3.66 ± 0.48^{a}	3.23 ± 0.31^{a}
Brain (g/kg body weight)	16.6 ± 2.0^{a}	12.7 ± 1.3^{b}	13.7 ± 0.7^{b}

All values are means ± SD. $^{a\text{-}b}$indicates significant differences between values in the same row ($P < 0.05$).
CON: high-fat diet; ALC: high-fat diet and alcohol treated; CUR: curcumin containing high-fat diet and alcohol treated.

Table 2: Concentrations of total lipids, triglyceride, and total cholesterol in the livers and brains.

(mg/100 mg wet tissue)		CON[1]	ALC	CUR
Liver	Total lipid	8.72 ± 2.19^{b}	16.8 ± 5.5^{a}	15.2 ± 3.9^{ab}
	Triglyceride	5.94 ± 0.56^{c}	12.5 ± 0.6^{a}	9.34 ± 0.87^{b}
	Total cholesterol	3.15 ± 0.92^{b}	5.06 ± 2.12^{a}	3.17 ± 0.78^{b}
Brain	Total lipid	11.8 ± 2.3	12.9 ± 1.7	13.2 ± 2.0
	Triglyceride	8.34 ± 0.77	9.99 ± 2.22	8.73 ± 1.30
	Total cholesterol	1.16 ± 0.45	0.96 ± 0.35	1.03 ± 0.61

All values are means ± SD. $^{a-c}$indicates significant differences between values in the same row ($P < 0.05$).
CON: high-fat diet; ALC: high-fat diet and alcohol treated; CUR: curcumin containing high-fat diet and alcohol treated.

Table 3: The phosphatidylcholine hydroperoxide (PC-OOH) level of the liver and brain in mice.

(pmol/g lipid)		CON	ALC	CUR
PC-OOH*	Liver	286 ± 35^{b}	366 ± 58^{a}	157 ± 44^{c}
	Brain	44.4 ± 12.9	53.0 ± 20.0	40.8 ± 5.9

All values are means ± SD. *was calculated by total lipid, which was extracted with triglyceride and total cholesterol concentrations. $^{a-c}$indicates significant differences between values in the same row ($P < 0.05$).
CON: high-fat diet; ALC: high-fat diet and alcohol treated; CUR: curcumin containing high-fat diet and alcohol treated.

(Figure 3). It was thought that dietary 20% ethanol during 12 weeks did not affect the brain lipid contents in this study.

3.3. PC-OOH Content of the Liver and Brain. The hepatic PC-OOH content per total lipids did not differ between each group (data not shown). However, the content in the ALC group was significantly ($P < 0.05$) higher than in the CON and CUR groups, when the data were expressed by the modified lipid concentration, which was extracted by hepatic TG and TC concentrations from the total lipid (Table 3), because those lipids are not concerned with the oxidation of phospholipids. This finding may be attributable to liver damage induced by alcohol-related oxidative stress [2]. The decreased hepatic PC-OOH level in the CUR group indicates that curcumin consumption effectively protected the liver against alcohol-related oxidative stress.

Several *in vitro* data indicate that curcumin has antioxidant, antiinflammatory, and anti-amyloid activities [17–20]. Furthermore, studies in animal models of Alzheimer's disease reviewed a direct effect of curcumin in decreasing the amyloid pathology of Alzheimer's disease [17]. However, the brain PC-OOH concentration did not significantly differ among all, suggesting that the dosage of alcohol could not increase a lipid peroxide level in brain and the reduced brain weight was not attributable to cell destruction caused by alcohol consumption. The differential effects of alcohol on the liver and brain PC-OOH levels might be the different mechanism of alcohol-related liver or brain disease because brain is affected in the final phase of alcohol-related disease while liver is affected in the primary phase [32]. Furthermore, brain damage by excessive alcohol consumption is linked to various conditions, such as alcohol-related liver diseases and thiamine deficiency. The mechanisms have not yet been clearly elucidated [32]. Therefore, further studies will be required to determine the effects of long-term treatment and behavioral tasks to better define the protective effect of curcumin on alcohol-related brain disease.

4. Conclusion

In this study, we demonstrated the effects of curcumin on alcohol-induced oxidative stress in liver but not in brain in mice treated with 20% ethanol. After 12 weeks, the hepatic PC-OOH level in the ALC group was observed to be higher than in the CON and ALC groups. This finding suggests that daily curcumin consumption is effective in protecting the liver against alcohol-related oxidative stress and indicates the possible role of hepatic lipid composition in altering the effect of excessive alcohol consumption. Therefore, further study is required for a detailed lipid mechanism of curcumin in mice fed an alcohol. In contrast, no significant difference was observed in the PC-OOH concentration among all groups. Therefore, additional studies may be required to investigate the effects of curcumin on the brains of alcohol-treated mice.

Conflict of Interests

The authors declare that they have no conflict of interests.

Acknowledgment

This research was supported by Technology Development Program for iPET (Korea Institute of Planning and Evaluation for Technology in Food, Agriculture, Forestry and Fisheries), Republic of Korea (610002-03-3-SB110).

References

[1] E. Albano, "Alcohol, oxidative stress and free radical damage," *Proceedings of the Nutrition Society*, vol. 65, no. 3, pp. 278–290, 2006.

[2] R. E. Mann, R. G. Smart, and R. Govoni, "The epidemiology of alcoholic liver disease," *Alcohol Research and Health*, vol. 27, no. 3, pp. 209–219, 2003.

[3] K. Moriya, K. Nakagawa, T. Santa et al., "Oxidative stress in the absence of inflammation in a mouse model for hepatitis C virus-associated hepatocarcinogenesis," *Cancer Research*, vol. 61, no. 11, pp. 4365–4370, 2001.

[4] K. Lee, L. Møller, F. Hardt, A. Haubek, and E. Jensen, "Alcohol-induced brain damage and liver damage in young males," *Lancet*, vol. 2, pp. 759–761, 1979.

[5] J. Soxton, C. A. Munro, M. A. Butters, C. Schramke, and M. A. McNeil, "Alcohol, dementia, and alzheimer's disease: comparison of neuropsychological profiles," *Journal of Geriatric Psychiatry Neurology*, vol. 13, no. 3, pp. 141–149, 2000.

[6] C. Harper and I. Matsumoto, "Ethanol and brain damage," *Current Opinion Pharmacology*, vol. 5, no. 1, pp. 73–78, 2005.

[7] M. A. Lovell and W. R. Markesbery, "Oxidative damage in mild cognitive impairment and early Alzheimer's disease," *Journal of Neuroscience Research*, vol. 85, no. 14, pp. 3036–3040, 2007.

[8] T. F. Slater, "Free-radical mechanisms in tissue injury," *Biochemistry Journal*, vol. 222, no. 1, pp. 1–15, 1984.

[9] T. F. Slater, "Free radicals and tissue injury: fact and fiction," *The British Journal of Cancer*, vol. 8, pp. 5–10, 1987.

[10] L. J. Machlin and A. Bendich, "Free radical tissue damage: protective role of antioxidant nutrients," *The FASEB Journal*, vol. 1, no. 6, pp. 441–445, 1987.

[11] T. Miyazawa, T. Suzuki, K. Fujimoto, and K. Yasuda, "Chemiluminescent simultaneous determination of phosphatidylcholine hydroperoxide and phosphatidylethanolamine hydroperoxide in the liver and brain of the rat," *Journal of Lipid Research*, vol. 33, no. 7, pp. 1051–1058, 1992.

[12] M. Suzuki, K. Fukuhara, M. Unno et al., "Correlation between plasma and hepatic phosphatidylcholine hydroperoxide, energy charge, and total glutathione content in ischemia reperfusion injury of rat liver," *Hepato-Gastroenterology*, vol. 47, no. 34, pp. 1082–1089, 2000.

[13] J. Adachi, S. Matsushita, N. Yoshioka et al., "Plasma phosphatidylcholine hydroperoxide as a new marker of oxidative stress in alcoholic patients," *Journal of Lipid Research*, vol. 45, no. 5, pp. 967–971, 2004.

[14] B. B. Aggarwal and S. Shishodia, "Suppression of the nuclear factor-κB activation pathway by spice-derived phytochemicals: reasoning for seasoning," *Annals of the New York Academy of Sciences*, vol. 1030, pp. 434–441, 2004.

[15] K. Kohli, J. Ali, M. J. Ansari, and Z. Raheman, "Curcumin: a natural antiinflammatory agent," *Indian Journal of Pharmacology*, vol. 37, no. 3, pp. 141–147, 2005.

[16] H. Hatcher, R. Planalp, J. Cho, F. M. Torti, and S. V. Torti, "Curcumin: from ancient medicine to current clinical trials," *Cellular and Molecular Life Sciences*, vol. 65, no. 11, pp. 1631–1652, 2008.

[17] J. M. Ringman, S. A. Frautschy, G. M. Cole, D. L. Masterman, and J. L. Cummings, "A potential role of the curry spice curcumin in Alzheimer's disease," *Current Alzheimer Research*, vol. 2, no. 2, pp. 131–136, 2005.

[18] M. Balasubramanyam, A. A. Koteswari, R. S. Kumar, S. F. Monickaraj, J. U. Maheswari, and V. Mohan, "Curcumin-induced inhibition of cellular reactive oxygen species generation: novel therapeutic implications," *Journal of Biosciences*, vol. 28, no. 6, pp. 715–721, 2003.

[19] G. P. Lim, T. Chu, F. Yang, W. Beech, S. A. Frautschy, and G. M. Cole, "The curry spice curcumin reduces oxidative damage and amyloid pathology in an Alzheimer transgenic mouse," *Journal of Neuroscience*, vol. 21, no. 21, pp. 8370–8377, 2001.

[20] R. A. Kowluru and M. Kanwar, "Effects of curcumin on retinal oxidative stress and inflammation in diabetes," *Nutrition and Metabolism*, vol. 4, article 8, 2007.

[21] S. Samuhasaneeto, D. Thong-Ngam, O. Kulaputana, D. Suyasunanont, and N. Klaikeaw, "Curcumin decreased oxidative stress, inhibited NF-κB activation, and improved liver pathology in ethanol-induced liver injury in rats," *Journal of Biomedicine and Biotechnology*, vol. 2009, Article ID 981963, 8 pages, 2009.

[22] A. A. Bachmanov, D. R. Reed, G. K. Beauchamp, and M. G. Tordoff, "Food intake, water intake, and drinking spout side preference of 28 mouse strains," *Behavior Genetics*, vol. 32, no. 6, pp. 435–443, 2002.

[23] R. Rukkumani, M. S. Balasubashini, and V. P. Menon, "Protective effects of curcumin and photo-irradiated curcumin on circulatory lipids and lipid peroxidation products in alcohol and polyunsaturated fatty acid-induced toxicity," *Phytotherapy Research*, vol. 17, no. 8, pp. 925–929, 2003.

[24] G. P. Lim, T. Chu, F. Yang, W. Beech, S. A. Frautschy, and G. M. Cole, "The curry spice curcumin reduces oxidative damage and amyloid pathology in an Alzheimer transgenic mouse," *Journal of Neuroscience*, vol. 21, no. 21, pp. 8370–8377, 2001.

[25] J. M. Ringman, S. A. Frautschy, G. M. Cole, D. L. Masterman, and J. L. Cummings, "A potential role of the curry spice curcumin in Alzheimer's disease," *Current Alzheimer Research*, vol. 2, no. 2, pp. 131–136, 2005.

[26] R. Polavarapu, D. R. Spitz, J. E. Sim et al., "Increased lipid peroxidation and impaired antioxidant enzyme function is associated with pathological liver injury in experimental alcoholic liver disease in rats fed diets high in corn oil and fish oil," *Hepatology*, vol. 27, no. 5, pp. 1317–1323, 1998.

[27] J. Folch, M. Lees, and G. H. Sloane-Stanley, "A simple method for the isolation and purification of total lipides from animal tissues," *The Journal of Biological Chemistry*, vol. 226, no. 1, pp. 497–509, 1957.

[28] *Official and Tentative Methods of AOCS, Cd 8-53*, American Oil Chemists' Society, 1964.

[29] P. M. Suter, E. Häsler, and W. Vetter, "Effects of alcohol on energy metabolism and body weight regulation: is alcohol a risk factor for obesity?" *Nutrition Reviews*, vol. 55, no. 5, pp. 157–171, 1997.

[30] A. L. Pazo, E. M. Godfrey, and K. M. Bowles, "Splenomegaly: invetigation, diagnosis and management," *Blood Reviews*, vol. 23, no. 3, pp. 105–111, 2009.

[31] C. S. Lieber, "Liver disease and alcohol: fatty liver, alcoholic hepatitis, cirrhosis, and their interrelationships," *Annals of the New York Academy of Sciences*, vol. 252, pp. 63–84, 1975.

[32] R. F. Butterworth, "Pathophysiology of alcoholic brain damage: synergistic effects of ethanol, thiamine deficiency and alcoholic liver disease," *Metabolic Brain Disease*, vol. 10, no. 1, pp. 1–8, 1995.

Hindawi Publishing Corporation
BioMed Research International
Volume 2013, Article ID 853083, 6 pages
http://dx.doi.org/10.1155/2013/853083

Research Article

Vaccine Adverse Events Reported during the First Ten Years (1998–2008) after Introduction in the State of Rondonia, Brazil

Mônica P. L. Cunha,[1] José G. Dórea,[2] Rejane C. Marques,[3] and Renata S. Leão[4]

[1] *Department of Nursing, Fundação Universidade Federal de Rondônia, 76801-974 Porto Velho, RO, Brazil*
[2] *Faculty of Health Sciences, Universidade de Brasília, 70919-970 Brasilia, DF, Brazil*
[3] *Universidade Federal do Rio de Janeiro, Campus Macaé, 27971-550 Rio de Janeiro, RJ, Brazil*
[4] *Instituto de Biofísica Carlos Chagas Filho, Universidade Federal do Rio de Janeiro, 21941-902 Rio de Janeiro, RJ, Brazil*

Correspondence should be addressed to José G. Dórea; dorea@rudah.com.br

Received 2 October 2012; Revised 7 January 2013; Accepted 11 January 2013

Academic Editor: Tanjore Balganesh

Despite good safety records, vaccines given to young children can cause adverse events. We investigated the reported adverse events following immunization (AEFI) of vaccines given to children of less than seven years of age during the first ten years (1998 to 2008) in the state of Rondonia, Brazil. We worked with the events related to BCG (Bacillus Calmett-Guérin), HB (hepatitis B), DTwP/Hib (diphtheria-tetanus-pertussis+Hemophillus influenza b), DTP (diphtheria-tetanus-pertussis), MMR (mumps, measles, rubella), and YF (yellow fever) vaccines because they were part of the recommended scheme. The number of doses of vaccines given was 3,231,567 with an average of AEFI of 57.2/year during the studied period. DTwP/Hib was responsible for 298 (57.8%), DTP 114 (22.9%), HB 31 (6%), MMR 28 (5.4%), BCG 24 (4.7%), and YF 20 (3.9%) of the reported AEFI. The combination of the AEFI for DTwP/Hib vaccines showed the highest number of systemic (61.4%) and local events (33.8%). Young children (≤1-year old) were more susceptible to AEFI occurring in the 6 hours (54.2%) following vaccine uptake. This study suggests significant differences in reactogenicity of vaccines and that despite limitations of the AEFI Brazilian registry system we cannot ignore underreporting and should use the system to expand our understanding of adverse events and effects.

1. Introduction

Immunization is an essential component of public health policies to control infectious diseases. Its success in worldwide eradication of smallpox and, regionally, in clearing out other infectious diseases makes vaccines one of the most trusted cost-effective public-health interventions [1]. Therefore, because of its universal use which in many cases or circumstances is mandatory, issues of effectiveness and safety take on paramount importance. Despite the stringent protocol for vaccine licensure, some individuals can react to the vaccine's antigens (and formulation ingredients). Discomfort, induration at the site of the inoculation, and pain are common features following vaccination in children but are regarded as inconsequential. However, more serious events, albeit rare, can occur in susceptible individuals [2].

As vaccine coverage increases for the intended infectious diseases, and additional recommended booster doses, there has been an attendant increase in the number of doses a child is now receiving. Therefore, as a consequence of the increased number of vaccinations the risk of an adverse event is proportionally increased. Paradoxically, when the immunization program is effective the incidence of vaccine-preventable disease will drop, resulting in higher numbers of adverse events following immunization (AEFI) and its easier perception [3]. Indeed, in the USA, the number of reported AEFI (registered by the vaccine adverse event reporting system-VAERS) exceeded the incidence of most preventable childhood diseases combined [3].

Vaccine safety surveillance and followup are central to address actual and perceived issues related to AEFI [4]. However, such surveillance and followup infrastructure lags behind vaccine development in industrialized countries [3] and is absent in most developing countries. As an example, despite the known toxicity of mercury, until the early 2000s there was no research on the toxicology of low doses of

Thimerosal/ethylmercury used as preservative in certain vaccines [1]. As a result, a significant gap between perceived and actual risks has developed, and now we need appropriate strategies to maintain the high vaccination rates which are crucial to control infectious diseases [5]. Parents' trust, in tandem with maintaining a high uptake of vaccines, relies mainly on primary health care workers.

Because pharmaceutical products carry risks, vaccines are no exception; however, expected serious events are rare; furthermore, prior to its licensure, as observed by Autret-Leca et al. [6] the size of clinical trials is insufficient to identify rare or deferred adverse effects. Therefore, AEFI systems are important tools to monitor temporal associations between vaccination and a suspected serious or mild adverse or unintended reaction to a given licensed product. The information collected can be used by government agencies in charge of public health, stakeholders, vaccine manufactures, scientists, and the general public. Zhou et al. [7] summarized the objectives of such systems as "(1) detect new, unusual, or rare vaccine adverse events; (2) monitor increases in known adverse events; (3) determine patient risk factors for particular types of adverse events; (4) identify vaccine lots with increased numbers or types of reported adverse events; and (5) assess the safety of newly licensed vaccines." As a consequence, such systems will be central to give public health authorities the necessary plasticity to act rapidly and accurately on an unintended effect of a specific vaccine.

Most AEFI systems are passive and designed for the specific purpose of pharmacovigilance of vaccines; therefore, beyond that, they are of limited use. Nevertheless, they all share a central role in providing crucial information regarding safety of postlicensure vaccine monitoring [8]. Inherent limitations related to diversity of vaccine type, vaccination schemes, and adopted protocol of AEFI by countries, as well as vaccine brands, have made it difficult to compare outcomes. Therefore it is crucial to understand and use the existing AEFI systems in order to improve competence and build expertise among public health workers in dealing with the uncertainties that surround vaccine-related unintended effects.

Since 1998, Brazil has implemented a nationwide program of reporting AEFI. The objective of this work was to use the notified adverse events in the state of Rondônia during the first ten years of the program's implementation as a case study to address current safety issues related to vaccines used in children.

2. Materials and Methods

The study was approved by the Ethics Committee of the Universidade Federal de Rondônia (protocol #43/09). AEFI data (*Eventos Adversos Pos Vacina-EAPV*) were collected directly from the specific pharmacovigilance agency (*Gerência do Programa de Imunizações da Secretaria Estadual de Saúde de Rondônia*). The data are presented collectively in order to safeguard the integrity and anonymity of those involved (patients and health care agents), and results are used only for the purpose of the study and not as an advocacy for or against a specific vaccine.

Vaccines in Brazil are free of charge to the consumer and are available in all public-run (federal, state, or municipal) hospitals, or equally public-run medical clinics throughout the country. In large cities, vaccines are also available from the private clinics where Thimerosal-free and brand-name products can be purchased. Most vaccines in newborns and young children are delivered in primary care vaccine clinics run by local public health qualified professionals; public health nurses or specifically trained health professionals administer the vaccinations and provide guidance for parents. In the maternity wards of public institutions, vaccination of newborns against hepatitis B is mandatory in the first 24 hours after birth; for mothers delivering in private institutions, this vaccine is procured later in private and public medical centers.

Adverse events here are defined "as any severe and/or unexpected adverse sign or symptom occurring after vaccination" [9]. A detailed account of how the Brazilian AEFI system is organized is described by Waldman et al. [9]. The data is captured by primary care medical offices and hospitals. Public health professionals (doctors and nurses specifically in charge of postvaccination adverse events) are required to report postvaccine events that received medical attention. All information is compiled in a specific form that is digitalized and electronically sent to a central office (*Programa Nacional de Imunização-PNI*). The notification form is a structured sheet that captures data related to the patients (age, sex, date of vaccine, and the adverse event); the characteristic of the adverse event is provided and encompasses systemic and localized reactions. The occurrence of an AEFI in a hospital or in medical clinics is required to be reported to the specific state or regional office; the first stage of data generation is by attending physician that reports on the evolution and releases the structured form to the AEFI office. However, after the registry, there are no verification checks. Once the information is properly entered in the appropriate form (with a structured list of 48 AEFI items) it is digitalized into the national data bank. Public medical offices (*postos de saúde*), where most vaccines are dispensed, are rarely contacted for adverse events. However, the processing office is part of all state-run hospitals; private-run vaccination clinics and hospitals are required to report AEFI in the same format.

The Brazilian reporting system of adverse events started in 1998 in a systematic form as specified in the "*Manual de Vigilância Epidemiológica dos Eventos Adversos Pós-Vacinação.*" In year 2000 a national program of vigilance of adverse events was implemented for the entire country (*Sistema de Informação da Vigilância Eventos Adversos Pós-Vacinação, SI-EAPV*). Although the system is backed by the national health authority there is no legal provision to compensate or attenuate sequels, other than what is provided by state run hospital and services.

Since then the SI-EAPV information on AEFI has been provided in a consistent and regular fashion by all states. We included all notified cases of adverse events attributed to any of the vaccines during the studied period (2000 to 2008) for children less than seven years of age. The years 1998 and 1999 were not available in the agency database. We excluded all cases with duplicated notification (only five

Table 1: Distribution of reported adverse events and type of vaccine; Rondônia 1999–2008.

Event type	Vaccines											
	DTP		DTP/Hib		HB		MMR		YF		BCG	
	N	%	*N*	%	*N*	%	*N*	%	*N*	%	*N*	%
Systemic												
Headache and vomiting	3	2.61	6	2.01	0	0.00	1	3.57	0	0	0	0.00
Afebrile seizure	2	1.74	9	3.02	1	3.23	0	0.00	0	0	0	0.00
Febrile seizure	19	16.52	37	12.42	1	3.23	0	0.00	0	0	0	0.00
Induration	2	1.74	4	1.34	3	9.68	0	0.00	1	5	0	0.00
Hypotonic hyporesponsive episodes	35	30.43	124	41.61	1	3.23	1	3.57	0	0	0	0.00
Generalized rash	2	1.74	12	4.03	3	9.68	8	28.57	4	20	0	0.00
Fever ≥39.5°C	30	26.09	52	17.45	1	3.23	2	7.14	0	0	1	4.17
Fever ≤39.5°C	1	0.87	16	5.37	1	3.23	3	10.71	1	5	1	4.17
Other serious events and/or unusual	2	1.74	8	2.68	3	9.68	1	3.57	0	0	0	0.00
Hypersensitivity reaction to 2 h	2	1.74	3	1.01	1	3.23	5	17.86	5	25	0	0.00
Hypersensitivity reaction after 2 h	4	3.48	6	2.01	0	0.00	2	7.14	5	25	0	0.00
Others	1	0.88	2	0.67	0	0.00	2	7.1	2	10	0	0.00
Local												
Pain/redness/heat	4	3.48	7	2.35	0	0.00	0	0.00	1	5	0	0.00
Local hot abscess	4	3.48	2	0.67	13	41.94	1	3.57	0	0	0	0.00
Others	4	3.48	10	3.36	3	9.7	2	7.1	1	5	22	91.67
Total	115	100%	298	100%	31	100%	28	100%	20	100%	24	100%

Percentage (%) was calculated from the number of specific cases and total number of reported cases.
Source: "*SI-EAPV do Programa de Imunizações do Estado de Rondônia*" (EAPV Registry of Rondonia). BCG: Bacillus Calmette-Guérin; HB: hepatitis B; DTP+Hib: diphtheria-tetanus-pertussis+Hemophillus influenza b; DTP: diphtheria-tetanus-pertussis; MMR: mumps, measles, rubella; YF: yellow fever.

cases) and those with incomplete information, that is, those cases without date of vaccine administration, type of vaccine, and associated AEFI symptoms (only six cases). Localized reactions that required hospitalization for more than 24 hours were counted as systemic. We considered the following vaccines: BCG (Bacillus Calmett-Guérin), HB (hepatitis B), DTP+HIB (diphtheria-tetanus-pertussis+Hemophillus influenza b), DTP (diphtheria-tetanus-pertussis), MMR (mumps, measles, rubella), and YF (yellow fever); they represented 516 of a total of 530 cases in the period.

Data were summarized with the Statistical Package for Social Sciences(SPSS) version 12.0 (IBM Corporation, Somers, NY, USA) and Microsoft Office EXCEL software (version 2007; Microsoft Corp, Redmond, WA, USA). Statistical analysis with Friedman and Kendall test was applied with software *Statistica* 7.0 (Tulsa, OK, USA).

3. Results

The rate of adverse events per individual vaccine is shown in Table 1 and is also illustrated in Figure 1. The time series illustrates a different pattern for the DTP and DTwP/Hib vaccines. These vaccines showed the highest rates of AEFI (52.7 and 70.6 per 100,000 resp.,). Year 2004 was particularly high only for these vaccines with the tetravalent (DTP/DTwP/Hib) maintaining the highest levels during the study; coincidently this year had the highest number of vaccinated children. Indeed of the 516 total cases for all vaccines, the tetravalent accounted for more than half (298). The other vaccines (HB, MMR, BCG, YF) together showed less than 20%.

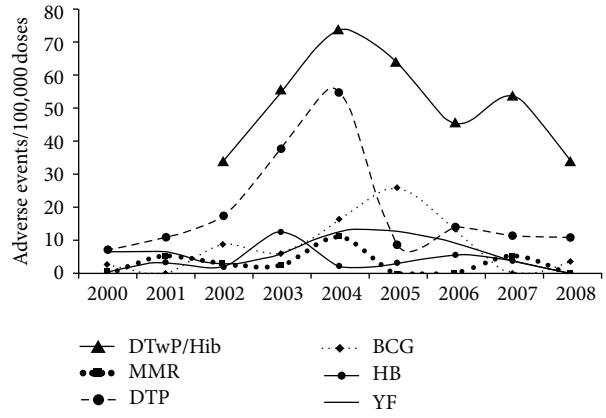

Figure 1: Distribution of notified adverse events and vacines; Rondônia 2000–2008. Source: "*SI-EAPV do Programa de Imunizações do Estado de Rondônia*" (EAPV Registry of Rondonia). Statistically significant differences between vaccines (Friedman ANOVA and Kendall Coefficient of concordance; ANOVA Chi Square (N = 8, df = 6) = 34.48227; P = 0.00001 Coefficient of concordance = 0.71838). BCG: Bacillus Calmett-Guérin; HB: hepatitis B; DTP+Hib: diphtheria-tetanus-pertussis+Hemophillus influenza b; DTP: diphtheria-tetanus-pertussis; MMR: mumps, measles, rubella; YF: yellow fever.

The distribution of adverse events as a function of the type of the reaction—systemic or local—is shown in Figure 2. Overall, systemic adverse events accounted for 86.6% of all

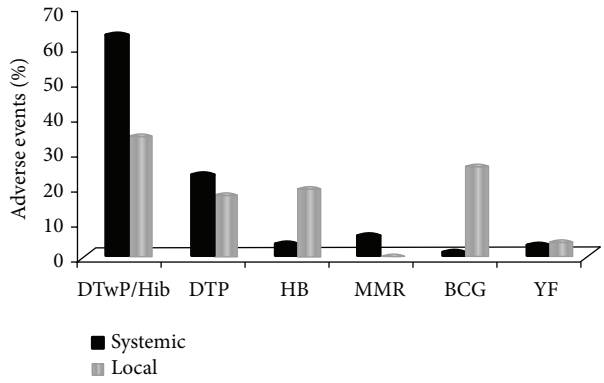

Figure 2: Type of reported adverse event and type of vaccine; Rondônia 2000–2008. Source: "*SI-EAPV do Programa de Imunizações do Estado de Rondônia*" (EAPV Registry of Rondonia). BCG: Bacillus Calmett-Guérin; HB: hepatitis B; DTP+Hib: diphtheria-tetanus-pertussis+Hemophillus influenza b; DTP: diphtheria-tetanus-pertussis; MMR: mumps, measles, rubella; YF: yellow fever.

the reported cases and the tetravalent vaccine (DTwP/Hib) showed the highest rate of systemic (61.4%) as well as local (33.8%) events. For the adverse events considered unexpected or of serious gravity, the DTP and Hib were reported in 57.1% of the cases, and HB alone was responsible for 21.4%. Together, the DTwP/Hib/DTP vaccines showed the highest rate for both systemic and local reactions; as for the other vaccines, the pattern was different for local (BCG>HB> YF>MMR) and systemic (MMR, HB>YF>BCG) reactions.

The most frequent systemic adverse events were hypotonic-hyporesponsive episodes (HHEs), fever >39.5°C, febrile convulsion, and generalized exanthema. HHE was almost exclusively related to the DTP (30.4%) and DTwP/Hib (41.6%) vaccines. These vaccines were also related to 75% of convulsions without fever, and 69.5% of fever (≤39°C), as well as local reactions with reddening, pain, and induration. Most of the EAPI (54.2) were reported to occur in <6 hs after the vaccine in children <12 months.

It is notable that in the majority of cases the AEFI occurred after the first and second dose of the vaccine and more frequently in children of less than 12 months of age. In more severe cases, like HHE, the recommendation is that the following vaccination should be conducted in a hospital facility; in cases of fever and seizures, the regular use of analgesic and antipyretic medication is advised.

4. Discussion

The notified AEFI seem to be associated more with the type of vaccine than with the child's age. The first vaccine (HB) is given on the first postnatal day, and this showed the second highest rate of AEFI, but the vaccine that produced the highest rate of AEFI (DTP/DTwP/Hib) is usually administered at two months of age. It is important to emphasize that in Brazil the rate of reported AEFI is positively associated with the human development index of the state [10], suggesting that underreporting occurs. Indeed, Gomes Monteiro et al. [10] showed the lowest reported AEFI of DTP (from 2002 to 2005) to be in the Northern region of Brazil which has the lowest development indices in the country. Therefore, it is likely that the notified AEFI are underestimated for the state of Rondonia, a representative Northern state.

Fever, HHE, and seizures were the most common systemic AEFI reported in this study. Although in the case of DTwP/Hib (along with convulsions) recovery without after effects was achieved in 98.4% of the cases [11], practical counseling does exist, which can help improve management of cases. Fever, irritability, and feeding disturbances (even anorexia) are transient adverse events that are widely observed, especially in children aged less than seven months, and these events may impact breastfeeding rates and nutrition; in such cases it is important to remind parents that breastfeeding protects against decreased energy intakes, decreasing pain and alleviating discomfort and stress of vaccination in very young children [12].

AEFI can vary as a function of the vaccine (formulation and manufacturers), vaccinee (age of children), and country (vaccination scheme adopted, AEFI reporting systems, and adverse event compensation policies); hence the difficulty in comparing outcomes of AEFI within and between countries. Because of such difficulties, this is a subject that has not been well studied [3], and we can only make inferences from indirect sources. Evans [13] compiled information on compensations available for a few countries and showed that compensated claims (which refer to severe AEFI) by vaccine type differ greatly. It seems that DTP was, at the time of the study, the vaccine showing the highest claims [13] and still is the vaccine with the highest occurrence of AEFI in young children.

For few individuals AEFI are severe, acute, with outcome clearly perceived as harmful. When a severe adverse event happens, an individual bears a significant burden for the greater good or "herd immunity" [14]. Concerns with the long-lasting after effects of disabling illness caused by or associated with the use of vaccines have led a number of countries to create effective systems of surveillance for AEFI and respective compensation programs [14].

During the last decade, however, we have seen an increased awareness related to AEFI that has extended beyond specific vaccine antigens to include low doses of excipients (preservative-Thimerosal and adjuvant-aluminum). Both ethylmercury (a breakdown product of Thimerosal) and aluminum are known neurotoxicants *per se* and, in the case of Hg, with a long history of known toxicity that also includes its organic form—ethylmercury [15]. These excipients (with neuronal effects) are used at low doses as part of some vaccine formulations (Thimerosal-containing vaccines [TCV], and aluminum-adjuvanted vaccines) and are considered safe. Indeed none of the rare neurologic adverse events (encephalopathy, Guillain-Barre syndrome, meningoencephalitis, polyneuropathy, peripheral neuritis, *per se* or in combination) associated with vaccine-antigens [16] can be attributed to low doses of either mercury or aluminum. However, the untested concept of low-dose safety of these excipients originated in the 1930s in the wake of vaccine development. New experimental research designed to model

low-dose exposure relevant to vaccines has established proof-of-concept that Thimerosal-Hg has the potential to produce nonclinical effects in the central nervous system [17] not contemplated by AEFI.

Since late 1990s industrialized countries of Europe and North America have restricted the use of Thimerosal as a preservative in vaccines intended for infants and young children. Although experimental studies can demonstrate toxic effects of low doses of Thimerosal we cannot predict neurological disorders for vaccine-Thimerosal. The few epidemiological studies taken together can at best be interpreted as inconclusive; they cannot show a clear association of ethylmercury with mental disability [18, 19]. However, several studies point to transient delays in neurodevelopment as measurable by neurobehavioral tests [20–23] as well as decreased pain associated with Thimerosal-free vaccine [24, 25]. Additionally, regarding immunologic effects, epidemiological studies have suggested an association of Thimerosal and patch-test sensitivity; countries that eliminated Thimerosal from vaccines such as Austria, Denmark, Poland, and the USA [26] observed a decrease in Thimerosal patch-test reactions. Moreover, both experimental [27] and clinical [28] studies have addressed autoimmune (autoinflammatory) syndrome induced by adjuvants (ASIA) in association with some adjuvanted vaccines. Although this emerging information is not part of the AEFI recording system the collected data are nevertheless shaping perceptions among health workers and stakeholders.

The importance of the study is that it the first attempt to address the AEFI after its implementation. The main limitation is that this system in the state of Rondonia, one with a low score of developmental index, has no means to assess reporting bias (i.e., full medical histories of patients) or to estimate nonreported adverse events.

5. Concluding Remarks

There is a need to improve vigilance of vaccine adverse events and implement compensation for those few children that are severely affected by unintended effects of vaccines. Public health workers need to develop competence to interpret AEFI in this new era of increased infectious diseases prophylaxis by vaccination. Stakeholders should be served with the best and most reliable information to ensure that public health immunization policies can live up to their mission.

References

[1] A. R. Hinman, W. A. Orenstein, and A. Schuchat;, "Centers for Disease Control and Prevention (CDC). Vaccine-preventable diseases, immunizations, and MMWR—1961–2011," *MMWR Surveillance Summary*, vol. 60, supplement 4, pp. 49–57, 2011.

[2] G. A. Poland, I. G. Ovsyannikova, and R. M. Jacobson, "Adversomics: the emerging field of vaccine adverse event immunogenetics," *Pediatric Infectious Disease Journal*, vol. 28, no. 5, pp. 431–432, 2009.

[3] R. T. Chen, "Vaccine risks: real, perceived and unknown," *Vaccine*, vol. 17, no. 3, pp. S41–S46, 1999.

[4] R. T. Chen, V. Pool, H. Takahashi, B. G. Weniger, and B. Patel, "Combination vaccines: postlicensure safety evaluation," *Clinical Infectious Diseases*, vol. 33, no. 4, pp. S327–S333, 2001.

[5] D. S. Diekema, "Improving childhood vaccination rates," *The New England Journal of Medicine*, vol. 366, no. 5, pp. 391–393, 2012.

[6] E. Autret-Leca, L. Bensouda-Grimaldi, A. P. Jonville-Béra, and F. Beau-Salinas, "Pharmacovigilance of vaccines," *Archives de Pediatrie*, vol. 13, no. 2, pp. 175–180, 2006.

[7] W. Zhou, V. Pool, J. K. Iskander et al., "Surveillance for safety after immunization: Vaccine Adverse Event Reporting System (VAERS)—United States, 1991–2001," *MMWR Surveillance Summaries*, vol. 52, no. 1, pp. 1–24, 2003.

[8] R. T. Chen, S. C. Rastogi, J. R. Mullen et al., "The vaccine adverse event reporting system (VAERS)," *Vaccine*, vol. 12, no. 6, pp. 542–550, 1994.

[9] E. A. Waldman, K. R. Luhm, S. A. M. G. Monteiro, and F. R. M. de Freitas, "Surveillance of adverse effects following vaccination and safety of immunization programs," *Revista de Saude Publica*, vol. 45, no. 1, pp. 173–184, 2011.

[10] S. A. M. Gomes Monteiro, O. A. Takano, and E. A. Waldman, "Evaluation of the Brazilian surveillance system for adverse events following vaccination," *Revista Brasileira de Epidemiologia*, vol. 14, no. 3, pp. 361–371, 2011.

[11] S. A. M. G. Monteiro, O. A. Takano, and E. A. Waldman, "Surveillance for adverse events after DTwP/Hib vaccination in Brazil: sensitivity and factors associated with reporting," *Vaccine*, vol. 28, no. 18, pp. 3127–3133, 2010.

[12] J. G. Dòrea, "Breastfeeding is an essential complement to vaccination," *Acta Paediatrica, International Journal of Paediatrics*, vol. 98, no. 8, pp. 1244–1250, 2009.

[13] G. Evans, "Vaccine injury compensation programs worldwide," *Vaccine*, vol. 17, supplement 3, pp. S25–S35, 1999.

[14] C. Lookera and H. Kellya, "No-fault compensation following adverse events attributed to vaccination: a review of international programmes," *Bulletin of the World Health Organization*, vol. 89, no. 5, pp. 371–378, 2011.

[15] D. A. Geier, L. K. Sykes, and M. R. Geier, "A review of Thimerosal (Merthiolate) and its ethylmercury breakdown product: specific historical considerations regarding safety and effectiveness," *Journal of Toxicology and Environmental Health—Part B*, vol. 10, no. 8, pp. 575–596, 2007.

[16] K. Lapphra, L. Huh, and D. W. Scheifele, "Adverse neurologic reactions after both doses of pandemic H1N1 influenza vaccine with optic neuritis and demyelination," *Pediatric Infectious Disease Journal*, vol. 30, no. 1, pp. 84–86, 2011.

[17] J. G. Dórea, "Integrating experimental (in vitro and in vivo) neurotoxicity studies of low-dose thimerosal relevant to vaccines," *Neurochemical Research*, vol. 36, no. 6, pp. 927–938, 2011.

[18] C. J. Clements, "The evidence for the safety of thiomersal in newborn and infant vaccines," *Vaccine*, vol. 22, no. 15-16, pp. 1854–1861, 2004.

[19] J. G. Dórea, "Making sense of epidemiological studies of young children exposed to thimerosal in vaccines," *Clinica Chimica Acta*, vol. 411, no. 21-22, pp. 1580–1586, 2010.

[20] R. C. Marques, J. G. Dórea, J. V. E. Bernardi, W. R. Bastos, and O. Malm, "Prenatal and postnatal mercury exposure, breastfeeding and neurodevelopment during the first 5 years," *Cognitive and Behavioral Neurology*, vol. 22, no. 2, pp. 134–141, 2009.

[21] D. Mrozek-Budzyn, R. Majewska, A. Kieltyka, and M. Augustyniak, "Neonatal exposure to Thimerosal from vaccines and child

development in the first 3years of life," *Neurotoxicology and Teratology*, vol. 34, no. 6, pp. 592–597, 2012.

[22] B. E. Lee and E. H. Ha, "Response to commentary 'Co-exposure and confounders during neurodevelopment: we need them in the bigger picture of secondhand smoke exposure during pregnancy'," *Environmental Research*, vol. 112, article 235, 2012.

[23] J. G. Dórea, R. C. Marques, and C. Isejima, "Neurodevelopment of Amazonian infants: antenatal and postnatal exposure to methyl- and ethylmercury," *Journal of Biomedicine and Biotechnology*, vol. 2012, Article ID 132876, 9 pages, 2012.

[24] Y. Tsuji, I. Ichihashi, K. Morita, and K. Itabashi, "Difference of the pain during the DPT (Diphtheria-Pertussis-Tetanus) vaccination," *World Journal of Vaccines*, vol. 2, pp. 91–95, 2012.

[25] K. Terada, M. Inoue, T. Yamaguchi, S. Ogita, K. Kawasaki, and K. Ouchi, "Difference of response in an inoculation site and pain between vaccines with Thimerosal or Phenoxyethanol," *Infection and Immunity in Childhood*, vol. 22, no. 2, pp. 145–150, 2010.

[26] J. G. Dórea, "Concern regarding early exposure to thiomersal and mercury poisoning: comment on the article by Bensefa-Colas et al," *Revue de Medecine Interne*, vol. 33, no. 2, pp. 115–116, 2012.

[27] A. Katzav, S. Kivity, M. Blank, Y. Shoenfeld, and J. Chapman, "Adjuvant immunization induces high levels of pathogenic antiphospholipid antibodies in genetically prone mice: another facet of the ASIA syndrome," *Lupus*, vol. 21, no. 2, pp. 210–216, 2012.

[28] E. Israeli, "Gulf War Syndrome as a part of the autoimmune (autoinflammatory) syndrome induced by adjuvant (ASIA)," *Lupus*, vol. 21, no. 2, pp. 190–194, 2012.